OUKA

Title	Nuclear Magnetic Resonance Study of Uranium Based Heavy Fermion Superconductors
Author(s)	藤, 秀樹
Citation	大阪大学, 1996, 博士論文
Version Type	VoR
URL	https://doi.org/10.11501/3110116
rights	
Note	

Thesis

Nuclear Magnetic Resonance Study
of
Uranium Based
Heavy Fermion Superconductors

by
Hideki Tou

OSAKA UNIVERSITY
Graduate School of Engineering Science
Department of Material Physics
Toyonaka Osaka

January 1996

Abstract

NQR and NMR studies have been performed for two types of heavy fermion compounds. One is the heavy fermion superconductors, UPd_2Al_3 and UPt_3, and the other is the heavy fermion antiferromagnet, $CePd_2Al_3$.

In UPd_2Al_3, which exhibits a record superconducting transition temperature $T_c = 2$ K and the narrowest Al-NQR line width of 12 kHz, the nuclear spin lattice relaxation rate, $^{27}(1/T_1)$, below T_c has been found to obey the T^3 law at least down to 200 mK, giving a strong evidence that the energy gap vanishes along lines on the Fermi surface. In addition, from the isotropic reduction of ^{27}Al-Knight shift below T_c, an even parity d-wave state characterized by lines of zero gap on the Fermi surface is considered to be realized in UPd_2Al_3.

On the other hand, in UPt_3 no change of ^{195}Pt-Knight shift has been found across T_c down to 28 mK, regardless of the directions of applied magnetic fields and independently of the superconducting multiphases. It is demonstrated that UPt_3 is an odd-parity superconductor with an equal spin pairing and the pinning of the order parameter does not take place, suggesting the spin-orbit coupling for the pairing interaction to be not so strong.

These novel results provide us with an evidence for a non phonon-mediated-superconducting-mechanism in the strongly correlated system.

In $CePd_2Al_3$, systematic measurements of the NQR spectrum and the nuclear-spin-lattice relaxation rate, $1/T_1$, of ^{27}Al have revealed that the magnetic nature dramatically changes from showing long-range and inhomogeneous AF ordering for annealed and as-cast poly-crystals, respectively, to a disappearance of any type of magnetic ordering for single crystals. A close relationship between the magnetic ordering and the structural disorder in the Al layers isolated from the Ce-Pd layers is demonstrated.

Contents

1   Introduction

1.1   General Introduction

Since the discovery of a class of intermetallic compounds, the so-called "*heavy fermion*" (HF) system, containing the rare earth and actinide elements in the late 70's, various HF compounds have been found and extensive studies have been carried out in order to clarify their ground state properties.

The HF systems have attracted special interests as exotic materials in the solid state physics because of rich varieties of their ground states. Their remarkable feature is that the effective mass of quasiparticles is extremely enhanced owing to electron-electron interactions and is larger than that of the free electron by two to three orders of magnitude [1].

The HF system is constituted from periodically arranged magnetic atoms originated in the localized character of 4f- or 5f-electrons. In the most HF compounds, the $-\ln T$ dependence of the resistivity associated with the single site Kondo scattering and the Curie-Weiss law like temperature dependence of susceptibility which are peculiar to the dilute Kondo alloys are commonly observed in the high temperature region. Below the Kondo temperature T_K, differently from the dilute Kondo alloys, the localized f-electrons are delocalized through a hybridization with conduction electrons, forming a heavy Fermi liquid state due to strongly correlated quasiparticles far below T_K. In addition, the indirect RKKY interaction among magnetic atoms also develops with decreasing temperature and competes with the dense Kondo effect. As a result, the heavy Fermi liquid state is not always stable as a ground state, but rather the heavy quasiparticles may fall into other ground state, e.g., magnetic ordered state, superconducting state and gapped state and so on.

After the first discovery of the heavy fermion superconductor (HFS), $CeCu_2Si_2$, by F. Steglich *et al.* [2], the HFS's were found in UPt_3 [1], UBe_{13} [3], URu_2Si_2[4], UNi_2Al_3 [5] and UPd_2Al_3 [6]. Most of the HFS's coexist or compete with magnetically ordered state in their superconducting ground state. The various results from thermodynamics and transport experiments have revealed anisotropic natures of their ground state properties.

1

Thus the formation of a superconducting state in the strongly correlated electron system leads to a possibility of an unconventional superconducting mechanism different from the conventional BCS one.

In this thesis, in order to clarify the mechanism of superconductivity in the strongly correlated system, we present, analyze and discuss the NMR experimental results on UPd_2Al_3, UPt_3 and $CePd_2Al_3$. In this chapter, we begin with reviewing the normal and the ground state properties of these systems established so far.

1.2 Review of Heavy Fermion Superconductor UPd$_2$Al$_3$

1.2.1 Crystal Structure

UPd$_2$Al$_3$ has a hexagonal PrNi$_2$Al$_3$ type structure with lattice parameters of $a = 5.365$ Å and $c = 4.186$ Å, as displayed in Fig.1.2.1. This structure is described by the space-group of $P6_3/mmm$ with following site occupations:

$$\text{U} \;:\; (0,0,0)$$

$$\text{Pd} \;:\; \left(\frac{1}{3},\frac{2}{3},0\right) ; \left(\frac{2}{3},\frac{1}{3},0\right)$$

$$\text{Al} \;:\; \left(\frac{1}{2},0,\frac{1}{2}\right) ; \left(0,\frac{1}{2},\frac{1}{2}\right) ; \left(\frac{1}{2},\frac{1}{2},\frac{1}{2}\right).$$

$\bigcirc$ U $\circledS$ Pd $\bullet$ Al
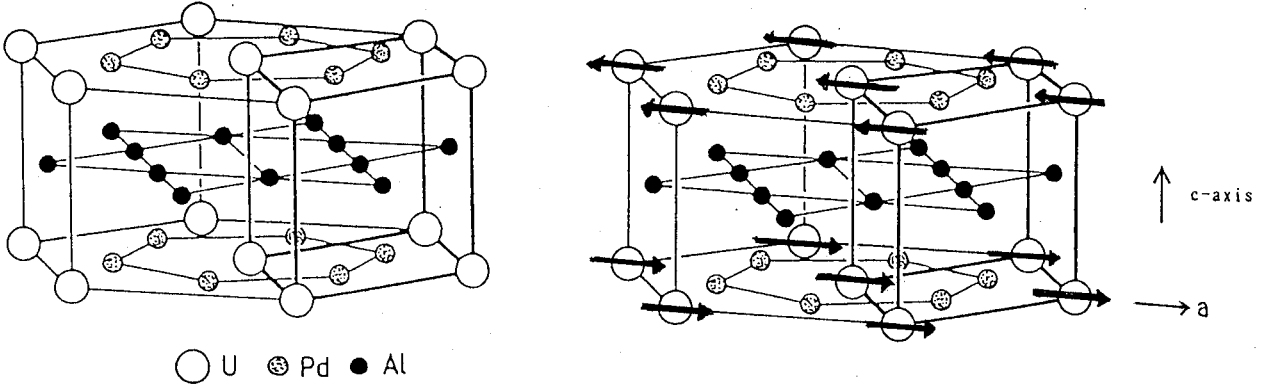
Figure 1.2.1 (a) The hexagonal PrNi$_2$Al$_3$ crystal structure and (b) the magnetic structure below T_N of UPd$_2$Al$_3$. Black arrows show the magnetic moment of U ions.

1.2.2 Experimental Approaches

UPd$_2$Al$_3$ was found to exhibit antiferromagnetic (**AF**) and superconducting (**SC**) transitions at the Néel temperature T_N=14.5K and the superconducting transition temperature T_c=2 K with a rather moderate mass enhancement, i.e., the T-linear coefficient of specific heat, γ_0=150 mJ/moleK^2 [6]. In Figs.1.2.2 and 1.2.3, we show the results of the electric resistivity, $\rho(T)$ [25] and the dc-susceptibility, $\chi(T)$ [26]. In the high temperature region above 70 K, $\chi(T)$ and $\rho(T)$ exhibit a Curie-Weiss law like temperature dependence with

$p_{eff} \sim 3.6\mu_B/$U and $\theta \sim -33$ K and a Kondo-like $-\ln T$ increase followed by a broad maximum around 70 K, respectively [6, 25]. Below 70 K $\rho(T)$ shows a rapid decrease, implying the formation of the Kondo lattice. Thus UPd_2Al_3 is recognized as the "dense Kondo system" [6].
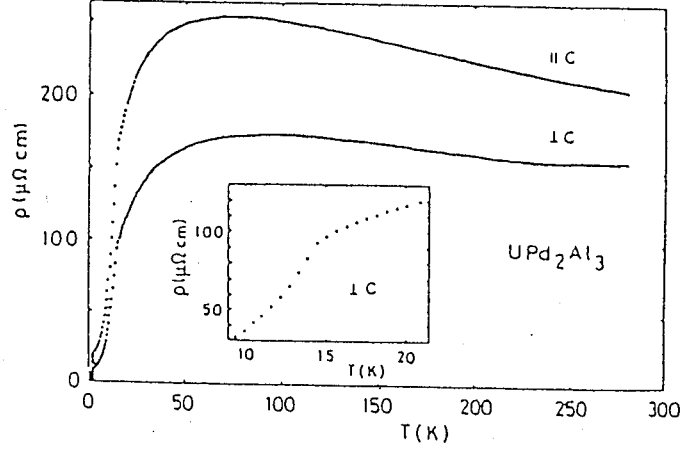
Figure 1.2.2 Temperature dependence of electrical resistivity for single crystal UPd_2Al_3. The inset shows the data around T_N [25].
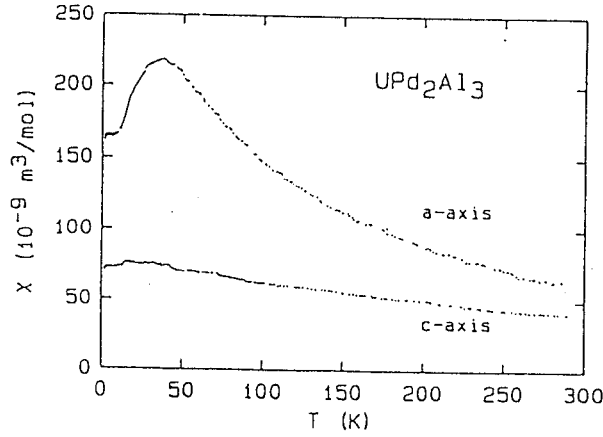
Figure 1.2.3 Temperature dependence of dc-susceptibility for single crystal UPd_2Al_3 [26].

On lowering temperature, the system undergoes the **AF** transition at $T_N \sim 15$ K as clearly displayed by λ like peak of specific heat in Fig.1.2.4 [6]. The electronic specific heat coefficient in the paramagnetic state is γ_p =210 mJ/moleK^2, which means that 5f-

4

electrons with localized character at high temperature gradually delocalize through the dense Kondo effect and are reformed as heavy-quasiparticles. The **AF** ordered state was reported to be a commensurate antiferromagnet with a wave vector $\vec{k}=(0,\ 0,\ \frac{1}{2})$ and an ordinary size of uranium-derived moments of $\mu_s \sim 0.85\mu_B/\text{U}$ [29] which is the largest in the HFS's (for instance, the magnitude of the **AF** moments of UPt$_3$, URu$_2$Si$_2$ are about an order of $10^{-2}\mu_B/\text{U}$). We should note that the Al site is ideally located at the magnetically symmetric site in such a spin structure that the ferromagnetic basal plane is antiferromagnetically stacked along the c-axis, as displayed in Fig.1.2.1.

With further decreasing temperature, the system undergoes a superconducting transition at T_c =2 K. Although the electronic specific heat is reduced by the magnetic phase transition from γ_p = 210 to γ_s =150 mJ/moleK^2 just above T_c as shown in Fig.1.2.4 [6], both the large γ_s value and specific heat jump, $\Delta C/C_e(T_c)$ =1.2 associated with the **SC** transition indicate that the heavy-quasiparticle itself takes part in the formation of the Cooper pairs. Especially, UPd$_2$Al$_3$ is the first compound where the HFS coexists with the AF ordering caused by U-derived moments with ordinary size.
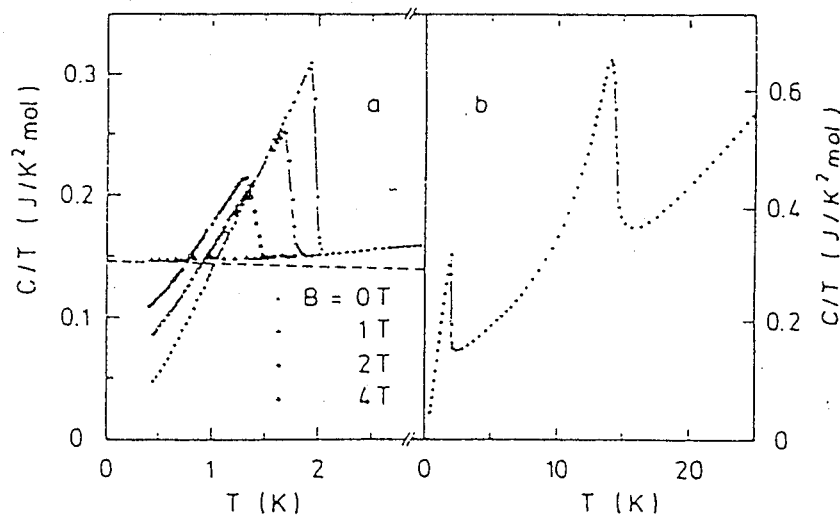

Figure 1.2.4 Temperature dependence of specific heat. (a) C/T near T_c in various magnetic fields. (b) C/T below 30 K. λ -like peak at around 14 K corresponds to an antiferromagnetic phase transition, while that at around 2 K to a superconducting phase transition. Dashed curve in (a) represents electronic contribution [6].

In the superconducting state, various thermodynamics, e.g., specific heat [27, 81], thermal conductivity [30] and NMR relaxation rate[31], exhibit a power-law temperature dependence, in contrast with the exponential one in the conventional BCS superconductors, suggesting the anisotropic nature of the superconducting state. Furthermore, both NMR-[31, 32] and μ^+-Knight shift [33] studies in UPd$_2$Al$_3$ gave evidences for a singlet nature of the Cooper pairing from the isotropic decrease of the spin susceptibility regardless of the crystal directions as displayed in Fig.1.2.5, in contrast to the case of UPt$_3$ [49] where the invariance of the Pt Knight shift below T_c suggests a possibility of a triplet pairing state. Also the isotropic Pauli limiting like temperature dependence of upper critical fields $H_{c2}(T)$ was reported (see Fig.1.2.6 [30]), also suggesting that a singlet nature of the Cooper pairing is realized in UPd$_2$Al$_3$.
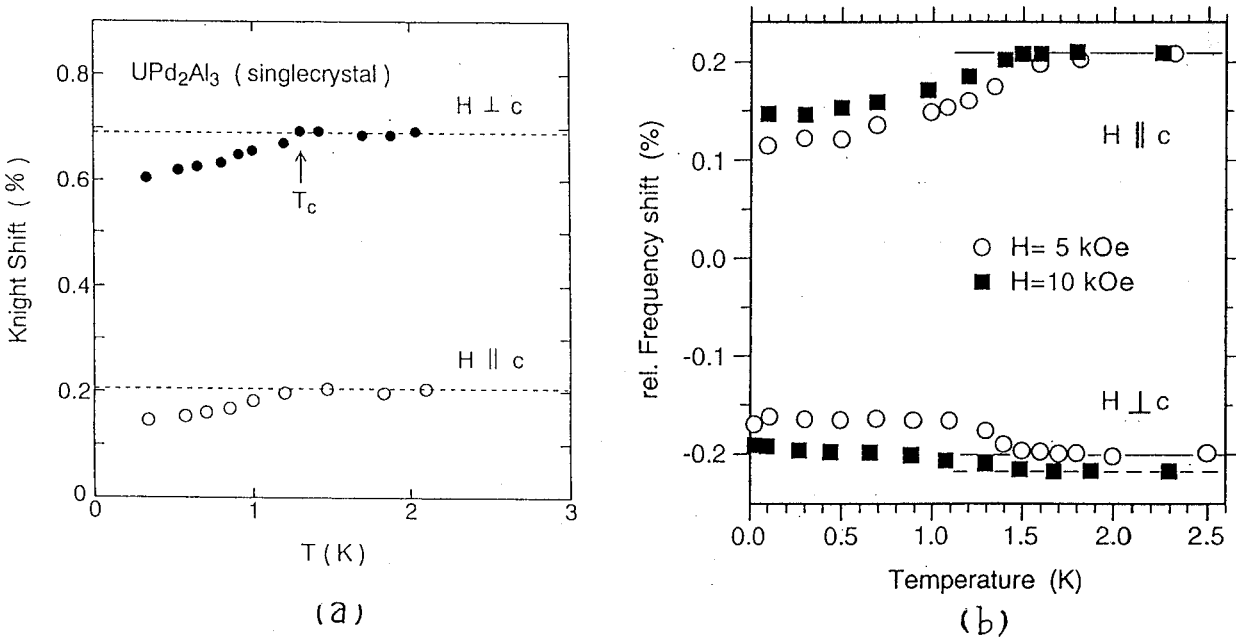
Figure 1.2.5 (a) Temperature dependence of the ^{27}Al Knight shift for single crystal UPd$_2$Al$_3$ under the applied magnetic field perpendicular and parallel to the hexagonal c-axis at f=15.1 MHz. (b) temperature dependence of μ^+SR Knight shift [31, 33].

Recent NMR studies clarified the T^3 dependence of $^{27}(1/T_1)$ in the temperature region from T_c=1.8 K to 0.65 K (see Fig.1.2.7) [31], suggesting a vanishing gap on line at the Fermi surface as in the case for other HFS compounds reported so far. On the other hand, the specific heat results provided the T^3 dependence (Fig.1.2.8) which is compatible with
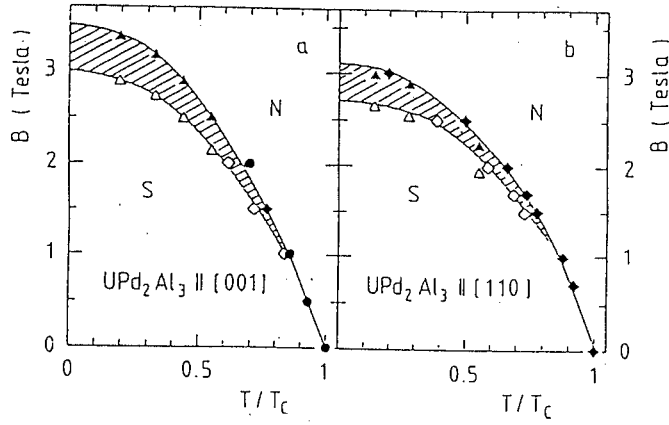
Figure 1.2.6 Temperature dependence of the upper critical field for the single crystal UPd_2Al_3 in the applied magnetic field perpendicular and parallel to the hexagonal c-axis [30].

a vanishing gap on points at the Fermi surface and was inconsistent with the NMR results [27, 81].

Since the previous measurement of $1/T_1$ made in the magnetic field has revealed a deviation from the T^3 dependence associated with the presence of the vortex cores, the identification of the anisotropic energy gap has not yet reached to a consensus. In Chapter 4, we report a precise measurement of the nuclear-spin-lattice relaxation rate, $^{27}(1/T_1)$ of ^{27}Al of the high-quality polycrystalline UPd_2Al_3 in zero field. In addition, we present a comment on the residual Knight shift below T_c.
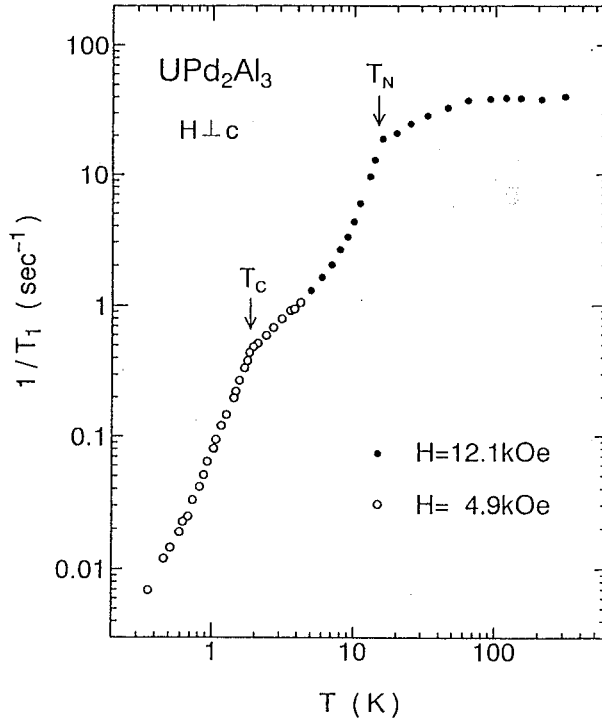
Figure 1.2.7 Temperature dependence of $1/T_1$ of ^{27}Al in UPd$_2$Al$_3$ at f=13.5 MHz (•) and 5.5 MHz (o) [32].
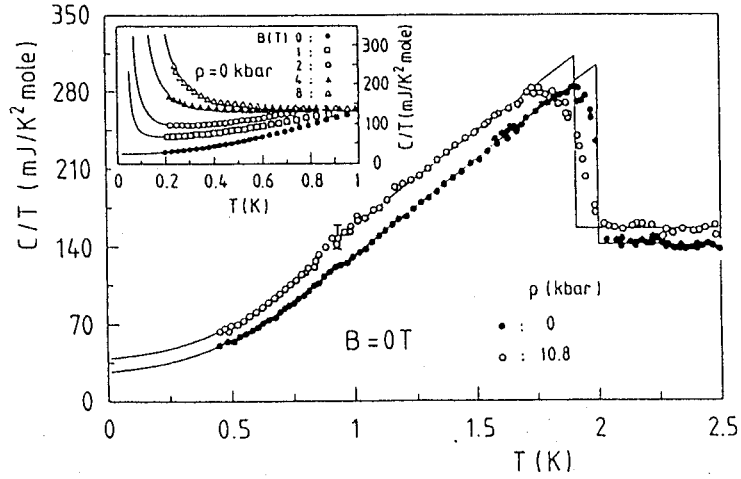
Figure 1.2.8 Temperature dependence of C/T in UPd$_2$Al$_3$ under various pressures. The inset shows C/T below 1 K. The solid lines are calculated by using a formula of $C/T = \gamma_{res} + \alpha T^2$ [27].

1.3 Review of Heavy Fermion Superconductor UPt$_3$

1.3.1 Crystal Structure

UPt$_3$ shows the MgCd$_3$ type hexagonal close-packed structure with lattice parameters of $a = 5.764$ Å and $c = 4.899$ Å, as displayed in Fig.1.3.1(a). The MgCd$_3$ type structure is described by the space-group of $P6_3/mmc$ with following site occupations:

$$U \quad : \quad \left(\frac{1}{3}, \frac{2}{3}, \frac{1}{4}\right) ; \left(\frac{2}{3}, \frac{1}{3}, \frac{3}{4}\right)$$

$$Pt \quad : \quad \left(x, 2x, \frac{1}{4}\right) ; \left(2\bar{x}, \bar{x}, \frac{1}{4}\right) ; \left(x, \bar{x}, \frac{1}{4}\right) ; \left(\bar{x}, 2\bar{x}, \frac{3}{4}\right) ; \left(2x, x, \frac{3}{4}\right) ; \left(\bar{x}, x, \frac{3}{4}\right)$$

$$, \text{and} \quad x = \frac{5}{6}, \bar{x} = -\frac{5}{6}.$$

The shortest U-U interatomic distance and the unit-cell volume are 4.132 Å and 140.96 Å^3, respectively. In Fig.1.3.1(b), we show the Brillouin zone of UPt$_3$. In the reciprocal space of hexagonal structure, [11$\bar{2}$0] and [0001] directions correspond to a and c-axis in real space, respectively.

Figure 1.3.1 (a) Hexagonal close-packed MnCd$_3$ crystal structure of UPt$_3$. (b) The Brillouin zone of UPt$_3$ (after Ref.[68]).

1.3.2 Experimental Approaches

Among heavy fermion superconductors, UPt$_3$ discovered in the middle of 80th has been clearly established as an unconventional superconductor [1]. In the normal state at low temperature below 1.5 K, UPt$_3$ displays a Fermi-liquid behavior characterized by a

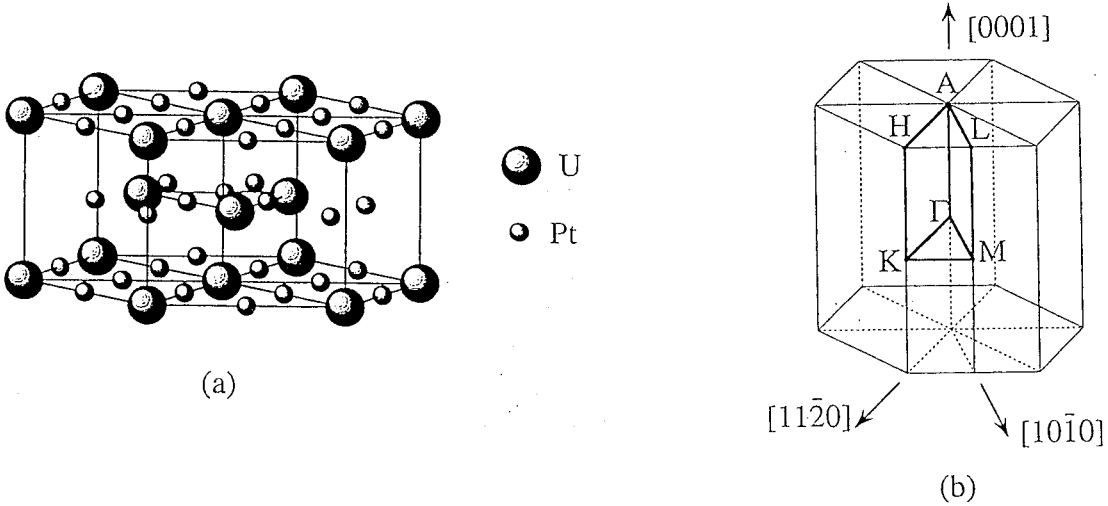linear temperature dependence of the specific heat ($C = \gamma T$), a nearly constant magnetic susceptibility ($\chi(T) = \chi(0)$), and a T^2 behavior in resistivity ($\rho = \rho_0 + AT^2$)[40]. The low temperature electronic specific heat coefficient, γ, is $\sim$420mJ/moleK^2, indicating that the effective mass of the quasiparticles amounts to 400 times as large as free electron mass [1, 40]. In addition, the large specific heat jump associated with superconducting transition of $\Delta C / \gamma T_c$ $\sim$0.5 implies that the heavy quasiparticles participate in the superconductivity. Furthermore neutron scattering studies have shown that UPt$_3$ exhibits **AF** correlation with a wave vector of $\vec{k}$ =(0,0,1) below 30 K [41] and undergoes phase transition to an **AF** ordered state with relatively small moment $\sim 0.02\mu_B$ with $\vec{k}$ =(0.5,0,1) at T_N $\sim$5 K (Fig.1.3.2) [42]. In this context, the formation of superconducting state is considered to be a non-BCS type of pairing mechanism.
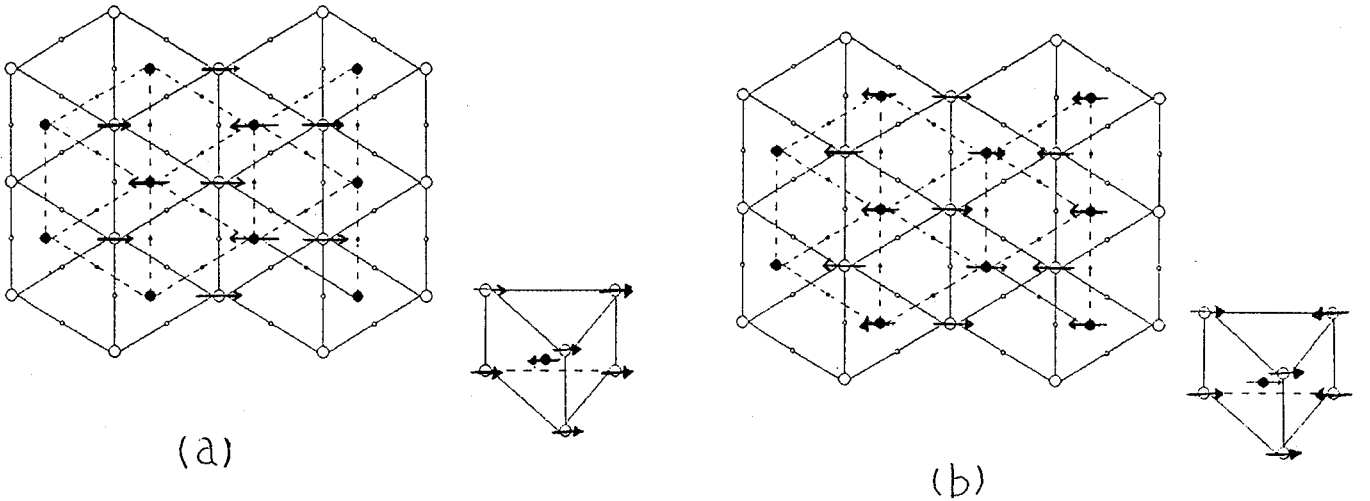
Figure 1.3.2 Magnetic structure of UPt$_3$. The open and closed circles (large) denote the positions of U atoms in two adjacent plane, respectively. Small ones denote the positions of Pt atom. (a) a snapshot of AF correlation with $\vec{k} = (0,0,1)$ below 30 K and (b) arrangement of AF ordered moments with $\vec{k} = (0.5,0,1)$ of UPt$_3$ [41, 42].

In order to elucidate the mechanism of superconductivity in UPt$_3$, extensive experimental works have been carried out and the characteristic features of the unconventional superconductivity in UPt$_3$ have been clarified. The temperature dependence of various thermodynamics in the superconducting state follows a power law, $e.g.$ the longitudinal ultrasonic attenuation $\sim T$ [43], the NMR relaxation rate $\sim T^3$ (Fig.1.3.3 [44]) and the specific heat $\sim T^2$ [45, 46], $etc.$, being in consistent with gap zeros on line at the Fermi

surface. Moreover μSR experiment on the penetration depth [48] and the transverse ultrasonic attenuation [47] clarified the energy gap vanishes both on points at the poles in addition to the line along the equator of the Fermi surface (Fig.1.3.4). A possibility of an odd-parity of the Cooper pairing was pointed out from NMR [49] and μSR [50] experiments as shown in Figs.1.3.5, where the spin susceptibility χ_s is invariant below T_c. However, a possibility that the invariance of χ_s is not ascribed to the odd-parity but to an even-parity pairing with the spin-orbit scattering due to impurities and/or defects cannot be ruled out *completely* [49, 51]. The *spin-orbit scattering* effect may bring about a similar invariant behaviors in **SC** state even for an even parity superconductor and prevent us from extracting the intrinsic phenomena.
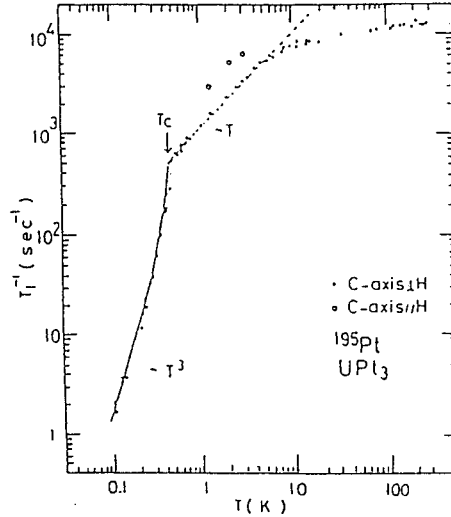
Figure 1.3.3 Temperature dependence of the $^{195}(1/T_1)$ in polycrystal UPt$_3$ [44].

In 1989, Fisher *et al.* and Hasselbach *et al.* discovered independently the successive **SC** transitions at T_{c1} =0.51 K and T_{c2} =0.46 K in the high-quality single crystal UPt$_3$ from the specific heat experiments (Fig.1.3.6) [45, 46]. Moreover, the ultrasonic absorption presented a remarkably complex superconducting phase diagram, as a function of the temperature and the magnetic field, in which three kinds of superconducting phases, the so called "**A**","**B**" and "**C**"-phases on the analogy of ^{3}He superfulid, meet each other at a tetracritical point [45, 46], [52]–[57] (Fig.1.3.7). This is an evidence that there exist internal degrees of freedom in the superconducting state. These results stimulated us to study on the novel superconducting state,*i.e.*, on both the origin of the internal degrees of freedom in the superconducting state and the mechanism of superconductivity of UPt$_3$

11
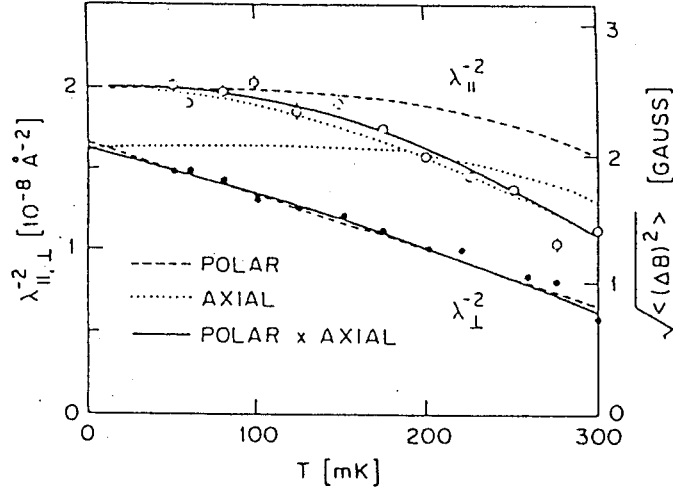
Figure 1.3.4 Temperature dependence of the μ^+SR penetration depth for single crystal UPt_3 in the applied magnetic field perpendicular and parallel to the hexagonal c-axis. Solid lines are fits assuming various model structure in the superconducting energy gap [48].
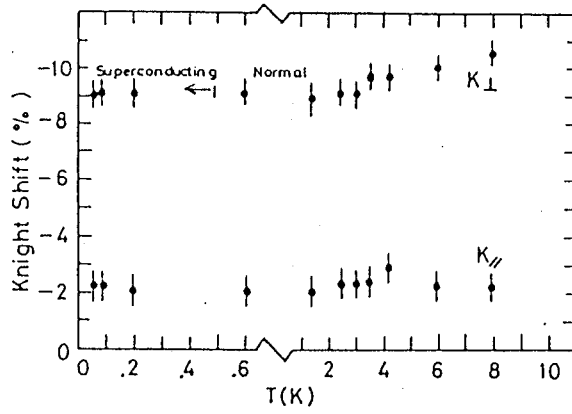
Figure 1.3.5 Temperature dependence of the ^{195}Pt Knight shift for polycrystal UPt_3 [49].
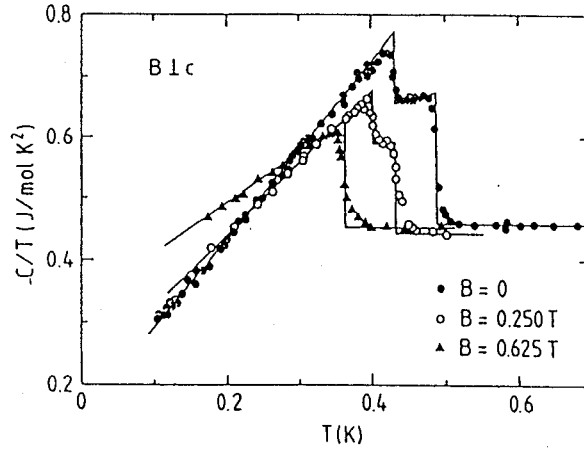
Figure 1.3.6 Specific heat C of UPt_3 plotted as C/T vs T under the magnetic fields applied perpendicular to the c-axis [46].
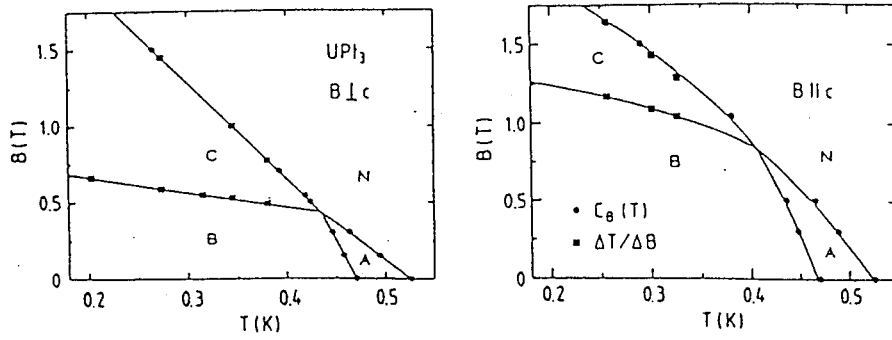
Figure 1.3.7 B-T phase diagram of UPt_3 for a field applied perpendicular and parallel to the hexagonal c-axis as determined from the specific heat (closed circles) and the magnetocaloric effect (closed square). Solid lines are guide for the eye [57].

13

1.3.3 Theoretical Approaches

In order to describe such unconventional natures of superconducting state, especially on the anomalous phase diagram, various attempts based on phenomenological theories have been made. So many phenomenological theories of UP_3 have been presented that we do not go into detail. Instead, we mention here only the main trends in the theories. At present, phenomenological theories are classified into two main trends. The first is the "*symmetry breaking field* (**SBF**)" model based on the odd-parity pairing. The most popular candidate for **SBF** is considered to be a weak antiferromagnetic order with small moment of $\mu_s = 0.02\mu_B/U$ below $T_N \sim 5$ K, in which the superconducting double transition is originated from a weak interaction between **SBF** and a multicomponent superconducting order parameter (OP) with internal degrees of freedom either in pseudo-spin (one-dimensional A_{1u} or A_{2u} [58] and two-dimensional E_{1u} [59] representations) or orbital (two-dimensional E_{2u} representation [60]) part of pairing function. Above scenarios based on the **SBF** were suggested to be consistent with the result that the double transition in zero field is merged into a single transition at the same critical pressure of 3.2 kbar as that beyond which the AF ordering disappears [61]. It is assumed that the spin-orbit coupling (**SOC**) in the Cooper pair is weak for A_{1u} or A_{2u} scenario [58], while is strong for both E_{1u} [59] and E_{2u} [60] ones. Therefore theoretical prediction for the T dependence of the spin susceptibility, χ_s's are quite different among them : (1) both for A_{1u} and A_{2u} with the weak **SOC**, χ_s is invariant regardless of directions of the magnetic field because the $\vec{d}$-vector can behave always as $\vec{d} \perp \vec{H}$, (2) for E_{1u} with the strong **SOC**, χ_s decreases in the hexagonal basal plane because the $\vec{d}$-vector is locked to the hexagonal basal plane and (3) for E_{2u} with the strong **SOC**, χ_s along the c-axis should decrease because the $\vec{d}$-vector is locked to the hexagonal c-axis.

Another is the "*two-components d-wave*" model based on accidentally degenerate two independent even-parity order parameters, *e.g.* of A_{1g} and E_{1g} representations [62, 63], in which the degeneracy is considered to be lifted not by **SBF**, but by a weak crystal field effect. Therefore, in this model it is based on a standpoint that the invariant spin susceptibility is not ascribed to the nature of odd-parity but rather to the impurities-induced *spin-orbit scattering* mechanism as reported previously [51, 49, 44]. Thus in *d-wave*

scenario, it is evident that the χ_s should decrease below T_c in a clean limit because of the singlet nature of the OP.

The temperature dependence of the spin susceptibilities below T_c predicted by various models are summarized in Table 1.

			$\Delta(\vec{k})$	$\chi_s^a \ (T \leq T_c)$	$\chi_s^c \ (T \leq T_c)$
SBF	1D	A_{1u}	$k_z \tau_+$	$\rightarrow$	$\rightarrow$
		A_{2u}	$k_z(k_x^2 + k_y^2)\tau_+$	$\rightarrow$	$\rightarrow$
	2D	E_{1u}	$k_+^2 k_z \tau_-$	$\searrow$	$\rightarrow$
		E_{2u}	$k_+^2 k_z \tau_z$	$\rightarrow$	$\searrow$
d-wave	E_{1g}		$(kx \pm ik_y)k_z$	$\searrow$	$\searrow$
	A_{1g}		$k_x^2 + k_y^2 - 2k_z^2$	$\searrow$	$\searrow$

Table 1 Temperature dependence of the spin susceptibility $\chi(T)$ in the superconducting state predicted by various model [58, 59, 60, 62, 63].

In spite of many experimental and theoretical efforts, the details of the superconducting mechanism even on the choice of pairing symmetry remain unresolved. Furthermore, although the **SOC** in the Cooper pair is generally considered to be strong in HFS system [23] because the **intra-atomic SOC** and the crystal field are strong, it is not at all clear at present whether or not the **SOC** in the Cooper pair is strong. In Chapter 5, in order to unravel a possible OP representation in UPt$_3$, we report precise ^{195}Pt Knight shift measurement on high quality single crystal UPt$_3$. In addition, in order to gain further insight into **AF** ordering which has not been confirmed by any macroscopic measurement yet (also previous NMR measurements failed to direct evidence of **AF** order), we present the precise NMR measurements in the high temperature region of 1−50 K.

1.4 Review of Heavy Fermion Antiferromagnet $CePd_2Al_3$

1.4.1 Crystal Structure

$CePd_2Al_3$ has a hexagonal $PrNi_2Al_3$ type with lattice parameters of $a = 5.470$ Å and $c = 4.216$ Å, which is the same as that of UPd_2Al_3 (See Fig.1.2.1).

1.4.2 Experimental Approaches

$CePd_2Al_3$ is characterized as a heavy fermion antiferromagnet with T_N ~3 K and a large electronic specific heat, γ =340 mJ/moleK^2 [72, 73, 74, 78].

The $PrNi_2Al_3$ type structure in the Ce-123 system consists of cerium-palladium layers, stacked along the c-axis, alternating with isolated aluminum layers. Antiferromagnetic ordering was found in annealed polycrystals below T_N =2.7 K and the magnetic structure determined by neutron scattering experiment belongs to the same planar class as that in UPd_2Al_3, where the ferromagnetic sheets of Ce moments lying in the hexagonal basal plane are coupled antiferromagnetically along the c-axis [29, 73, 74, 75]. The ordered Ce-moment of $0.47\mu_B$ is smaller than the U-moment of $0.85\mu_B$ in UPd_2Al_3 [29]. The onset of the **AF** order in the *annealed* $CePd_2Al_3$ was established by means of various experiments (Figs.1.4.1−1.4.3). On the other hand, no long-range ordering was observed down to 1.5 K both for *as-cast poly-* and *single*-crystals and even for *annealed single*-crystals in the Ce-123 system (Fig.1.4.1−1.4.4). The **AF** ordering in this system disappears depending on the method of sample preparation.

In the early stage of research, an inter-atomic disorder between Pd and Al atoms, *i.e.*, the Al atom partially occupying the Pd-site, was suggested by means of x-ray scattering experiment for polycrystalline samples, where the reduction of the x-ray intensity of (001) and (003) reflections was observed [74]. It was argued that this type of structural disorder was responsible for the sample dependence of the occurrence of the **AF** ordering. By contrast, the neutron scattering experiment for an annealed single crystal revealed a large reduction of the strongest (002) reflection, though the reduction of the intensity of (001) and (003) reflections was significantly improved by annealing. The precise neutron scattering experiment has suggested that Al atoms are statically or dynamically displaced from $z =$
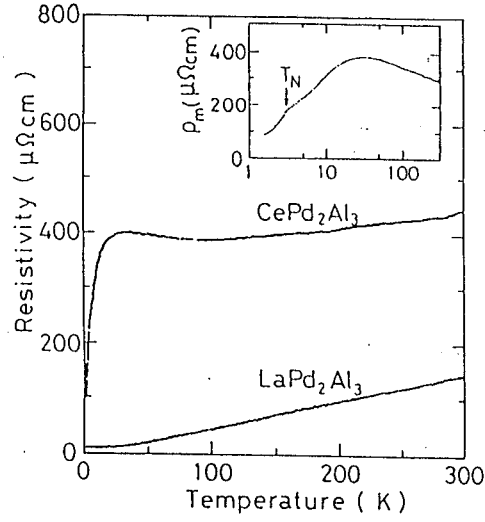
Figure 1.4.1 Temperature dependence of the electrical resistivity of CePd2Al$_3$ and LaPd$_2$Al$_3$. The inset shows a log$T$ plot of magnetic part of resistivity $\rho_m = \rho(\text{Ce123}) - \rho(\text{La123})$ [72].
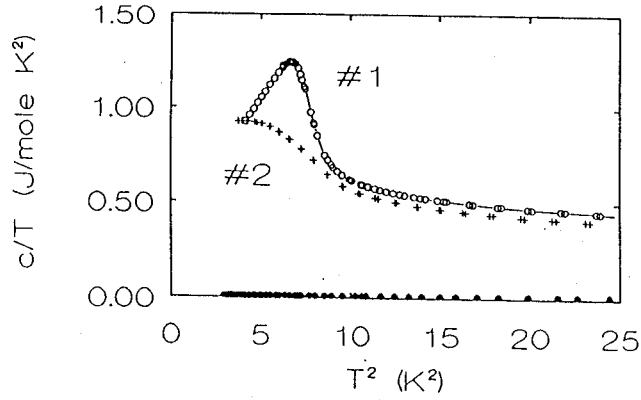
Figure 1.4.2 Specific heat divided by temperature versus temperature squared for annealed (o) and as-cast (+) CePd$_2$Al$_3$. The data of the reference compound LPd$_2$Al$_3$ (•) are given for comparison. [74].
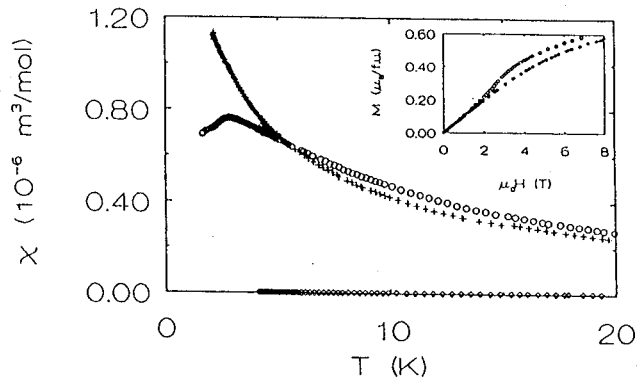
Figure 1.4.3 Susceptibility $\chi(T)$ for annealed (o) and as-cast (+) samples of CePd$_2$Al$_3$. The insets show the magnetization versus field. [74].
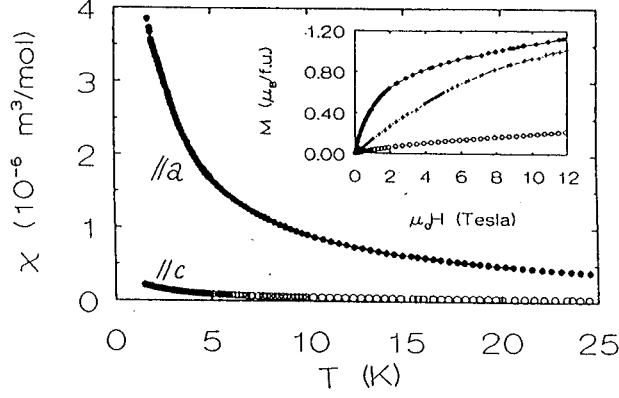
Figure 1.4.4 Susceptibility $\chi(T)$ for single crystal CePd$_2$Al$_3$. The insets show the magnetization versus field [78].

1/2 plane isolated from the Ce-Pd plane [78].

Recently, it was reported from susceptibility, specific heat and Al NQR experiments that the **AF** ordering in CePd$_2$Al$_3$ critically depends on the degree of randomness in the Al-layer [79]. In order to account for the sample dependence of the **AF** ordering in CePd$_2$Al$_3$, Mentink *et al.* proposed a model that an interplane exchange coupling parameter, J_c, along the c-axis is affected sensitively by the different occupation and distribution of Al atoms over two possible sites in the Al layers isolated from the Ce-Pd layers. It was considered that the lack of any long range magnetic ordering in the single crystals is due to the reduction of interplane exchange coupling, J_c, caused by the Al-displacement and/or deficiency. Furthermore, it was supposed that the same effect of the Al site-disorder in UPd$_2$Al$_3$ and UNi$_2$Al$_3$ brought about the sample dependence of the superconducting transition temperature [81, 82].

The study of the sample dependence of the magnetic character in the Ce-123 system is anticipated to provide an important information on a relationship between the antiferromagnetic ordering and the structural disorder in this system. It is, however, still unclear how the magnetic nature is distinguished between the *as-cast* polycrystals and the *single* crystals, both exhibiting no long-range **AF** ordering from the macroscopic experiments. Furthermore, it is of great interest to inspect to what extent the **AF** ordered state is affected by the site-disorder, which may exist inevitably in the Al layers to some extent. In Chapter 5, in order to clarify microscopically the static and dynamical properties for well-

18

characterized antiferromagnetic $CePd_2Al_3$, and to unravel those underlying issues in the Ce-123 system, we report the results of more detailed ^{27}Al NMR and NQR experiments.

2 Introduction to Nuclear Magnetic Resonance

2.1 Static Hyperfine Interaction

2.1.1 Origin of Hyperfine Interaction

The NMR parameters mostly depend on the local atomic configurations and conduction electron density around a nucleus. Here, we summarize the origin of the hyperfine interaction and principles of NMR [7, 8].

In general, the nuclear spin Hamiltonian $\mathcal{H}_N$ is expressed as follows,

$$\mathcal{H}_N = \mathcal{H}_z + \mathcal{H}_{hf}^M + \mathcal{H}_{hf}^Q. \tag{2.1}$$

The first term is the Zeeman interaction between a nuclear spin moment $\vec{\mu}_N = \gamma_N \hbar \vec{I}$ and the external field $\vec{H}_0$;

$$\mathcal{H}_z = -\gamma_N \hbar \vec{I} \cdot \vec{H}_0. \tag{2.2}$$

The second term $\mathcal{H}_{hf}^M$ is the magnetic hyperfine interaction given as

$$
\begin{aligned}
\mathcal{H}_{hf}^M = \gamma_N \gamma_e \hbar^2 \Bigg\{ &\frac{8\pi}{3}\delta(\vec{r})\vec{I}\cdot\vec{S} - \left(\frac{\vec{I}\cdot\vec{S}}{r^3} - \frac{3(\vec{I}\cdot\vec{r})(\vec{S}\cdot\vec{r})}{r^5}\right) \\
&+ \frac{\vec{I}\cdot\vec{l}}{r^3} + \frac{8\pi}{3}\sum_i\left(\left|\Psi_i(0)^\uparrow\right|^2 - \left|\Psi_i(0)^\downarrow\right|^2\right)\vec{I}\cdot\vec{S} + \ldots\ldots \Bigg\}.
\end{aligned}
\tag{2.3}
$$

Here, $\vec{I}$, $\vec{S}$ and $\vec{l}$ are the nuclear spin, the total electron spin ($\vec{S} = \sum \vec{s}$) and the orbital angular momentum of electron, respectively. γ_N and γ_e are the nuclear and electron gyromagnetic ratios. $|\Psi_i(0)|^2$ is the probability density of closed s-electrons. Each term in eq.(2.3) is the Fermi contact interaction due to s-electrons, the spin dipolar interaction due to only unpaired non s-electrons, the orbital interaction due to the orbital current of non s-electron and the indirect interaction due to core polarization effect where the closed inner s-electrons are polarized by the unpaired non s-electrons through exchange polarization effects. In general, eq.(2.3) is divided into two parts of a spin and a orbital part as

$$\mathcal{H}_{hf}^M = \vec{I} \cdot \tilde{A} \cdot \vec{S} + \gamma_N \gamma_e \hbar^2 \frac{\vec{I}\cdot\vec{l}}{r^3}, \tag{2.4}$$

where $\tilde{A}$ is the hyperfine coupling tensor.

The third term in eq.(2.1) is the electrostatic hyperfine interaction between the electric field gradient (EFG) due to non-spherical distribution of the electron charge and the nuclear electric quadruple moment for the nuclear spin ($I \geq 1$);

$$\mathcal{H}_{hf}^Q = \frac{e^2 qQ}{4I(2I-1)} \left\{ 3I_z^2 - I(I+1) + \frac{1}{2}\eta(I_+^2 + I_-^2) \right\},\qquad(2.5)$$

with

$$eq \equiv \frac{\partial^2 V}{\partial z^2}, \; \eta = \frac{\frac{\partial^2 V}{\partial x^2} - \frac{\partial^2 V}{\partial y^2}}{\frac{\partial^2 V}{\partial z^2}},\qquad(2.6)$$

where x, y, z are the principle axes of the electric field gradient tensor and $\frac{\partial^2 V}{\partial z^2} \geq \frac{\partial^2 V}{\partial x^2} \geq \frac{\partial^2 V}{\partial y^2}$.

2.1.2 Knight Shift

For metals, the resonance condition is modified by the effect that the nuclear dipole moment interacts not only with the external magnetic field $\vec{H}_0$ but also with the local hyperfine field $\vec{H}_{hf}$ due to the surrounding electrons [7, 8]. Neglecting the quadruple interaction for simplicity, eq.(2.1) can be expressed as

$$\mathcal{H}_N = -\gamma_N \hbar I \cdot (\vec{H}_0 + \vec{H}_{hf}),\qquad(2.7)$$

and

$$\begin{aligned}\vec{H}_{hf} =\; & \gamma_e \hbar \left\{ \frac{8\pi}{3}\delta(\vec{r})\vec{S} - \left(\frac{\vec{S}}{r^3} - \frac{3\vec{r}(\vec{S}\cdot\vec{r})}{r^5} \right) \right.\\ & \left. + \frac{\vec{l}}{r^3} + \frac{8\pi}{3}\sum_i (\left|\Psi_i(0)^\uparrow\right|^2 - \left|\Psi_i(0)^\downarrow\right|^2)\vec{S} + ... \right\}.\end{aligned}\qquad(2.8)$$

Since the spin and orbital susceptibilities are expressed as

$$\chi_s = -g\mu_B \frac{\langle S_z \rangle}{H_0},\qquad(2.9)$$

$$\chi_{vv} = -\mu_B \frac{\langle l_z \rangle}{H_0},\qquad(2.10)$$

where $\langle s_z \rangle$ and $\langle l_z \rangle$ are the average value of the spin and orbital momentum parallel to the external magnetic field $\vec{H}_0$. Therefore, the average value of eq.(2.8) parallel to $\vec{H}_0$, $\langle H_{hf}^z \rangle$, is divided into two parts of a spin and a orbital term as

$$H_{hf} \equiv \langle H_{hf}^z \rangle = (A_{hf}^s \chi_s + A_{hf}^{vv} \chi_{vv})H_0,\qquad(2.11)$$

21

where A_{hf}^s and A_{hf}^{vv} are the hyperfine coupling constant associated with the spin and the orbital parts. The additional field $\langle H_{hf} \rangle$ causes a energy shift and then the resonance condition would be expressed as

$$\omega_{res} = \gamma_N (H_0 + H_{hf}).$$ (2.12)

The Knight shift is defined as the fractional displacement of the frequency in a fixed field $\vec{H}_0$ from its value in a nonmetalic, nonmagnetic environment ω_0,

$$K = \frac{\omega_{res} - \omega_0}{\omega_0}$$ (2.13)

By substituting eqs.(2.11) and (2.12) into eq.(2.13), we have a relation of

$$K = K_s + K_{vv},$$ (2.14)

where

$$K_s \equiv \frac{A_{hf}^s}{g\mu_B} \chi_s,$$ (2.15)

and

$$K_{vv} \equiv \frac{A_{hf}^{vv}}{\mu_B} \chi_{vv}.$$ (2.16)

Here, K_s and K_{vv} are the spin and Van Vleck parts of Knight shifts, respectively.

Since the NMR experiment is usually performed at a fixed frequency with sweeping external magnetic field, the Knight shift is sometimes expressed as the fractional change in the field for resonance at a fixed frequency ω_0,

$$K = \frac{H_0 - H_{res}}{H_{res}},$$ (2.17)

in which K is defined as positive if the field for resonance in the metal is lower than that found in the reference material.

When both K and χ show a temperature dependence, we can make K vs χ plot, with temperature as an implicit parameter. In general in case of transition metals, since the orbital part of both χ and K is temperature independent, hence we can separate the contributions from the spin and the orbital parts by taking this procedure.

Whereas in the heavy fermion system, the state is generally defined by the total angular momentum, $J = L + S$, since the intra-atomic spin-orbit coupling is so strong. Furthermore,

the lowest J manifold is split into several doublets and singlets owing to the crystal electric field (CEF). In this case, we should pay attention that the temperature dependence of both K and χ is arising from fictitious spin J, i.e., not only S but also L.

2.2 Dynamic Hyperfine Interaction

2.2.1 Nuclear Spin-lattice Relaxation Rate $1/T_1$

The Knight shift is a measure of the time average value $\langle H_{hf} \rangle$ of the hyperfine field. On the other hand, the relaxation time T_1 is a measure of the fluctuating components of the hyperfine fields perpendicular to the quantization direction, $\delta \vec{H}^\pm$ [7]. Here we will comment the relaxation time T_1. The longitudinal relaxation rate $1/T_1$ can be expressed as [9]

$$\frac{1}{T_1} = \frac{\gamma_N^2}{2} \int_{-\infty}^{\infty} \left\langle \left\{ \delta H^-(t)\delta H^+(0) \right\} \right\rangle_{AV} \exp(i\omega_0 t) dt. \tag{2.18}$$

Here, γ_N is the gyromagnetic ratio of nucleus, $\delta H^\pm$ is the transverse component of the fluctuation of local field $\vec{H}_{loc}$, $\{AB\}$ is $\frac{AB+BA}{2}$ and ω_0 is the nuclear resonance frequency. Since $\vec{H}_{loc}$ is expressed as

$$\vec{H}_{loc} = \sum A_i \vec{S}_i(\vec{r}), \tag{2.19}$$

where A_i and $\vec{S}_i(\vec{r})$ are the hyperfine coupling constant and the electron spin, respectively, eq.(2.18) is expressed as

$$\frac{1}{T_1} = \frac{\gamma_N^2}{2} \sum_q A_q A_{-q} \int_{-\infty}^{\infty} \left\langle \left\{ \delta S_q^-(t)\delta S_{-q}^+(0) \right\} \right\rangle_{AV} \cos(\omega_0 t) dt. \tag{2.20}$$

Here, A_q and S_q are the Fourier transform of A_i and $\vec{S}_i(\vec{r})$, respectively. By using the fluctuation-dissipation theorem, eq.(2.20) becomes [10]

$$\frac{1}{T_1} = \frac{2\gamma_N^2 k_B T}{(\gamma_e \hbar)^2} \sum_q A_q A_{-q} \frac{Im\chi_\perp(q,\omega_0)}{\omega_0}, \tag{2.21}$$

where $Im\chi_\perp(q,\omega_0)$ is the imaginary part of the transverse component of the dynamical susceptibility.

In the case of the free electron model, $Im\chi_\perp(q,\omega_0)$ is rewritten as follows,

$$Im\chi_\perp(q,\omega_0) \sim \frac{\pi}{2}(\gamma_e \hbar)^2 \sum_k \delta(\hbar\omega_0 - \varepsilon_{k+q} + \varepsilon_k)\{n(\varepsilon_k) - n(\varepsilon_{k+q\uparrow})\}$$

$$\sim \frac{\pi}{2}(\gamma_e \hbar)^2 (N(\varepsilon_F))^2 \hbar\omega_0, \tag{2.22}$$

where $n_{k\sigma}$ is the number of electron with the wave vector $\vec{k}$ and the spin σ. Then eq.(2.21) is expressed as

$$\frac{1}{T_1} = \frac{\pi}{\hbar} A^2 [N(\varepsilon_F)]^2 k_B T, \tag{2.23}$$

where $A^2 = \gamma_N^2 \hbar^2 < A_q A_{-q} >$, $N(\varepsilon)$ is the density of states and ε_F is the Fermi energy. By combining with the Knight shift, we have a relation of

$$\frac{1}{T_1 T K^2} = \frac{4\pi k_B}{\hbar} \left(\frac{\gamma_N}{\gamma_e}\right)^2, \tag{2.24}$$

when the s-electrons, which relates to the first term in eq.(2.3), play a dominant role in nuclear relaxation and Knight shift. This relation is the so called "**Korringa relation**" [11].

2.3 NMR in the Superconducting State

2.3.1 NMR in the BCS Superconducting State

(1)BCS theory

The microscopic theory of superconductivity which was provided by Bardeen, Cooper and Schrieffer in 1957 is based on the fact that, when an attractive interaction between fermions is present, the stable ground state is no longer the degenerated Fermi gas but is a coherent state in which the electrons are combined into pairs of the spin-singlet with zero total momentum (Cooper pairs) [18]. It is the pairing in the momentum space rather than real space. The attractive potential, which has the strong on-site attractive force, originates from the electron-phonon coupling and produces electron pair with isotropic s-wave symmetry. The BCS Hamiltonian is expressed as [18, 19]

$$\mathcal{H}_{BCS} = \sum_{\vec{k},\sigma} \xi_{\vec{k}} a_{\vec{k},\sigma}^\dagger a_{\vec{k},\sigma} + V \sum_{\vec{k},\vec{k}',q} a_{\vec{k}+\frac{q}{2},\uparrow}^\dagger a_{-\vec{k}+\frac{q}{2},\downarrow}^\dagger a_{-\vec{k}'+\frac{q}{2},\downarrow} a_{\vec{k}'+\frac{q}{2},\uparrow}. \tag{2.25}$$

Here $\xi_{\vec{k}}$ is the band energy measured relative to the chemical potential μ and V (<0) is an attractive interaction. By taking the mean field approximation, the order parameter (OP) in the superconducting state is expressed as

$$\Delta = -V \sum_{\vec{k}'} \langle a_{-\vec{k}',\downarrow} a_{\vec{k}',\uparrow} \rangle,$$

$$\Delta^* = -V \sum_{\vec{k}'} \left\langle a_{\vec{k}',\uparrow}^\dagger a_{-\vec{k}',\downarrow}^\dagger \right\rangle, \tag{2.26}$$

24

From eqs.(2.25) and (2.26), and by taking the unitary transformation, the energy eigenvalue of quasiparticles in the BCS superconducting state is obtained as $\pm\varepsilon_{\vec{k}}$, where

$$\varepsilon_{\vec{k}} = \sqrt{\xi_{\vec{k}}^2 + \Delta^2}. \tag{2.27}$$

Then the density of states in the BCS state is

$$
\begin{aligned}
N_{BCS}(E) &= \sum_{\vec{k}} \delta(\varepsilon_{\vec{k}} - E) \\
&\sim \begin{cases} \dfrac{N_0|E|}{\sqrt{E^2 - |\Delta|^2}} & E \geq \Delta \\ 0 & E \leq \Delta. \end{cases}
\end{aligned}
\tag{2.28}
$$

where N_0 is the density of states of one spin per unit energy at the Fermi level in the normal state. Since the order parameter, Δ, has the *s-wave* symmetry as clearly seen in eq.(2.26), the excitation gap is isotropic ($\vec{k}$-independent), leading to the exponential temperature dependence of various thermodynamics and transport quantities. In Fig.2.3.1, we show the density of states in the BCS state.
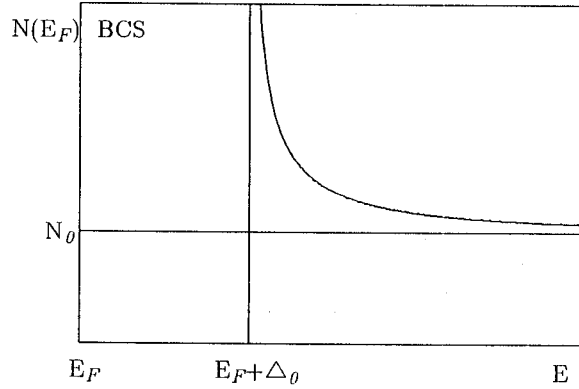
Figure 2.3.1 Density of states for the BCS model.

(2) Knight shift K

Since the Cooper pairs consisting of spin-up and spin-down do not contribute to the spin susceptibility χ_s, only the excited quasiparticles contribute to χ_s. Then χ_s is expressed by well known "Yosida function", $Y(T)$, as [13],

$$
\begin{aligned}
\chi_s &= 2\mu_B^2 N_0 Y(T), \\
Y(T) &= -\frac{2}{N_0} \int_0^\infty N_{BCS}(E) \frac{df}{dE} dE, \tag{2.29}
\end{aligned}
$$

25

where $N_{BCS}(E)$ is defined by eq.(2.28) and f is the Fermi-Dirac function. In Fig.2.3.2, we show the results of Knight shift on aluminum, together with a theoretical curve obtained from eq.(2.29) [15]. In the temperature region of $T \ll T_c$, χ_s decreases exponentially with decreasing temperature as

$$\chi_s(T) \sim e^{-\frac{\Delta}{k_B T}}, \tag{2.30}$$

reflecting the isotropic opening of superconducting excitation gap.
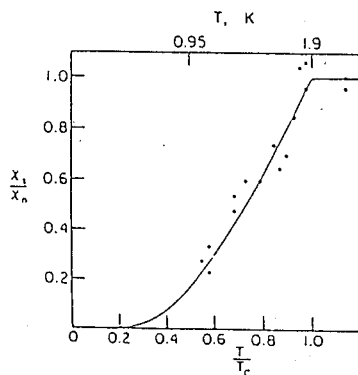
Figure 2.3.2 χ_s/χ_n vs T/T_c plot of aluminum [15].The solid curve is calculated by using eq.(2.29) [13].

(3)Nuclear spin-lattice relaxation rate $1/T_1$

Nuclear spin-lattice relaxation in the superconducting state is caused by the scattering of the normal electrons excited above the superconducting energy gap [12]. $1/T_1$ in the BCS state is expressed as

$$\frac{1}{T_1} = \frac{2\pi}{\hbar} A^2 \int_0^\infty \left\{ N_s(E)^2 + M_s(E)^2 \right\} \left(-\frac{\partial f}{\partial E} \right) dE, \tag{2.31}$$

where $N_s = N_{BCS}$, M_s is the so called "**the anomalous density of states**" related to the coherence effect. M_s is given by

$$M_s(E) = \begin{cases} \dfrac{N_0 \Delta}{\sqrt{E^2 - \Delta^2}} & E \geq \Delta \\ 0 & E \leq \Delta. \end{cases} \tag{2.32}$$

Thus just below T_c, $1/T_1$ shows anomalous enhancement the so called "**Hebel-Slichter peak**" or "**coherence peak**" originated not only from the divergence of N_s at the gap edge,

Δ, but also from the anomalous density of states M_s [14]. This effect is weakened by the life time broadening of the quasiparticle states and/or the dumping effect due to the electron-phonon coupling. In the temperature region of $T \ll T_c$, $1/T_1$ decreases exponentially with decreasing temperature as

$$\frac{1}{T_1} \sim e^{-\frac{\Delta}{k_B T}}, \tag{2.33}$$

reflecting the isotropic opening of the excitation gap. In Fig.2.3.3, we show the results of $1/T_1$ on aluminum [16].
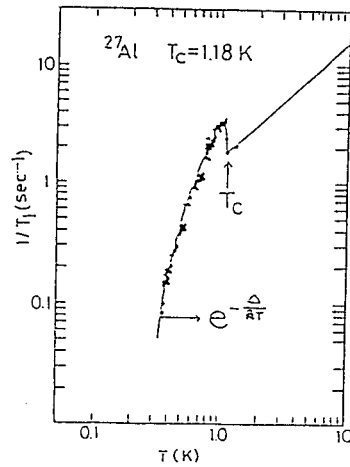
Figure 2.3.3 Temperature dependence of $1/T_1$ of aluminum [16]. The solid curve is calculated by using the density of states on BCS model with taking appropriate anisotropy into account.

2.3.2 NMR in Anisotropic Superconducting State

(1) Extended BCS theory

The electron-phonon coupling may not be the only possible mechanism to obtain an attractive interaction. Other interactions (spin fluctuation, charge fluctuation, etc.) could be an origin of the anisotropic pairing [19]. A good example is the superfulid of ^{3}He where the triplet p-wave pairing is realized through the agency of the paramagnon spin fluctuation [19, 20].

Since the pairing potential need not be spatially isotropic in general, the pairing potential in non-BCS superconductivity may have the anisotropic pairing wave function in $\vec{k}$-space.

Namely, the extended Hamiltonian from the BCS theory is generally expressed as [19, 20, 22]

$$\mathcal{H}_{non-BCS} = \sum_{\vec{k},\sigma} \xi_{\vec{k}} a^\dagger_{\vec{k},\sigma} a_{\vec{k},\sigma} + \frac{1}{2} \sum_{k,k',q} \sum_{\sigma_1,\sigma_2,\sigma_3,\sigma_4} V_{\sigma_1,\sigma_2,\sigma_3,\sigma_4}(\vec{k},\vec{k}') a^\dagger_{\frac{q}{2}-\vec{k},\sigma_1} a^\dagger_{\frac{q}{2}+\vec{k},\sigma_2} a_{\frac{q}{2}+\vec{k}',\sigma_3} a_{\frac{q}{2}-\vec{k}',\sigma_4},$$

(2.34)

and

$$V_{\sigma_1,\sigma_2,\sigma_3,\sigma_4}(\vec{k},\vec{k}') \equiv \left\langle -\vec{k},\sigma_1; \vec{k},\sigma_2 \left| \hat{V} \right| -\vec{k}',\sigma_4; \vec{k}',\sigma_3 \right\rangle,$$

(2.35)

where $\xi_{\vec{k}}$ is the band energy referred to μ. The operator $\hat{V}$ is a general effective electron-electron interaction which is attractive in a small range near the Fermi level. In the presence of this attractive interaction, the degenerated Fermi gas is unstable against falling into a superconducting state. By means of the mean field approach, the superconducting order parameter is expressed as

$$\Delta_{\sigma_1,\sigma_2}(\vec{k}) = - \sum_{\vec{k}',\sigma_3,\sigma_4} V_{\sigma_2,\sigma_1,\sigma_3,\sigma_4}(\vec{k},\vec{k}') \left\langle a_{\vec{k}',\sigma_3} a_{-\vec{k}',\sigma_4} \right\rangle,$$

$$\Delta^*_{\sigma_1,\sigma_2}(\vec{k}) = - \sum_{\vec{k}',\sigma_3,\sigma_4} V_{\sigma_4,\sigma_3,\sigma_1,\sigma_2}(\vec{k}',\vec{k}) \left\langle a^\dagger_{-\vec{k}',\sigma_4} a^\dagger_{\vec{k}',\sigma_3} \right\rangle.$$

(2.36)

From eqs.(2.34) and (2.36), and by taking the Bogoliubov transformation, the OP is rewritten by following two cases because the OP is restricted by the antisymmetric nature of a fermion wave function. For an even function for $\vec{k}$, the OP, $\hat{\Delta}(\vec{k})$, has to be antiparalell spin pairs (singlet nature of the Cooper pairing), therefore, $\hat{\Delta}(\vec{k})$ can be described by a single even function, $\hat{\Delta}(\vec{k}) = \Psi(\vec{k}) i\sigma_y$. While for an odd parity function of $\vec{k}$, since the OP has to be an parallel spin pairs (triplet nature of the Cooper pairing), therefore, the OP can be described by, $\hat{\Delta}(\vec{k}) = \left(\vec{d}(\vec{k}) \cdot \vec{\sigma} \right) i\sigma_y$, by using an odd vector function $\vec{d}(\vec{k})$ because the total spin "$S = 1$" behaves as vector under the symmetry transformation in the spin-$\frac{1}{2}$ space, as mentioned later. Then the OP's are expressed as

$$\hat{\Delta}(\vec{k}) = \begin{cases} \Psi(\vec{k}) i\sigma_y & \text{(singlet : } l = \text{even)} \\ \left(\vec{d}(\vec{k}) \cdot \vec{\sigma} \right) i\sigma_y & \text{(triplet : } l = \text{odd).} \end{cases}$$

(2.37)

We should note that the OP, $\hat{\Delta}(\vec{k})$, has the symmetry of a paring wave function in $\vec{k}$-space, differently from that in the BCS state.

The energy eigenvalue of quasiparticles in superconducting state is obtained as $\pm\varepsilon_{\vec{k}}$, where

$$\varepsilon_{\vec{k}} = \begin{cases} \pm\sqrt{\xi_k^2 + \left|\Psi(\vec{k})\right|^2} & (l = \text{even}), \\ \pm\sqrt{\xi_k^2 + \vec{d}(\vec{k}) \cdot \vec{d}^*(\vec{k}) \pm \left|\vec{d}(\vec{k}) \times \vec{d}^*(\vec{k})\right|} & (l = \text{odd}). \end{cases} \tag{2.38}$$

For $l =$ odd, it is called "*unitary*" ("*nonunitary*") if the $\left|\vec{d}(\vec{k}) \times \vec{d}^*(\vec{k})\right| = 0 (\neq 0)$. Therefore the density of states is

$$\begin{aligned} N_s(E) &= \sum_{\vec{k}} \delta(\varepsilon_{\vec{k}} - E) \\ &\sim \frac{N_0 |E|}{\sqrt{E^2 - \left|\Delta(\vec{k})\right|^2}}, \end{aligned} \tag{2.39}$$

where $\left|\Delta(\vec{k})\right|$ is the eigenvalue of $\left|\hat{\Delta}^\dagger(\vec{k})\hat{\Delta}(\vec{k})\right|$. Since the OP has $\vec{k}$ dependence, it can vanish for some directions *e.g.*, at points and/or lines on the Fermi surface. Namely, in the energy region far below gap edge Δ_0, the density of states with an anisotropic energy gap is expressed as

$$N_s(E) \propto \begin{cases} E & \text{line zeros} \\ E^2 & \text{point zeros}, \end{cases} \tag{2.40}$$

It is noted that there appear easily a finite (residual) density of states near the Fermi level (gapless state) in the case of resonant impurity scattering as discussed by Schmitt-Rink *et al.* [35]. Together with the case for the gapless state, eq.(2.40) is given as,

$$N_s(E) \propto \begin{cases} N_{res} & \text{gapless} \\ E & \text{line zeros} \\ E^2 & \text{point zeros}, \end{cases} \tag{2.41}$$

We did not refer to the detailed form of the OP in above treatments. Generally, in order to find the spatial symmetry of $\hat{\Delta}(\vec{k})$ we need the precise form of the pairing potential $\hat{V}$. A form of $\hat{\Delta}(\vec{k})$, however, can be obtained even without a detailed knowledge of $\hat{V}$ [21, 22]. Namely, the form of an OP can be found by using group theoretical argument which is the treatment based on the definition that, in the Bose condensation, there is only one function which should be transformed into itself under symmetry transformations that do not change the superconducting state. In the crystal symmetry, a possible OP which describes the superconducting state must be invariant under symmetry transformations for the crystal point group G of the crystal lattice symmetry, the spin rotation symmetry

group $SU(2)$, the time-reversal symmetry group R and the gauge symmetry group $U(1)$ as follows [21, 22],

$$\mathcal{G} = G \times SU(2) \times R \times U(1). \tag{2.42}$$

Under the restriction of eq.(2.42), we can find possible OP's, by referring to the crystal symmetry even when we do not have a detailed knowledge of $\hat{V}$.

(2) Knight shift

(a) Even parity

In the superconducting state as the same as BCS type, the spin susceptibility χ_s is expressed as

$$\chi_s = -4\mu_B^2 \int_0^\infty N_s(E)\frac{df}{dE}dE, \tag{2.43}$$

because the singlet pairs dose not contribute to χ_s. According to eqs.(2.39)−(2.41), χ_s far below T_c is expected as follows,

$$\chi_s \propto \begin{cases} \chi_{res}(const.) & \text{gapless} \\ T & \text{line zeros} \\ T^2 & \text{point zeros} \end{cases} \tag{2.44}$$

(b) Odd parity

Differently from the even parity pairing, the case of an odd parity paring must have a pair of $S = 1$ (triplet spin pairing) because the wave function of a Fermion system must be antisymmetric under the interchange of any two particles. In case of the equal spin pairing, since the population of the spin-up and spin-down remains even at $T = 0$ K[19, 20], therefore, the spin susceptibility χ_s is essentially the same as that of the normal state, regardless of crystal directions, unless the OP is locked to a certain crystal axis [23]. In the BW (Balian-Werthamer) state [20] where the Cooper pairs are composed of $(\vec{k}\uparrow, -\vec{k}\uparrow), (\vec{k}\uparrow, -\vec{k}\downarrow)$ and $(\vec{k}\downarrow, -\vec{k}\downarrow)$, χ_s decreases to two third of the value at T_c.

(3) Nuclear spin-lattice relaxation rate $1/T_1$

Since the OP has $\vec{k}$-dependence, $1/T_1$ dose not always behave exponentially below T_c. In addition, the coherence effect is weakened or disappears owing to the gap anisotoropy and

/or the life time broadening of the quasiparticle states. Then eq.(2.31) is reduced as [17]

$$\frac{1}{T_1} = \frac{2\pi}{\hbar} A^2 \int_0^\infty N_s(E)^2 \left(-\frac{\partial f}{\partial E} \right) dE, \tag{2.45}$$

therefore, from eqs.(2.41) and (2.45) we have relations as follows,

$$\frac{1}{T_1} \propto \begin{cases} T & \text{gapless} \\ T^3 & \text{line zeros} \\ T^5 & \text{point zeros.} \end{cases} \tag{2.46}$$

In Figs.2.3.4-2.3.6, we show the typical behaviors of $N_s(E), \chi_s(T)$ and $1/T_1$ in the case of BCS state ($\Delta = \Delta_0$), the polar state ($\Delta = \Delta_0 \cos \theta$) and the axial ABM state ($\Delta = \Delta_0 \sin \theta$) [19]. For Knight shift, we assume the case of singlet pairing state.

(4) The case of the strong spin-orbit coupling

So far, we have treated the properties of anisotropic superconductivity under the weak or absence of the **spin-orbit coupling (SOC)**among the Cooper pairs in which the above treatments are valid. On the other hand, those are not valid under the strong **SOC** case.

Here, we remark on the **SOC** in the Cooper pairs [23, 21, 22, 24]. It is said that, in the heavy fermion systems, the spin-orbit coupling and the crystal field should be taken into account for discussing Cooper pair formation. This idea was introduced by Anderson as follows:

"First, as in the $^3P_2$ state of neutron matter, there is strong spin-orbit coupling and the spin and orbital variables **may not** *be freely rotated independently; second, there is an underlying crystal structure and hence, the orbital variables—and through them the spin—have only a discrete rotation symmetry."*
[*quoted from* Phys.Rev.**B30**,4000,(1984)].

In this case, the spins have to be considered as "**frozen**" with the lattice, namely, its fundamental assumption is that the spin rotation symmetry group $SU(2)$ is absorbed into the crystal point group G as follows [21, 22],

$$\mathcal{G}' = G' \times R \times U(1), \tag{2.47}$$

where G' is the point group involving the spin rotation symmetry group. This restriction is important on considering an odd parity pairing. The behavior of $\vec{d}$-vector under each lattice rotation element $\hat{A}$ from a point group G' of the system acts in the case of odd parity as follows [21, 22, 24]

$$\hat{A} \cdot \vec{d}_\alpha(k_i) = A_{\alpha\beta}\vec{d}_\beta(A_{ij}k_j). \tag{2.48}$$

Therefore, even for an odd-parity pairing, the spin susceptibility, $\chi_s(T)$, should decrease for $H \parallel \vec{d}$ by analogy with even-parity pairing because $\vec{d}$-vector is locked to a certain direction of the crystal lattice, namely, the spin labels can be no longer treated independently with a symmetry rotation.
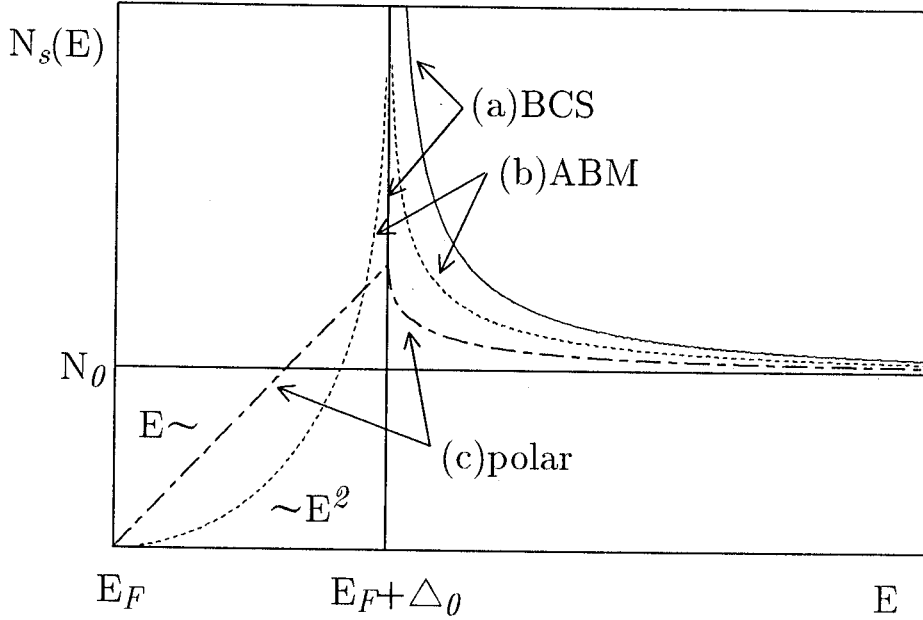
Figure 2.3.4 Density of states, $N_s(E)$, for (a) the BCS state ($\Delta = \Delta_0$), (b) the axial ABM state ($\Delta = \Delta_0 \sin\theta$) and (c) the polar state ($\Delta = \Delta_0 \cos\theta$).
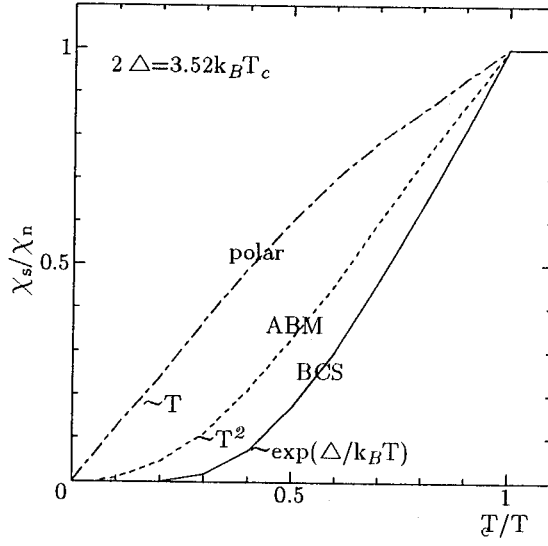
Figure 2.3.5 Temperature dependence of $\chi_s(T)/\chi_n$ for (a) the BCS state, (b) the axial ABM state and (c) the polar state, by using $2\Delta = 3.52 k_B T_c$.
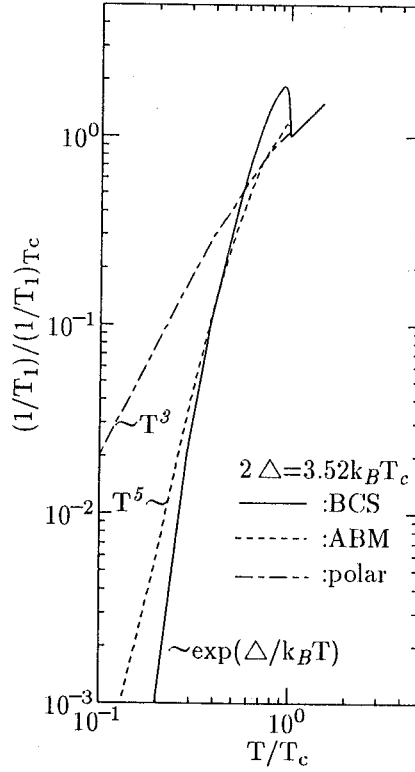
Figure 2.3.6 Temperature dependence of $(1/T_1)/(1/T_1)_{T_c}$ for (a) the BCS state, (b) the axial ABM state and (c) the polar state, with $2\Delta = 3.52 k_B T_c$ and with taking an appropriate damping effect into account.

33

3 Experimental Procedure

3.1 NMR Spectrometer

NMR and NQR measurements were carried out by the spin-echo method by using a conventional phase coherent type home-made spectrometer. NMR/NQR experiments have been performed by using either a monodyne type or a superheterodyne type receiver system. The block diagram of a superheterodyne type system is shown in Fig.3.1.1.

The NMR spectrum was obtained at fixed frequency by either tracing the spin-echo intensity as a function of external field or the Fourier-transform (FT) technique of the spin-echo signal. The NQR spectrum was obtained in the zero magnetic field by measuring the spin-echo intensity as a function of frequency or the FT technique of the spin-echo signals. Since the magnitude of the exciting rf field is about 50~150 Oe, the FT technique was utilized for the spectrum whose line width is narrower than 50 kHz (or 50 Oe for the gyromagnetic ratio $\gamma_N \sim 1$ MHz/T). Nuclear spin-lattice relaxation time T_1 was measured by the saturation recovery method.

Figure 3.1.1 NMR block diagram.

3.2 Magnet and Cryostat

The NMR experiments in the high temperature region above 1.3 K were performed by using a Helmholtz type magnet ($\sim$2 T). Below 1.3 K, the solenoid type superconducting magnet (2 T and 9 T) were used to generate magnetic field up to 1.8 T.

The NMR measurements were performed in the temperature range of 0.028–300 K. Above 4.2 K the sample was settled in the vaporized helium. The temperature was controlled by heat-balance between heating and cooling and was monitored by a thermocouple and a carbon glass resister.In the temperature range of 4.2–1.3 K, the sample was put in the evacuated liquid helium. The temperature was controlled by the pressure balance. Below 1.3 K, a ^{3}He refrigerator and an Oxford ^{3}He-^{4}He dilution refrigerator were used. The sample was immersed directly in ^{3}He liquid or ^{3}He-^{4}He mixture. Temperature was measured by using RuO_2 carbon resistor which was calibrated by measurement of T_1 of the high quality platinum powder which is known as $T_1 T$ =30 msecK.

In Figs.3.2.1–3.2.3, we show sketches of ^{4}He, ^{3}He cryostats and ^{3}He-^{4}He dilution refrigerator.

to ^{4}He recovery

heater for warm up

sample

heater for cooling

thermocouple

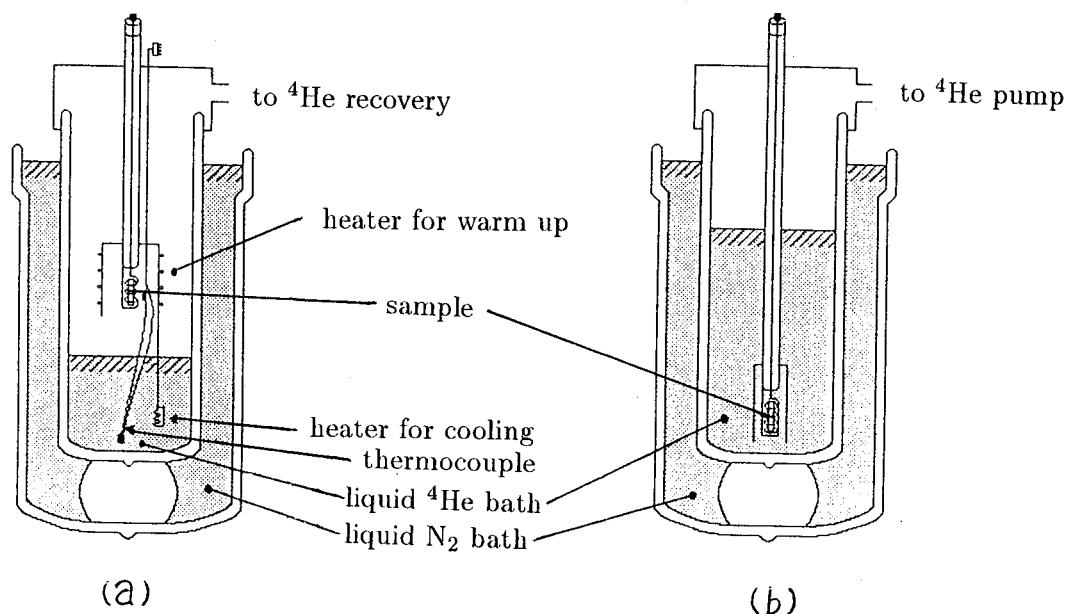liquid ^{4}He bath

liquid N_2 bath

to ^{4}He pump

(a)

(b)

Figure 3.2.1 ^{4}He cryostat for the temperature range of (a)$300\geq T \geq$4.2 K and (b)$4.2 \geq T \geq$1.3 K.
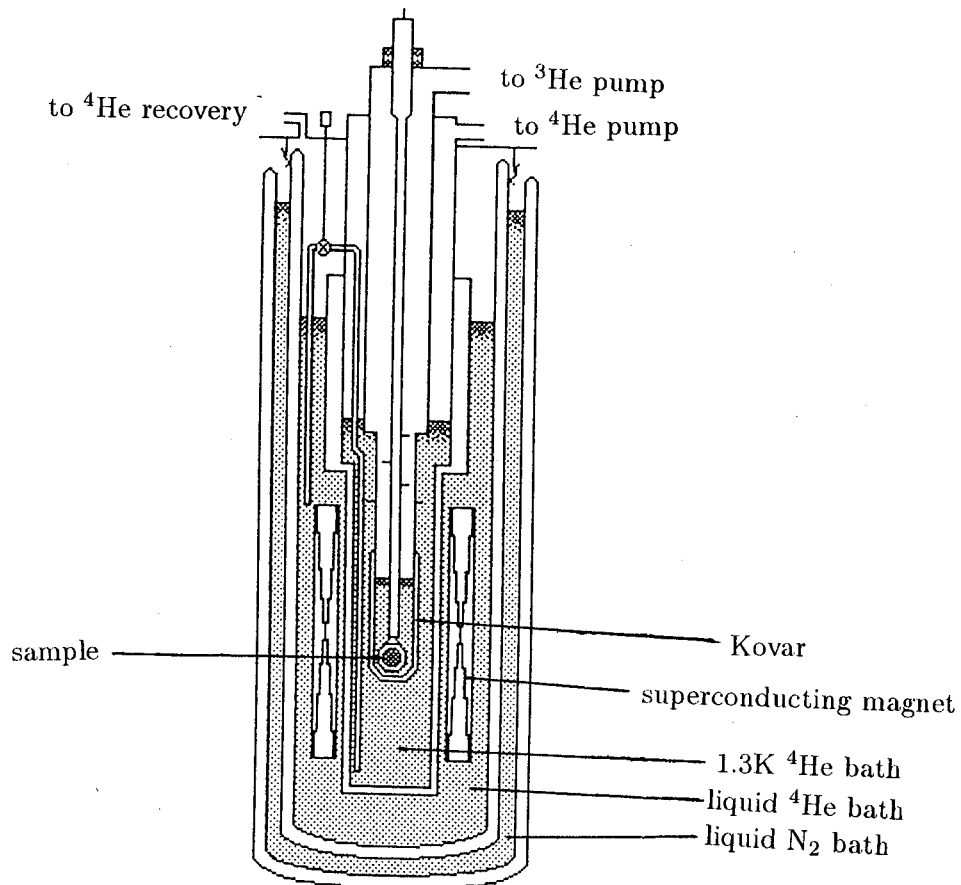
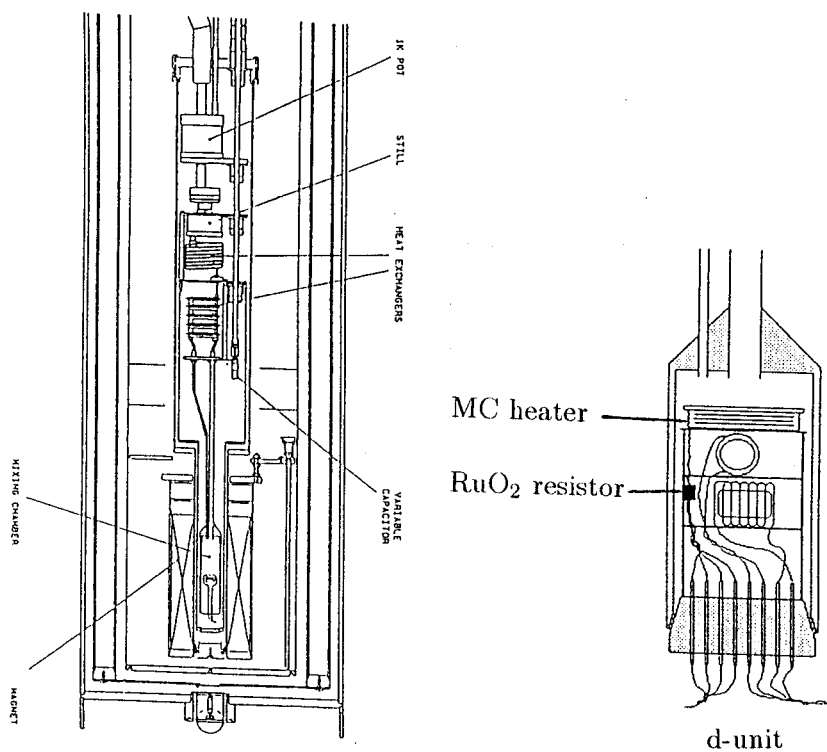Figure 3.2.2 ^{3}He cryostat for the temperature range of $1.3 \geq T \geq 0.35$ K.

Figure 3.2.3 ^{3}He-^{4}He dilution refrigerator for the temperature range of $1-0.028$ K.

3.3 Samples

3.3.1 UPd$_2$Al$_3$

The polycrystalline sample of UPd$_2$Al$_3$ was prepared by the group at Institute für Festkorperohysik, Technishe Hochschule, Darmstadt. The sample preparation and the characterizations are according to their report [6].

Polycrystalline UPd$_2$Al$_3$ was prepared by melting appropriate amounts of U, Pd and Al together in arc furnace under Ar atmosphere. In order to get rid of a few percent of secondary phases in as-cast samples, the samples were annealed at 900°C for 120hrs. X-ray powder diffractometry on annealed samples shows the single phase of hexagonal PrNi$_2$Al$_3$ structure. The specimen for the NMR measurement was cut from a ingot wich was diffrent from the ingot used for the specific heat measurement performed by Caspary et $al.$ [27]. The specimen was crushed into the powder with small grain size of 70μm.

^{27}Al-NQR experiment was carried out in the temperature range of 0.13-150 K. The NQR spectrum for ($\pm 3/2 \Leftrightarrow \pm 5/2$) transition was obtained by the Fourier-transform (FT) technique of the spin-echo. T_1 was measured by the saturation recovery method. The lowest temperature at which the measurements can be carried out was limited down to 0.13K because of an extremely long T_1 at low temperatures ($T_1 \sim 90$min. at 0.13K).

3.3.2 UPt$_3$

The single crystalline samples of UPt$_3$ were prepared by the group at Department of Physics, Faculty of Science, Osaka University. The sample preparation and the characterizations are according to their report [68].

The single crystalline UPt$_3$ was grown under Ar gas atmosphere by the Czochralski pulling method in a tetra-arc furnace, by using 99.95 % pure U and 99.999 % pure Pt as the starting materials. Subsequently, the sample was heated by a DC current flow with a density of 1000 A/m^2 through the single crystal rod and kept at 1200°C for 6 days in vacuum of 8×10^{-10} torr. After that the crystal was gradually cooled down to the room temperature for 10 days.

The double peak structures in the zero field specific heat experiment due to different

37

superconducting phase transitions are clearly observed as shown in Fig.3.3.1. The electronic specific heat coefficient and the two superconducting transition temperatures are obtained as $\gamma \sim 420$ mJ/moleK^2, $T_{c1} \sim 0.58$ K and $T_{c2} \sim 0.53$ K, respectively. The $H - T$ phase diagram is also shown in Fig.3.3.2. Both the residual resistivity ratio of $RRR \sim 510$ (Fig.3.3.3) and the transport mean free path of $l_{tr} \gg 2000$ Å expected from the dHvA experiments assure that the sample quality is sufficiently good.
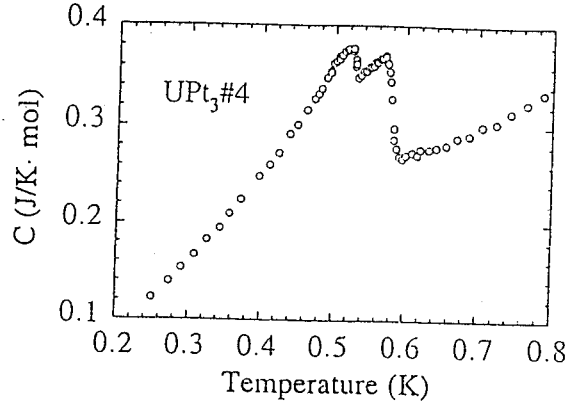

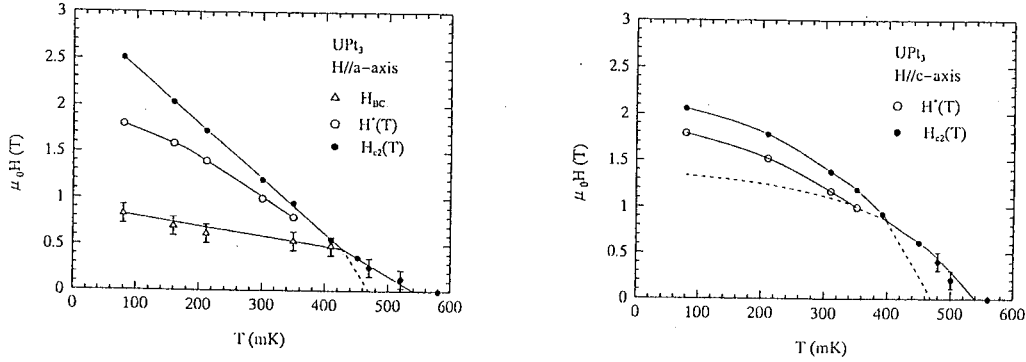Figure 3.3.1 Temperature dependence of specific heat [68].

Figure 3.3.2 $H - T$ phase diagram measured by Sakakibara *et al.* [69].

Two single-crystalline samples, whose typical dimensions of $2 \times 2 \times 5$ mm^3 and $1 \times 1 \times 4$ mm^3 with their length parallel to the hexagonal [0001] and [10$\bar{1}$0] axes, respectively, were prepared for NMR measurements. NMR spectrum was obtained at fixed frequency by using FT technique of spin echo signal.

The samples with powder form are usually utilized in NMR measurements in order to make the NMR signal intensity as strongly as possible because it depends on the number of
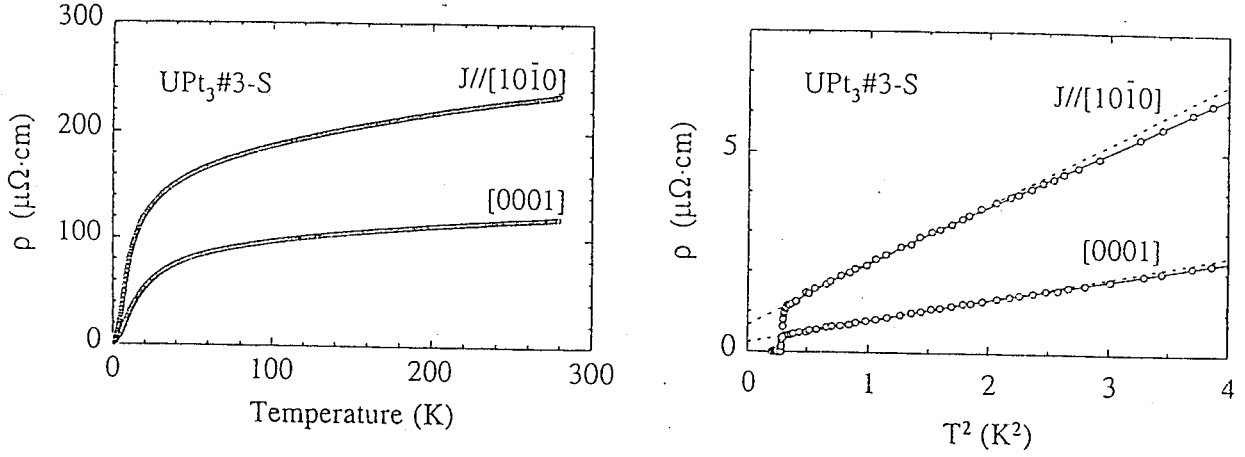
Figure 3.3.3 (a) Resistivity versus temperature and (b) that versus temperature squared for single crystal UPt₃[68].

nuclei, that is, the NMR signal comes from the nuclei in the surface region of each grain in the powder sample. On the other hand, the NMR measurements in single crystal metallic specimens are difficult for several reasons. For the single crystal UPt₃ whose skin depth is estimated as less than $\sim 2\mu m$, the signal comes only from the surface region of the bulk form and is therefore weak in comparison with that for the powder form. In addition, the effect of heating up of a sample due to eddy-current loss caused by exciting *rf* field and the spurious ringing due to excitation of *rf* acoustic modes in the static magnetic field usually disturb us to extract NMR signal. The improvement of the shape of *rf*-coil, the phase alteration technique for the 1*st* and 2*nd* *rf*-pulse sequence and, at the same time. the signal averager have made possible to remove the acoustic spurious ringing after *rf*-pulses and to improve the signal to noise ratio, *e.g.*, $S/N \sim 4$ at 4.2 K. Below 100 mK, the repetition time of the exciting *rf*-pulse sequence was increased more than at least ten minutes in order to avoid the heating up of the sample.

3.3.3   CePd₂Al₃

Polycrystalline samples of CePd₂Al₃ were prepared at Leiden University by arc-melting appropriate amounts of pure elements (Ce:4N; Pd:5N; Al:6N) in argon atmosphere under continuous titanium gettering. Subsequently, one of the samples was annealed at 800 °C for one week in quartz ampules, filled with high purity argon gas [74]. A single crystalline sample of CePd₂Al₃ was grown at the FOM-ALMOS facility at the University of Ams-

terdam with the "tri-arc" Czochralski method, using the pure elements with 2%-excess of aluminum [78]. Hereafter, annealed polycrystalline , as-cast polycrystalline and single crystalline samples are denoted as PC1, PC2 and SC1, respectively. All the samples were analyzed by Debye-Scherrer X-ray analysis and electron probe microanalysis (EPMA) in Leiden and showed the ideal $PrNi_2Al_3$ structure. Metallurgical and structural characterizations of the various samples are shown in Table 2. The single crystal contains approximately 3 at.% less aluminum than the polycrystals.

As shown in Figs.1.4.1 and 1.4.3, antiferromagnetic ordering temperature, T_N, was found for the annealed sample (PC1) by susceptibility and specific heat experiments which reveal a mean field type maximum and a λ—like peak at 2.7 K, respectively [74]. By contrast, the as-cast (PC2) and the single crystalline (SC1) samples did not exhibit those anomalies at 2.7 K, though specific heat for PC2 showed spin-glass like behavior below 2.7 K (see Figs.1.4.1–1.4.4) [74, 78]. Since the entropy released at 2.7 K is roughly equivalent for both PC1 and PC2, some static magnetic correlation is expected to develop below T_N even for PC2 [74, 79]. The samples were crushed into the powder with smaller grain size of

	Composition	lattice parameter($\mathring{A}$)	T_N
PC1	$Ce_{0.97}Pd_{2.02}Al_{3.01}$	a=5.470 c=4.216	2.7
PC2	$Ce_{0.98}Pd_{1.94}Al_{3.09}$	a=5.477 c=4.222	—
SC1	$Ce_{1.06}Pd_{1.99}Al_{2.96}$	a=5.469 c=4.214	—

Table 2 Metallurgical and structural characterizations of annealed poly- (PC1), as-cast poly- (PC2) and single-crystalline (SC1) $CePd2Al_3$.

$\sim 70\mu$m for NMR and NQR experiments. The NMR spectrum was obtained by tracing the spin echo intensity as a function of external magnetic field at a fixed frequency. The NQR spectrum was obtained by measuring the spin-echo intensity as a function of frequency in the zero magnetic field.

4 NMR Studies of UPd$_2$Al$_3$

4.1 Experimental Results

4.1.1 ^{27}Al NQR Spectra

Figure 4.1.1 shows ^{27}Al NQR spectra for the ($\pm 3/2 \Leftrightarrow \pm 5/2$) transition of ^{27}Al nuclei ($I = 5/2$) at (a) 16.5 and (b) 4.2 K, respectively. The full width at half maximum (FWHM) of ^{27}Al spectrum is very narrow of 12 kHz, assuring the sufficiently good quality of the sample from a microscopic level. No evidence for the incommensurate phase in the temperature range of 14.5K$\leq$ T $\leq$20K above T_N was observed.
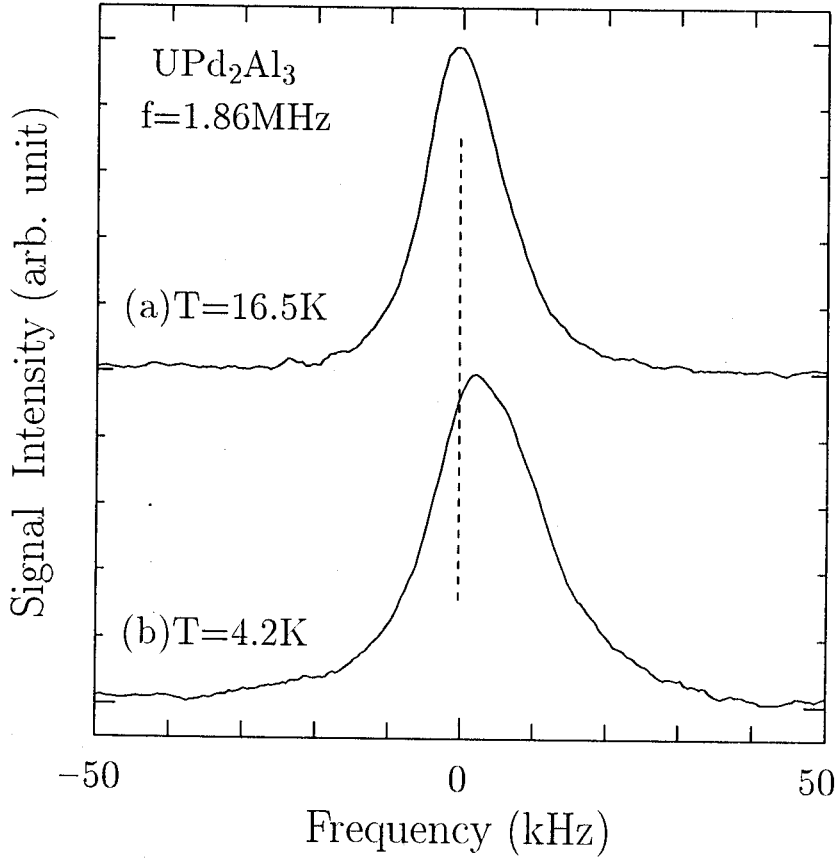

Figure 4.1.1 ^{27}Al NQR spectra for the ($\pm 3/2 \Leftrightarrow \pm 5/2$) transition of ^{27}Al nuclei at (a) 16.5 and (b) 4.2 K, respectively.

Upon cooling, slight shifts of the resonance frequency are observed below T_N =14.5 K, meaning the slight change of EFG at Al-site. Also FWHM increases abruptly from 12 kHz to 18 kHz at T_N =14.5 K as seen in Fig.4.1.2. The hyperfine broadening at the Al site is about 4 Oe. If the Al site is ideally located at the magnetically symmetric site in such

a spin structure that the ferromagnetic basal plane is antiferromagnetically stacked along the c-axis, the hyperfine broadening should not occur. However, a lattice imperfection or a slight displacement of Al atoms from the ideal position, which might prevent a perfect cancellation of the hyperfine field as discussed in Chapter 6 on $CePd_2Al_3$, may be the cause for the observed hyperfine broadening from 12 to 18 kHz. Differently from the case for $CePd_2Al_3$ where the Al NQR spectrum is asymmetrically broadened with a satellite peak at low frequency side, the symmetric broadening of the Al NQR spectrum in UPd_2Al_3 may be the case of a lattice imperfection and/or a deviation of the Al site from the ideal magnetically symmetric position, which are considered to be much smaller than those in $CePd_2Al_3$. From the fact that the FWHM does not change in the superconducting state at all, it is deduced that the onset of the superconductivity does not disturb the **AF** ordered state.
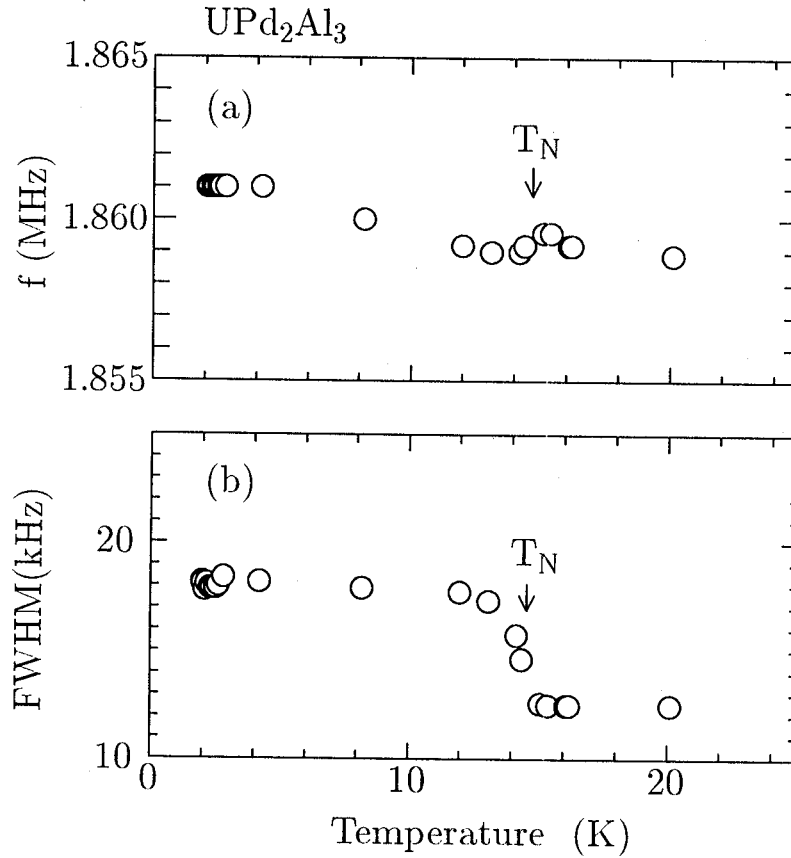

Figure 4.1.2 Temperature dependence of FWHM of ^{27}Al NQR spectra for the ($\pm 3/2 \Leftrightarrow \pm 5/2$) transition.

4.1.2 Nuclear Spin-lattice Relaxation Rate, $1/T_1$

In Figs4.1.3, we show the nuclear relaxation behavior at various temperatures. The nuclear relaxation for NQR transition of $(\pm 3/2 \leftrightarrow \pm 5/3)$ is given by

$$m(t) = \frac{M(\infty) - M(t)}{M(\infty)} = \frac{3}{7}\exp(-\frac{3t}{T_1}) + \frac{4}{7}\exp(-\frac{10t}{T_1}), \tag{4.1}$$

where $M(\infty)$ and $M(t)$ are the nuclear magnetization in the thermal equilibrium and at a time t after saturating pulses, respectively. The solid lines in figures are calculated by the least square fitting. As shown in the figures, T_1 can be determined uniquely above 0.2 K, independently of the **AF** and the **SC** transitions. On the other hand in the low temperature region below $T = 0.2$ K (see Fig.4.1.3(i)), the nuclear relaxation does not have unique solution on fitting to eq.(4.1) because of either the effect of heating up due to eddy-current losses caused by exciting *rf* field or a presence of only a few impurities which is responsible for the distribution of nuclear relaxation at low temperatures as discussed in Chapter 6. Therefore there remains an ambiguity in determining T_1 below $T = 0.2$K.
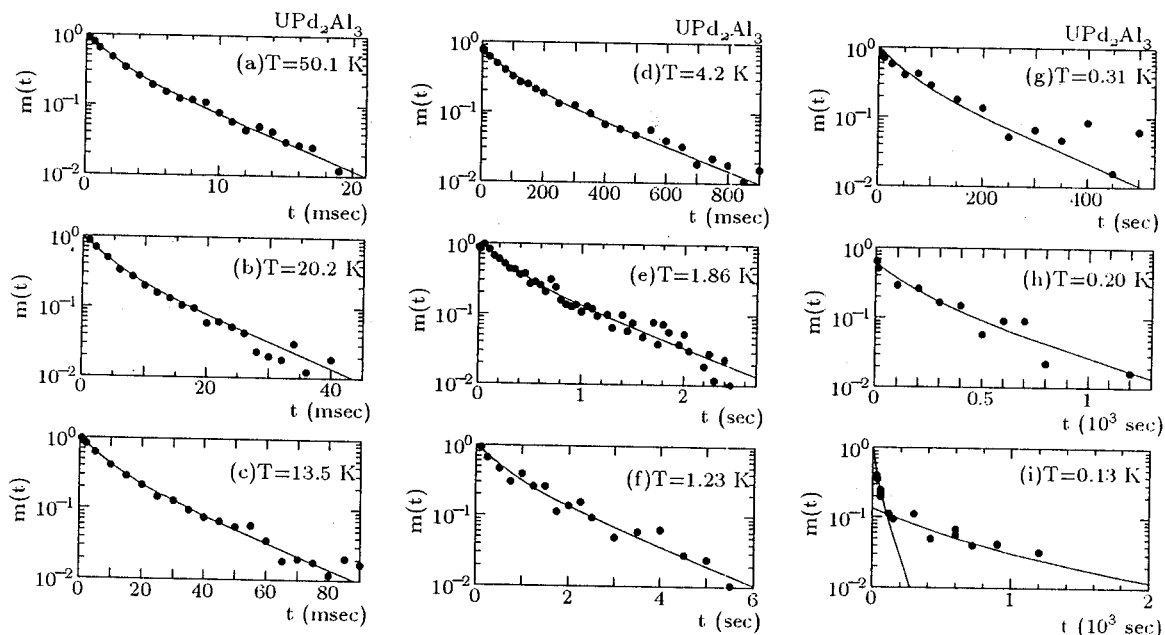

Figure 4.1.3 Relaxation curve of the nuclear magnetization of ^{27}Al NQR for the $(\pm 3/2 \Leftrightarrow \pm 5/2)$ transition at (a) 50.1, (b) 20.2, (c) 13.5 (just below T_N), (d) 4.2, (e) 1.86 (just below T_c), (f) 1.23 K, (g) 0.31, (h) 0.20 and (i) 0.13 K. An appreciable distribution of T_1 appears below 0.2K.

Figure 4.1.4 shows the temperature dependence of $^{27}(1/T_1)$ measured in **zero-field**, where T_1 is deduced from a fitting to above formula. The Néel temperature, T_N, and

the superconducting transition temperature, T_c, were also confirmed as 14.5 and 1.98 K, respectively, from each distinct kink in the temperature dependence of $^{27}(1/T_1)$ as seen in the figure. The relaxation behavior above 0.6 K is almost the same as the previous results measured in the magnetic field by the NMR technique [31, 32]. Above 80K, $^{27}(1/T_1) = const.$ behavior is observed as seen in Fig.4.1.4, which is commonly observed in the HF system at high temperatures where the magnetic susceptibility obeys the Curie-Weiss law, corresponding to the localized moment regime of $5f$-quasiparticles. When the magnetic susceptibility obeys Curie-Weiss law in the high temperature region and its wave number dependence is neglected, from eq.(2.21) we have following relation of T_1,

$$\frac{1}{T_1} \sim 2\gamma_N^2 k_B T A_{hf}^2 \chi(q = 0)\tau(T), \tag{4.2}$$

assuming a Lorentzian frequency spectrum for spin correlation time as

$$\frac{\chi''(q,\omega_n)}{\omega} = \chi(q)\frac{\Gamma(q)}{\Gamma(q)^2 + \omega^2}. \tag{4.3}$$

Here γ_N is the nuclear gyromagnetic ratio, A_{hf} is the transferred hyperfine field from $5f$-local moment and $\chi(q) \sim \chi(0)$ and $\Gamma(q) \sim 1/\tau(T)$. Since $\chi(q = 0) = \frac{c}{T+\theta}$, the temperature dependence of $1/T_1$ should be associated only with a correlation time $\tau(T)$. If the temperature dependence of τ is governed by the inter-site interaction among f-electrons, i.e., $\tau(T) \sim const.$, $1/T_1$ does not depend on temperature. Thus, at the high temperature region, it is considered that the temperature dependence of $1/T_1$ is determined by the exchange interaction among the f-electrons having localized character.

Upon cooling, $^{27}(1/T_1)$ is proportional to the temperature between $T_N = 14.5$ and 30 K as displayed in Fig.4.1.5, revealing a crossover to the Fermi-liquid state. Below T_N, $1/T_1$ drops rapidly without the critical fluctuation near the ordering temperature and becomes to be proportional to the temperature range of 5 to $T_c = 2$ K. Below T_N, $1/T_1$ is fitted by a simple form of

$$\frac{1}{T_1 T} = A + B\exp\left(-\frac{E_g}{k_B T}\right). \tag{4.4}$$

The first term is due to the Fermi-liquid excitation of itinerant quasiparticles near the Fermi level, which continues to be valid in the field-induced normal state where the superconductivity is suppressed by the magnetic field [31]. The second one should be related to
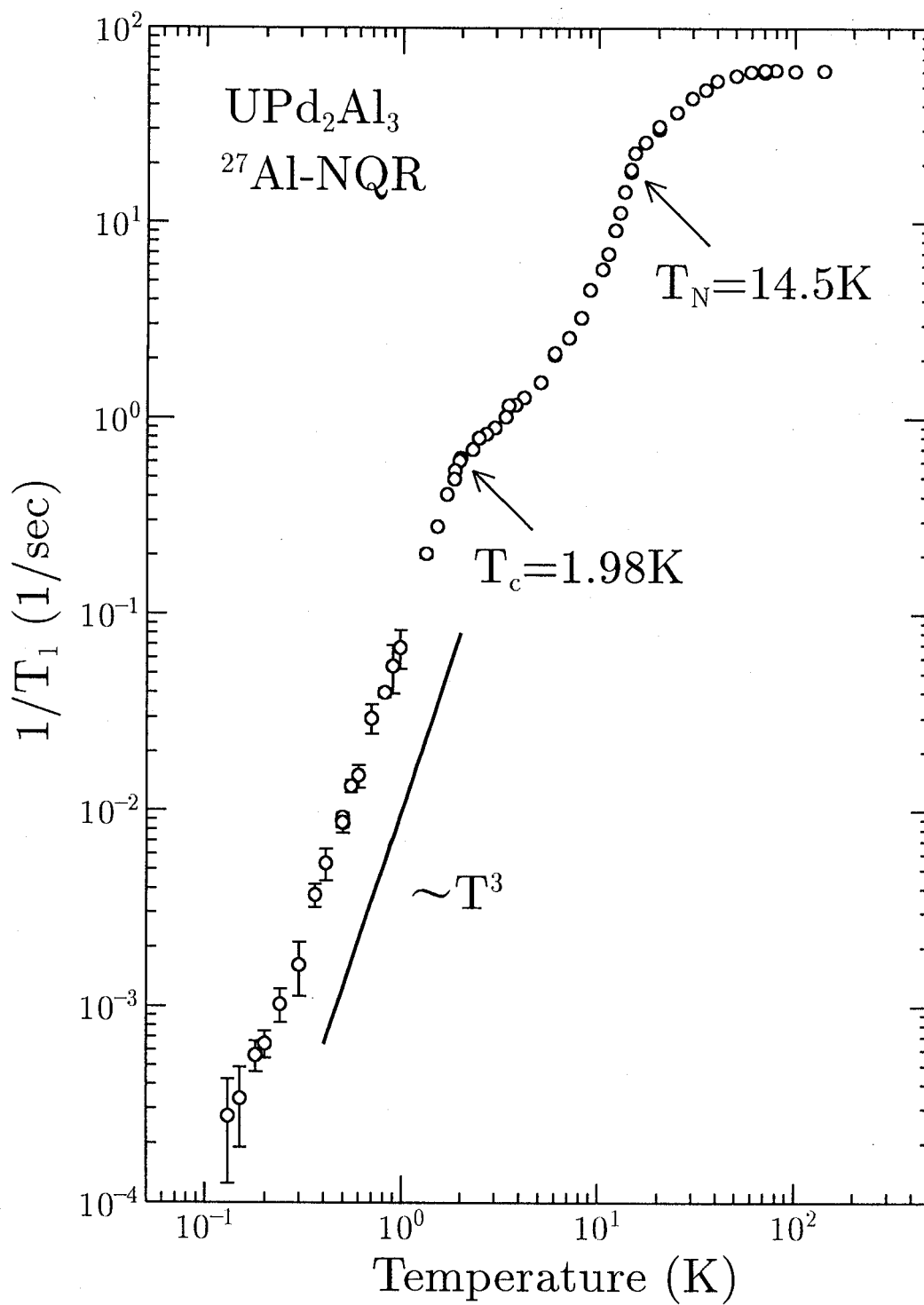
44

Figure 4.1.4 Temperature dependence of $^{27}(1/T_1)$ measured in zero external field.

a partial loss of the density of states due to an opening of the energy gap below T_N and/or a holding of the Fermi surface caused by the formation of the magnetic unit cell. In this temperature range, the specific-heat well below T_N was decomposed into two contributions of T linear and T^3 contributions as $C_{AF}(T)/T = \gamma_0 + \beta T^2$. Whereas the former is compatible with the $T_1T=$const. law observed in the temperature range of 6–2 K, the latter is claimed to be dominated by a spin-wave or magnon contribution [27, 81]. Differently from the specific heat results, the relaxation process far below T_N is not dominated by low-lying spin excitations from the **AF** ordered state, but only by a Fermi liquid excitation of quasiparticles near the Fermi level, since the fluctuating hyperfine fields from adjacent uranium planes are filtered away at Al site because of the magnetically symmetric form factor.
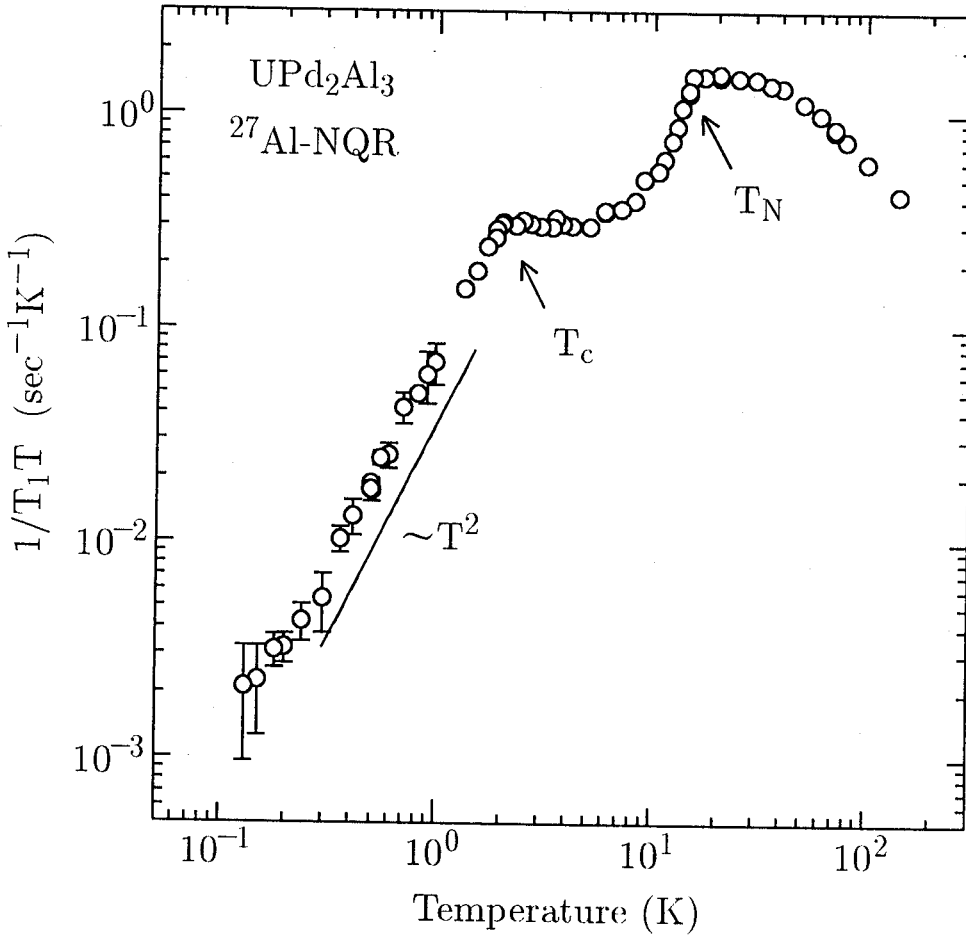

Figure 4.1.5 Temperature dependence of $^{27}(1/T_1T)$. The $T_1T = const.$ relation appears in the temperature range of 30–14.5 and 6–2 K.

In the superconducting state, $^{27}(1/T_1)$ does not show any coherence peak reflecting the intrinsic feature of conventional BCS superconductors, but rather a steep reduction just below T_c. A most remarkable finding is that $^{27}(1/T_1)$ in **zero-field** obeys a T^3 law over three orders of magnitude at least down to 0.2 K as seen in Figs.4.1.4 and 4.1.5. This is the first case where the T^3 dependence of $1/T_1$ has been observed down to such low T as $0.09T_c$.

4.2 Analysis and Discussion

4.2.1 D-Wave Superconductivity in UPd$_2$Al$_3$

So far, many experimental efforts have clarified anisotropic natures of superconducting order parameter in UPd$_2$Al$_3$. Previous Knight shift studies have identified that the singlet pairing state is realized in UPd$_2$Al$_3$ [31, 33]. The identification of the topology of the superconducting energy gap and the interpretation for the large residual shifts, however, has not yet reached to a consensus.

In order to unravel these underlying issue, we discuss here the results of T_1 and Knight shift. First, we begin to discuss the results of the $1/T_1$.

In the superconducting state, since the quasiparticles condense into only one ground state (the Bose condensation), various thermodynamics are caused by the scattering of the normal quasiparticles excited above the superconducting energy gap. As mentioned in Chapter 2, the thermodynamics in the BCS superconductors exhibit exponential temperature dependence, reflecting the opening of the isotropic superconducting energy gap. On the other hand, the thermodynamics in the heavy fermion superconductors exhibit a power-law like temperature dependence, T^n, reflecting the anisotropic quasiparticle excitation gap. As shown in Fig.4.1.4, differently from the exponential temperature dependence in BCS superconductors, the T^3 law of $1/T_1$ in the low temperature range of $0.5T_c(1$ K$)-0.09T_c(0.18$ K) provides a strong evidence for the anisotropic superconductivity with lines of vanishing gap on the Fermi surface because the order parameter stays constantly below $0.5T_c$.

This is, however, inconsistent with the specific heat result which is compatible with the octagonal d-wave state characterized by eight zeros at points on the Fermi surface as described by $C(T)/T = \gamma_{res} + \alpha T^2$. According to the literature [27], the first term, $e.g.$,

47

the large residual electronic specific heat coefficient, γ_{res}=24 mJ/moleK^2, is ascribed to a gapless magnetic excitation inherent to the **AF** ordered state, while the second, $C(T) \propto T^3$ term is ascribed to the zeros gap on points at Fermi surface. It is noteworthy that the temperature dependence of $^{27}(1/T_1)$ below T_c is determined only by quasiparticle excitations in the superconducting state, since the fluctuating hyperfine fields from two adjacent uranium planes are filtered away at the Al-site because of the magnetically symmetric form factor. By contrast, the specific heat probes not only quasiparticle excitations but also all contributions from magnetic excitations in the **AF** ordered state which coexists with the superconductivity. In fact, the T linear term γ_{res}=24 mJ/mole·K^2 well below T_c was proposed to originate from a gapless magnetic excitation for the *5f-localized subsystem* [27]. Thus, the reason why the temperature dependence of the specific heat is not dominated by a T^2 behavior expected for lines of zero gap may be due to an extra contribution from magnetic excitations in the **AF** ordered state.

From other viewpoint, if the T linear term were associated with the residual quasiparticles density of states at the Fermi level induced by strong impurity scattering, a $T_1 T = const.$ law should appear at low T as well discussed in the high T_c cuprates [36]. Since $(1/T_1 T) \propto N(E_F)^2$ and $\gamma \propto N(E_F)$ in the Fermi liquid state as mentioned in Chapter 2 (eq.2.22), corresponding to γ_{res}=24 mJ/mole·K^2, $(T_1 T)_{res}^{-1}$ is obtained to be 8.06×10^{-3} (sec·K)$^{-1}$ from a relation of

$$\frac{(T_1 T)_{res}^{-1}}{(T_1 T)_0^{-1}} = (\frac{\gamma_{res}}{\gamma_0})^2, \tag{4.5}$$

where γ_0=150 mJ/(mole·K^2) and $(T_1 T)_0^{-1}$=0.315 (sec·K)$^{-1}$ are the values in the Fermi liquid state far below T_N. As mentioned previously, we cannot decide clearly whether or not $1/T_1$ obeys T^3 below 0.2K because of the appreciable distribution of nuclear relaxation curve. If such distributions are ascribed to the residual density of states due to impurity scattering, we can estimate residual electronic specific heat coefficient as $\gamma_{res} \sim$ 14mJ/moleK^2 in case that $T_1 T = const.$ relation is assumed below 0.2 K. This value is, however, about a half of the specific heat result, γ_{res} =24mJ/moleK^2. In addition, if such a residual density of states is inherent in UPd$_2$Al$_3$, the relaxation curve below 0.2 K should obey the relation of eq.(4.1) without any distribution. Therefore, it is considered that the results of $^{27}(1/T_1)$ exclude the presence of such a large residual density of states

at the Fermi level below T_c, as drawn by a dashed line in Fig.4.2.1.

Kohori et $al.$[34] have actually reported such a T_1T=const. behavior on UPd$_2$Al$_3$ with lower T_c=1.75 K and larger FWHM=20 kHz than T_c=1.98 K and FWHM=12 kHz of our sample. Their $1/T_1$ data at low temperature are denoted by dash-dotted line in Fig.4.2.1. A slight inhomogeneity at the Al site evidenced from the larger FWHM of their sample decreases T_c from 1.98 to 1.75 K and yields the residual density of states. Apparently, the temperature dependence of $^{27}(1/T_1)$ can sensitively probe an intrinsic quasiparticle excitation near the Fermi level, even if the impurity scattering affects the quasiparticle density of states. Furthermore, as shown in Fig.4.2.2, it should be noted that the T_c-reduction rate, $R = \frac{T_c(1.75K)}{T_{c0}(1.98K)} = 0.88$ against the fraction of residual to normal density of states, $\frac{N_{res}}{N_0} = \sqrt{\frac{(T_1T)_{res}^{-1}}{(T_1T)_0^{-1}}} = 0.23$ is consistent with the prediction ($\frac{N_{res}}{N_0}$=0.36 for $\frac{T_c}{T_{co}} = 0.88$) from the $unitarity$ $scattering$ $limit$ for the anisotropic superconductivity with lines of vanishing gap as argued extensively in the literatures [35]. From the T^3 law of $^{27}(1/T_1)$ in the clean sample with the record T_c=1.98 K and the $T_1T = const.$ behavior in the sample with the lower T_c =1.75 K, it is thus identified that the superconducting gap function in UPd$_2$Al$_3$ vanishes along lines on the Fermi surface. In this case, since the low-lying quasiparticle excitation is expressed as $N_s(E) \sim N_{res} + \alpha' E$, the low temperature specific heat should obey a relation of $C(T) \sim \gamma_{res}T + \alpha T^2$, inconsistently with the experimental result of $C(T) \sim T^3$ as mentioned before. Another possible explanation for this discrepancy is that the low-lying quasiparticle excitations in the line-node gapless state with the impurities-induced residual density of states near the Fermi level, which leads to the crossover from $C(T) \sim T^2$ to $\sim T$ at low temperatures, may provide $\gamma_{res}T + \alpha T^3$ like temperature dependence of specific heat at low temperatures.

Thus the discrepancy with the specific heat result [27, 81] may be reconciled in such a context either that it involves contributions not only from quasiparticle excitations near the Fermi level but also from magnetic excitations in the **AF** ordered state leading to a complication of the analysis or that the existence of the residual density of states near the Fermi level in the line-node gapless state may give rise to E^2 like quasiparticle excitations in the low-lying energy region.

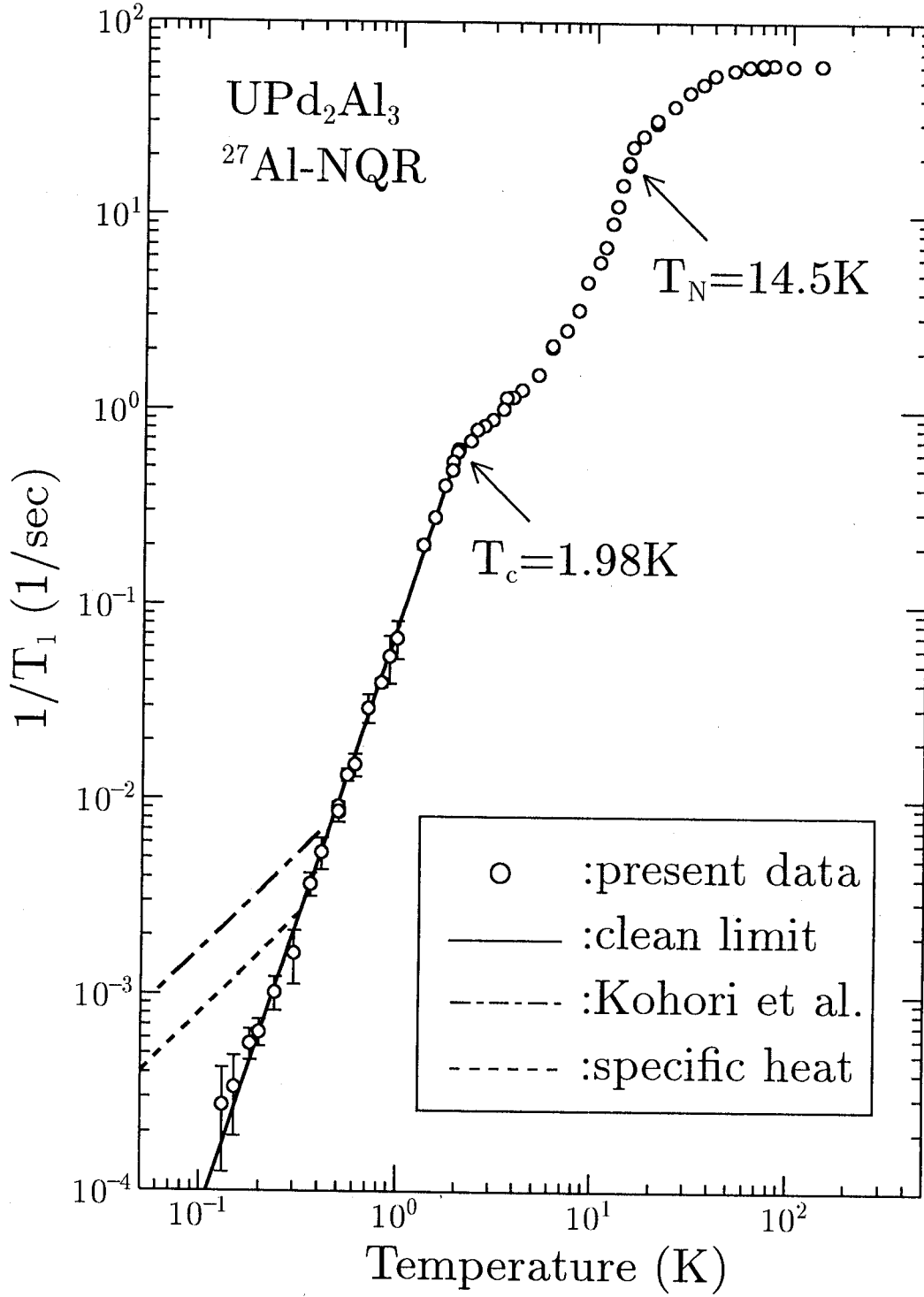Next, keeping in mind that our sample has been confirmed to be very clean from the

Figure 4.2.1 Temperature dependence of $^{27}(1/T_1)$. The solid line shows T^3 dependence as a guide for the eye. The dashed-dotted and the dashed lines show the low temperature behavior reported by Kohori *et al.* and the temperature dependence expected from the specific heat result in the case of unitarity limit, respectively (see text).
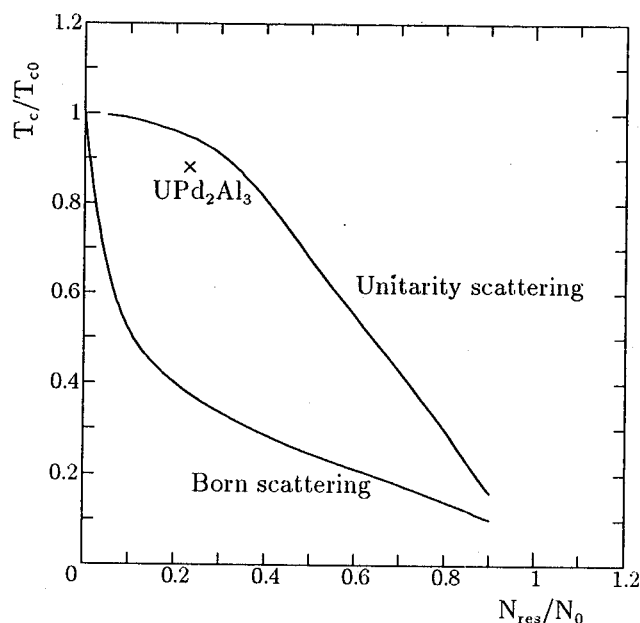
Figure 4.2.2 T_c/T_{c0} versus N_{res}/N_0 plot. The solid line show the theoretical calculations based on $d - wave$ model with node line where impurity scattering is treated in Born (weak) and unitarity (strong) scattering limits. The data ($\times$) was deduced from NQR measurement by Kohori *et al.* where N_{res} and N_0 are the residual density of states at Fermi level in the superconducting state and the density of states in the normal state.

narrow ^{27}Al-NQR line width and T_1 result at very low temperatures, we deal with the Knight shift results reported elsewhere in order to gain an insight into the pairing symmetry. Figure 4.2.3 shows the temperature dependence of the Knight shift below T_c for the polycrystalline and the single crystalline UPd$_2$Al$_3$ reported by Kyogaku *et al.* [31, 32]. The reduction of spin Knight shift, ΔK_s is about 0.08% $\sim$ 0.11% at 0.4 K regardless of the crystal axis direction, leaving large residual values.

In the previous paper, Kyogaku *et al.* pointed out that the *strong spin-orbit scattering* mechanism is not the primary cause for the origin of the residual shift [32]. What is the origin of the large residual shift? According to the high field magnetization studies [37], it was reported that the metamagnetic transition at $H \sim 20$ T can be well interpreted by introducing the model which consists of itinerant heavy Fermion state and the antiferromagnetic state due to the localized U-moment of $0.85\mu_B$. As well, it is reasonable to consider that the anomalous Knight shift behavior is not due to the impurity scattering but rather to the **AF** susceptibility which does not change below T_c, whereas the isotropic decrease of the spin shift, ΔK_s, is due to the formation of Cooper pairing among itinerant
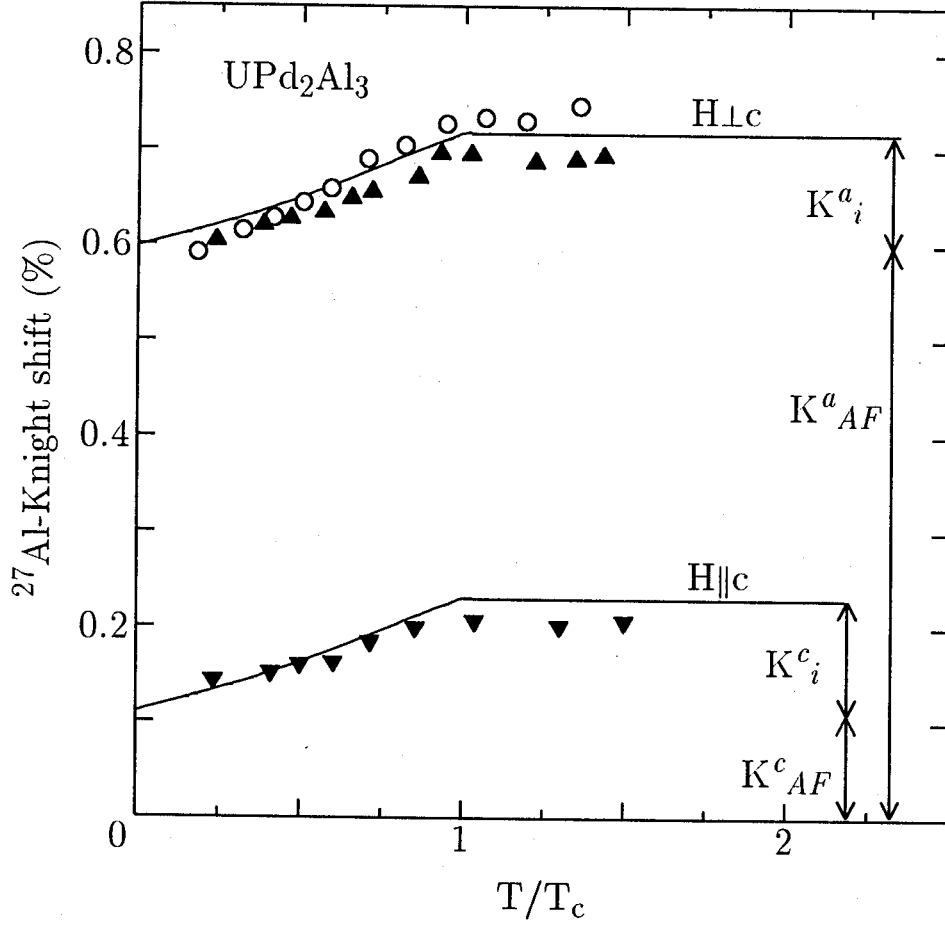
Figure 4.2.3 The T-dependence of Knight shifts reported by Kyogaku et al.[31, 32] ◯ shows the Knight shift perpendicular to the field in polycrystal UPd_2Al_3. ▲ and ▼ show the shifts perpendicular to and parallel to the field for single crystalline, respectively. The reduction of the shifts, $\Delta K_s \sim 0.08 \sim 0.11\%$, are nearly comparable to $K_i \sim 0.12\%$. The antiferromagnetic spin shifts are estimated as $\sim 0.6\%$ and $\sim 0.1\%$ for perpendicular and parallel to the field, respectively. The solid lines are calculated by using $\Delta(\theta) = 2\Delta\cos\theta$ with the parameters of $2\Delta = 5.5k_BT_c$.

quasiparticles near the Fermi level. Namely, the spin part of Knight shift is divided into two parts of itinerant, K_s^i, and localized parts, K_{AF}^i, as follows,

$$K_s(T) = K_s^i(T) + K_s^{AF}. \tag{4.6}$$

Then the observed Knight shift is expressed as

$$K(T)_{obs} \sim K_s^i(T) + K_s^{AF}, \tag{4.7}$$

where the "Van Vleck" part of the Knight shift is negligible, referring to the previous paper [31]. We can estimate $K_s^i(T)$ easily from a simple estimation. Just above T_c, since the Fermi liquid state is fully established, the spin susceptibility can be expressed as

$$\chi_s = \frac{\gamma g_J^2 \mu_B^2 J(J+1)}{\pi^2 k_B^2}, \tag{4.8}$$

where g_J, μ_B and k_B are the spectroscopic splitting factor, the Bohr magneton and the the Boltzmann factor, respectively. From eq.(4.8), we evaluated the itinerant part of susceptibility as $\chi_s \sim 2.0 \times 10^{-3}$(emu/mole), using $\gamma =$150mJ/moleK^2 and assuming $(g_J J) \sim 1$ (for instance, the localized picture of $J = 5/2$ and $g_J = 4/5$ in tetravalent 5f^2 state may not be valid far below T_K because quasiparticles form the "degenerated" heavy Fermi liquid state below T_K which is compatible with the renormalized heavy quasiparticle band width, but rather the magnetic moment, $\vec{\mu} = g_J \mu_B \vec{J}$, far below T_K is arising from either a low lying Kramerse doublet or two low lying non-Kramerse singlets. Namely magnitude of the localized moment should be reduced below T_K). Interestingly, the μ^+-Knight shift [33] and the polarized neutron scattering [39] studies have extracted values $\chi_i \sim 1.7 \times 10^{-3}$ and $\sim 2.14 \times 10^{-3}$ emu/mole, respectively, as the itinerant spin susceptibility, being nearly the same as the above value. By using the value of $\chi_i \sim 2.0 \times 10^{-3}$ emu/mole and ^{27}Al hyperfine coupling constant [32], H_{hf}=3.5 kOe/μ_B, the itinerant part of the spin shift, K_i, is estimated to be ~ 0.12 % from the formula of $K_i = \frac{H_{hf}}{(N_A \mu_B)} \chi_i$. The reduction of the shift, $\Delta K_s \sim 0.08 \sim 0.11\%$, is nearly comparable to K_i, which means that the spin Knight shift of quasiparticles becomes almost zero due to the pairing formation well below T_c regardless of the crystal direction. This result provides a strong evidence that the superconducting pairing state is singlet in a clean limit which is in consistent with the results of the μ^+ Knight shift[76] and the upper critical field, $H_{c2}(T)$ [30], exhibiting a pronounced paramagnetic limiting.

4.3 Conclusion

In conclusion, in a high-quality polycrystalline UPd_2Al_3, the T^3 law of $^{27}(1/T_1)$ holds down to a sufficient low temperature of 200 mK, unraveling the low-lying quasiparticle excitation in proportion to the energy near the Fermi level, $i.e.$, $N_s(E) \sim E$ resulting from the lines-node gapless [31, 32]. From the Knight shift result below T_c, it is shown that the large residual shift originates from the antiferromagnetic susceptibility while the isotropic reduction of the spin shift below T_c is due to the formation of a singlet pairing among quasiparticles near the Fermi level. Combining both the results of $^{27}(1/T_1)$ including the impurity effect and Knight shift, it has been clarified that the superconductivity in UPd_2Al_3 is of d-wave pairing type characterized by a vanishing gap on lines at the Fermi surface.

5 NMR Studies of UPt$_3$

5.1 Experimental Results

5.1.1 Knight Shift in the Normal State

Figure.5.1.1 shows the spectra for the single crystalline sample measured at (a) f=9.1 MHz at T =4.2 K and (b) f=3.925MHz and T =1 K for H ||[11$\bar{2}$0] (hereafter denoted as H_a). $\gamma_N/2\pi$ for ^{195}Pt is 9.094 MHz/T, so the K=0 position at f=9.1 MHz an 3.925 MHz correspond to H_0 ~10.007 kOe and 4.316 kOe, respectively. Whereas the full-width-at-half-maximum (FWHM) of ^{195}Pt spectrum is about 45 Oe at f=9.1MHz at 4.2 K, which is in agreement with the previous report on single-crystal UPt$_3$ with whisker shape [64], FWHM at $H_{a,c}$ ~4.5 kOe (f=3.925 MHz) are quite narrow with 9.5~ 11Oe, which are the narrowest to date in the heavy-fermion superconductors, assuring the sample quality is sufficiently good from a microscopic viewpoint.
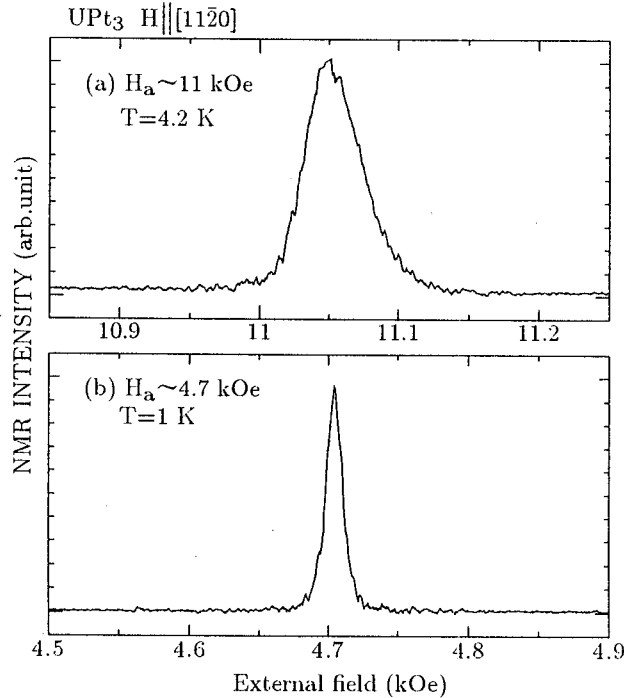

UPt$_3$ H||[11$\bar{2}$0]

(a) H_a~11 kOe
T=4.2 K

(b) H_a~4.7 kOe
T=1 K

NMR INTENSITY (arb.unit)

External field (kOe)

Figure 5.1.1 ^{195}Pt-NMR spectra of single crystal UPt$_3$ measured at (a)f=9.1 MHz and T = 4.2 K and (b) 3.925 MHz and 4.2 K for H ||[11$\bar{2}$0] (H_a).

In Fig.5.1.2, we present the ^{195}Pt-NMR spectra of single crystal UPt$_3$ for (a) H_a and (b) H ||[0001] (also hereafter denoted as H_c) measured at f = 9.1 MHz and T = 4.2 K. The

Knight shifts are extracted precisely as $K_a = -9.1\%$ and $K_c = -1.85\%$ from a relation of eq.(2.17), $K(\%) = \frac{H_0 - H_{res}}{H_{res}}$, with the typical errors of $\pm0.02\%$ and $\pm0.03\%$ for $H_{a,c} \sim 11$ kOe and ~ 4.5 kOe, respectively, which are by a twentieth smaller than previous NMR results of $\sim \pm0.5\%$ for the polycrystalline powder sample [44].
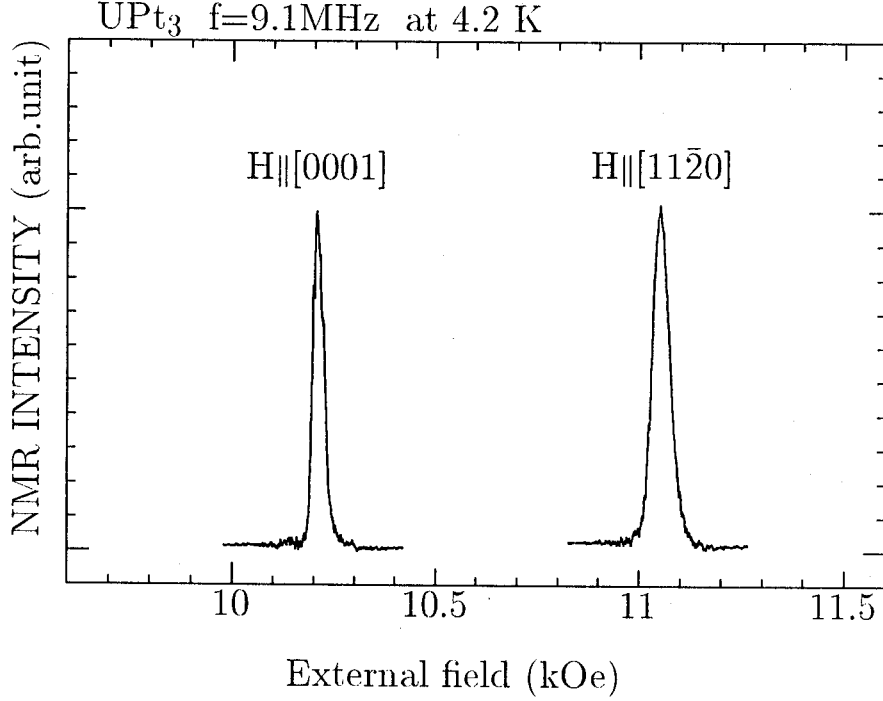

Figure 5.1.2 [195]Pt-NMR spectra of single crystal UPt$_3$ measured at f=9.1 MHz for $H \parallel [11\bar{2}0](H_a)$ and $H \parallel [0001]$ (H_c)

In Fig.5.1.3, we show the angular dependence of Knight shift at f=9.1 MHz and T =4.2 K. So far, the angular dependence of K for $H\perp[0001]$ was already measured by Lee et al. In addition, we succeeded to measure the angular dependence of K in the basal plane for the first time. In the hexagonal symmetry, the angular dependence of the Knight shift is generally expressed by the form

$$K(\theta, \phi) = K_{iso} + \frac{1}{2}(3\cos^2\theta - 1)K_c + \sin^2\theta\cos 6\phi(K_b - K_a), \qquad (5.1)$$

where the θ, ϕ are the polar angle of applied field with respect to the [0001]-axis. The angular dependence of the Knight shifts for $H\perp[10\bar{1}0]$ and $H\perp[0001]$ is in good agreement with above formula. The solid lines in Figs.5.1.3(a) and (b) are the best fits to $K(\theta,0)$ and $K(90°, \phi)$ of Eq(5.3), respectively. $K(\theta)$ is consistent with previous results on the single-crystal whisker UPt$_3$ [64].
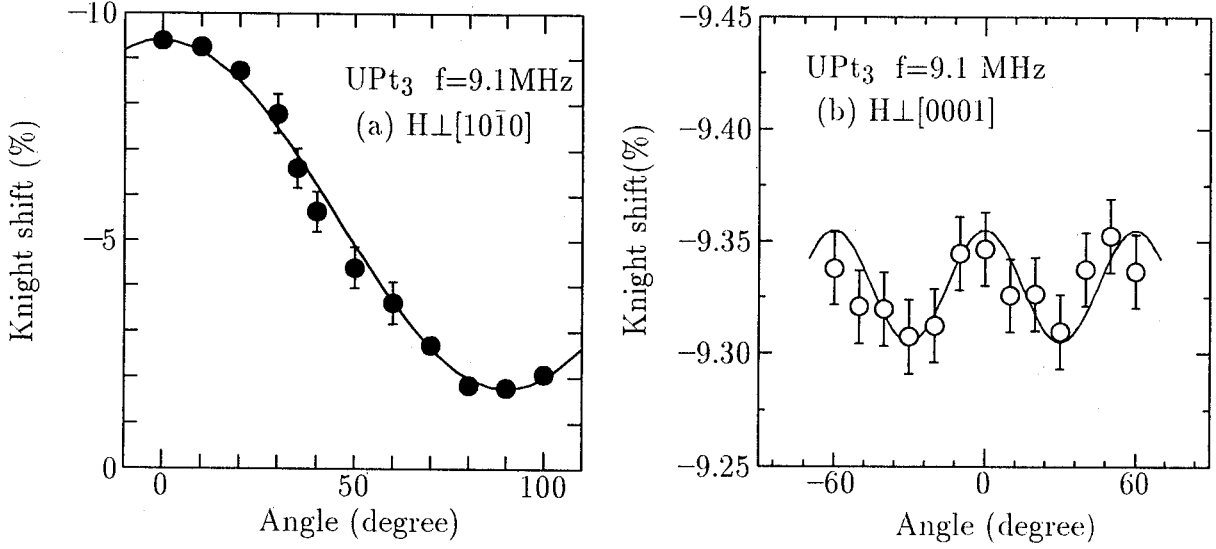
56

Figure 5.1.3 Angular dependence of [195]Pt-Knight shift of single crystal UPt₃ measured at f=9.1 MHz for H_a and H_c. The solid lines are the best fits to eq.(5.3). (see text)

In Figs.5.1.4 and 5.1.5, we show the temperature dependence of the NMR spectra for H_a and H_c. The resonance fields for both directions change gradually with decreasing temperature and any additional spectral broadening related to the antiferromagnetic order detected by neutron scattering were not observed at around $T_N \sim 5$ K.

The temperature dependence of both the Knight shifts for H_a and H_c are shown in Figs.5.1.6 together with the data (+) reported previously by Kohori et al. The origin of large negative shifts for both directions is ascribed to the transferred hyperfine field due to a polarization effect through Pt 6s- and 5d-electrons hybridized with U-5f electrons. The Knight shifts for both directions strongly depend on temperature. The temperature dependence of $K^a(T)$ and $K^c(T)$ measured up to 11K and 50K, respectively, are in agreement with the data reported on single crystal by Lee et al. and with those for oriented grains. The temperature dependence of $K^{a,c}(T)$ are quite similar to that of the the uniform susceptibility shown in Fig.5.1.7.
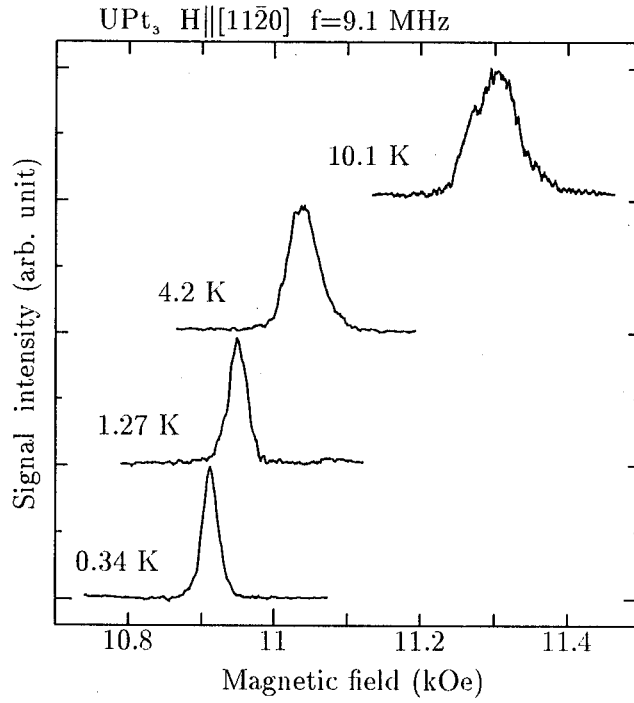
UPt$_3$ H||[11$\bar{2}$0]   f=9.1 MHz

Signal intensity (arb. unit)

10.1 K

4.2 K

1.27 K

0.34 K

Magnetic field (kOe)

10.8   11   11.2   11.4

Figure 5.1.4   Temperature dependence of ^{195}Pt NMR spectra of single crystal UPt$_3$ measured at f=9.1 MHz for H_a.

UPt$_3$ H||[0001]   f=9.1MHz

^{195}Pt-NMR Intensity (arb.unit)

50.2K

20.7K

10.1K

4.2K

1.6K

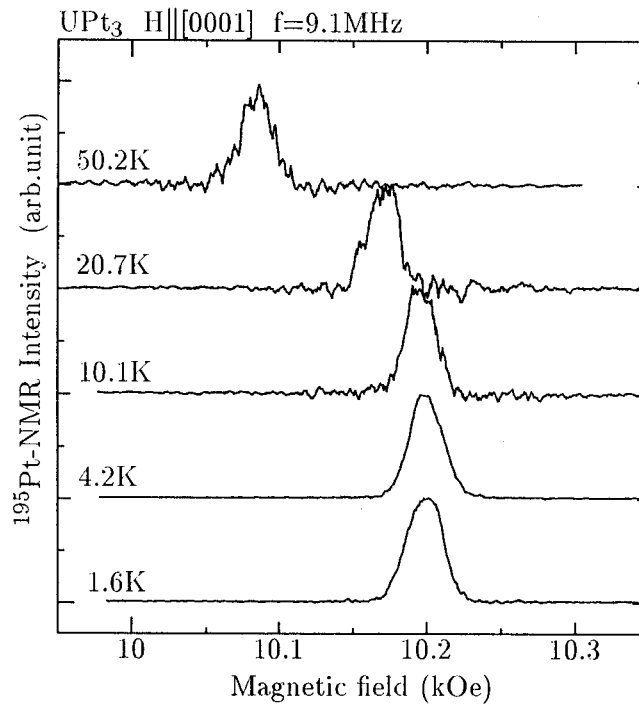Magnetic field (kOe)

10   10.1   10.2   10.3

Figure 5.1.5   Temperature dependence of ^{195}Pt NMR spectra of single crystal UPt$_3$ measured at f=9.1 MHz for H_c.
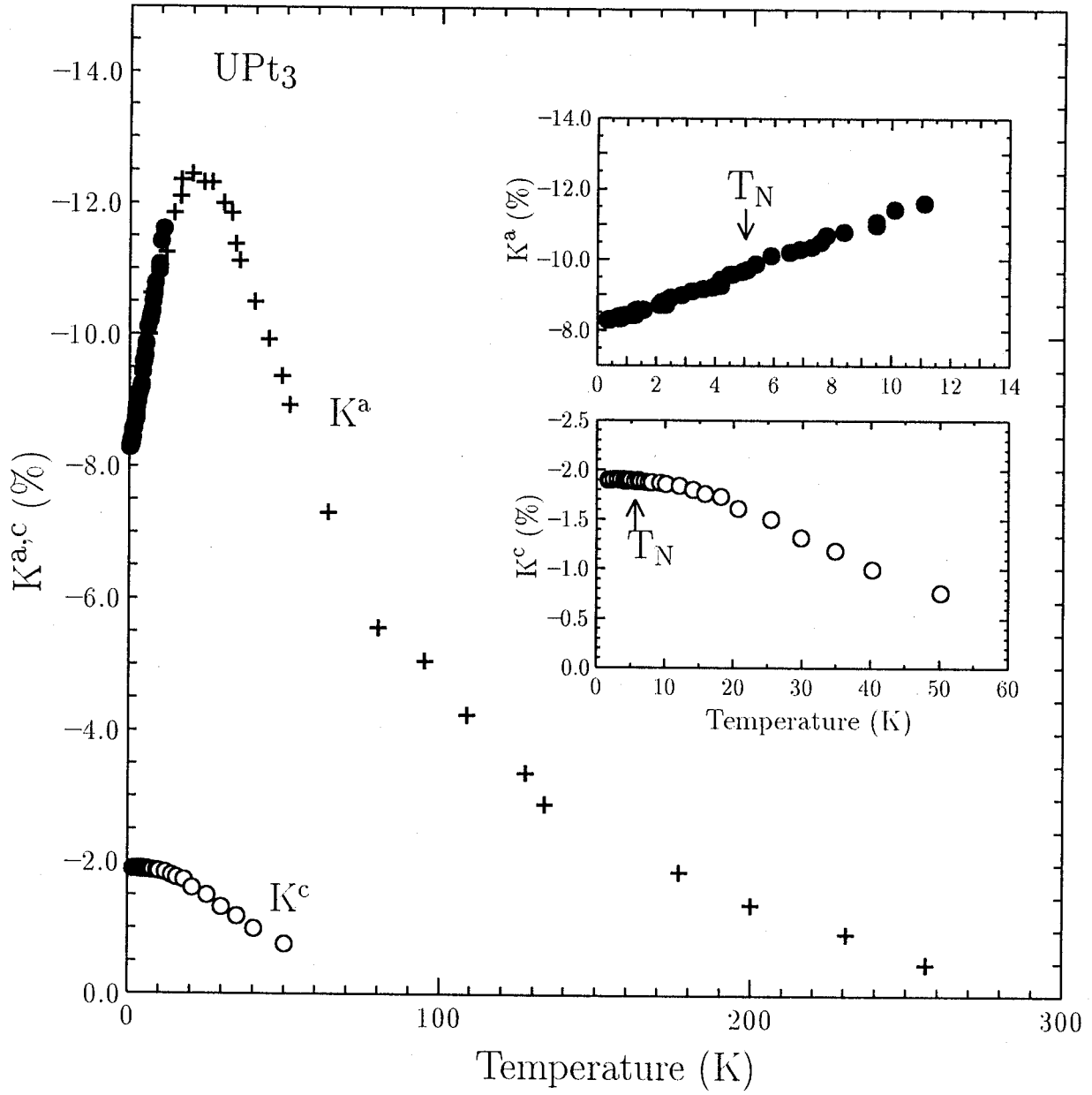
58

Figure 5.1.6 Temperature dependence of ^{195}Pt Knight shifts of single crystal UPt$_3$ for (a) H_a and (b) H_c. The data (+) are referred to the previous result [44]. The insets show the temperature dependence of K^a below $T = 14$ K and K^c below $T = 60$ K. Note that any anomalies appear at around T_N.
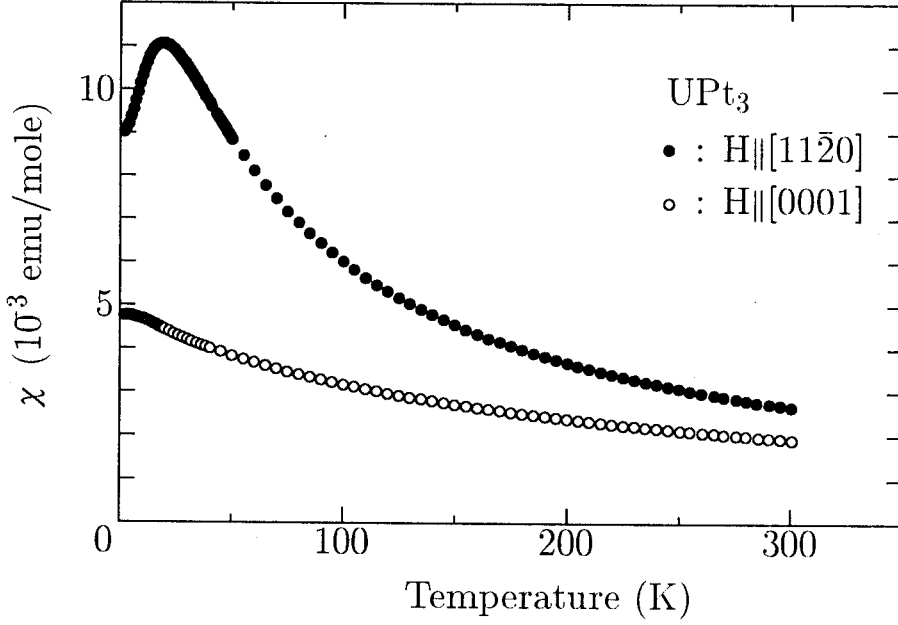
Figure 5.1.7 Temperature dependence of uniform susceptibility of single crystal UPt₃[69].

5.1.2 Knight Shift in the Superconducting State

In Fig.5.1.8, we show the temperature dependence of the ^{195}Pt-NMR spectrum at $H_a = 11$ kOe for C-phase and 4.7 kOe for **B**. We also performed ^{195}Pt-NMR measurement at $H_c = 15.5$ kOe for C-phase, $H_c = 10$ for **B**-phase and 4.4 kOe for **A**, **B**-phase as shown in Fig.5.1.9. The linewidth at $H_{a,c} \sim 10$ kOe is about 20~35 Oe, while that at $H_{a,c} \sim 4.5$ kOe is about 9~10 Oe. In Figs.5.1.10 and 5.1.11, we plot the Knight shift as a function of temperature down to $T = 28$ mK. As clearly seen in the figures, the Knight shift dose not change below T_c irrespective of the crystal directions and of the superconducting multiphases. Slight shifts to the negative side were observed in the low-field condition of $H_{a,c} \sim 4.5$ kOe.

In the superconducting mixed state of $H_{c1} \ll B \ll H_{c2}$, the contribution of the diamagnetic field can be estimated from the London equation:

$$H_{dia} = H_{c1}\frac{\ln\frac{H_{c2}}{B}}{\ln\kappa},\tag{5.2}$$

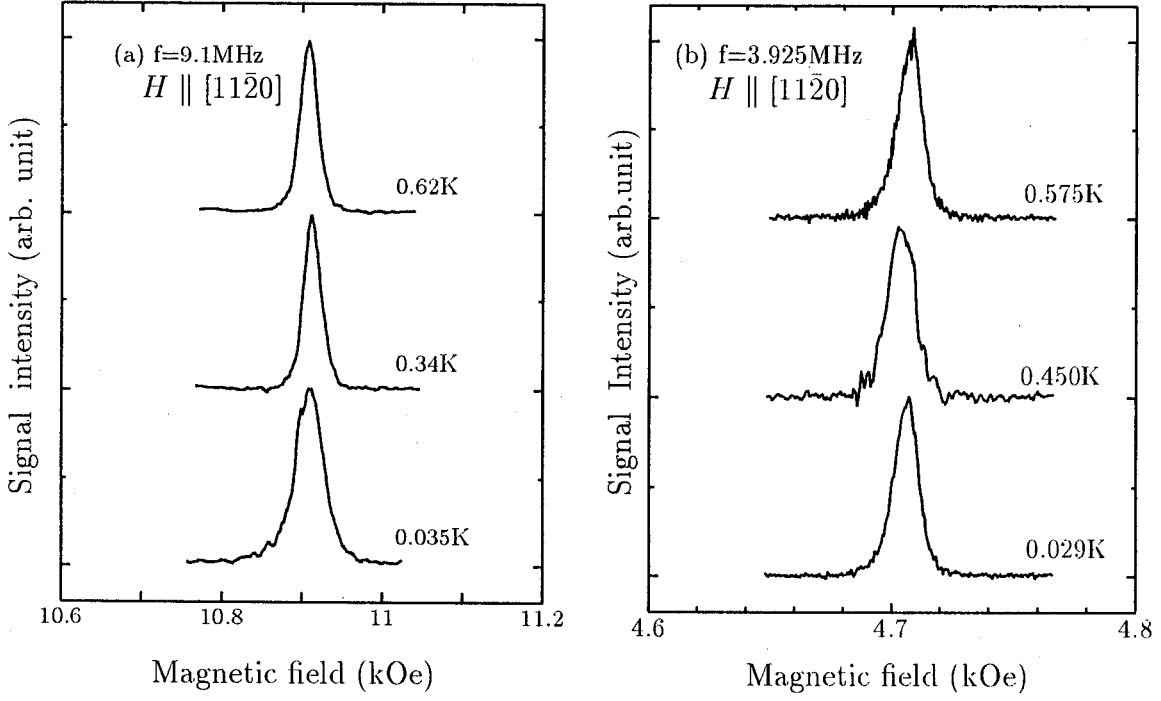where B is the applied magnetic field, κ is Ginzburg-Landau parameter, H_{c1} the lower

Figure 5.1.8 Temperature dependence of ^{195}Pt-NMR spectra of single crystal UPt$_3$ for $H \parallel [11\bar{2}0]$ (H_a) at (a) f=9.1 MHz ($H_a \sim 11$ kOe C-phase) and (b) 3.925 MHz ($H_a \sim 4.7$ kOe B-Phase).

critical field and H_{c2} the upper critical field. Using the value of $H_{c1} \sim 20$ mT, $H_{c2} \sim 2$ T and $\kappa \sim 100$, the diamagnetic field for $B \sim 10$ kOe and 5 kOe are estimated as 3 and 6 Oe, respectively. Then the diamagnetic contributions are -0.02% and -0.06% for $H_{a,c} \sim B \sim 11$ kOe and 4.5 kOe, respectively. Therefore, in the high field condition ($H \sim 10$ kOe), the diamagnetic shift is negligibly small within an experimental accuracy, while, in the low field condition ($H \sim 5$ kOe), it is observed as slight deviation to negative shift side. No marked change of the Knight shifts below T_c implies that possibilities of even parity superconductor with the *strong spin orbit-scattering* or an odd parity with equal spin pairing. While for odd parity superconductors, the χ_s dose not decrease below T_c except for that in BW state, which is found for B-phase of the ^{3}He-super fluid, and in an odd-parity with the strong SOC in the Cooper pairs, as described latter.
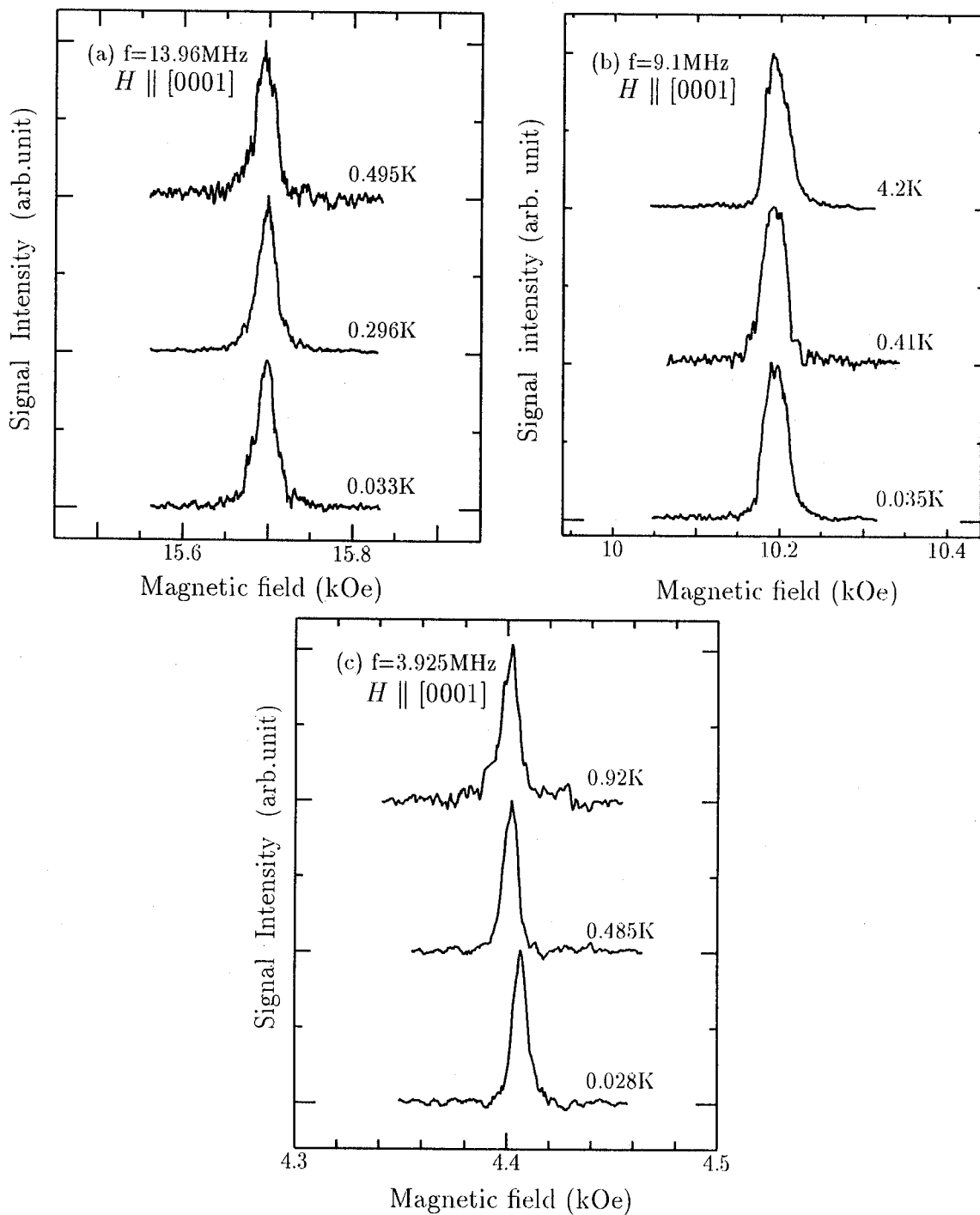
Figure 5.1.9 Temperature dependence of ^{195}Pt-NMR spectra of single crystal UPt$_3$ for $H \parallel [0001]$ (H_c) at (a) f=13.96 MHz ($H_c \sim$ 15.5 kOe, C-phase), (b) 9.1 MHz ($H_c \sim$ 10 kOe **B**, **C**-phase) and (c) 3.925 MHz ($H_c \sim$ 4.4 kOe **B-Phase**).
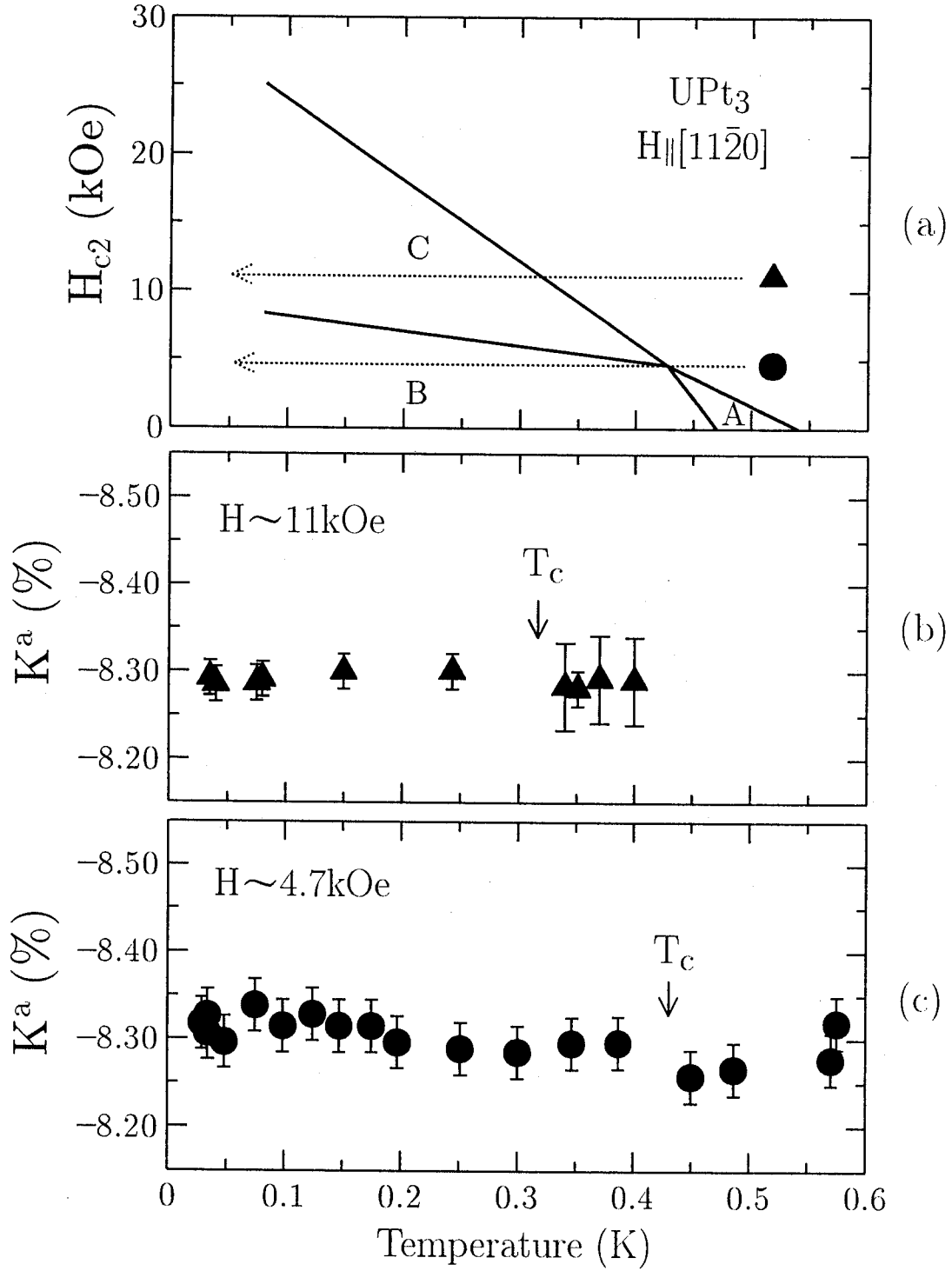
Figure 5.1.10 (a) Schematic $H - T$ phase diagram for $H \parallel [11\bar{2}0]$ (H_a). Temperature dependence of ^{195}K for H_a at (b) ~ 11 kOe (**C**-phase) and (b)~ 4.7 kOe (**B**-phase) below and near T_c.

30

H_{c2} (kOe)

20

UPt₃

H//[0001]

C

△

(a)

10

□

B

○

A

0

-2.10

H~15.6kOe

-2.00

T_c

K^c (%)

(b)

-1.90

-1.80

-2.10

□:H~10.2kOe

○:H~4.4kOe

-2.00

T_c(□) T_c(○)

K^c (%)

(c)

-1.90

-1.80
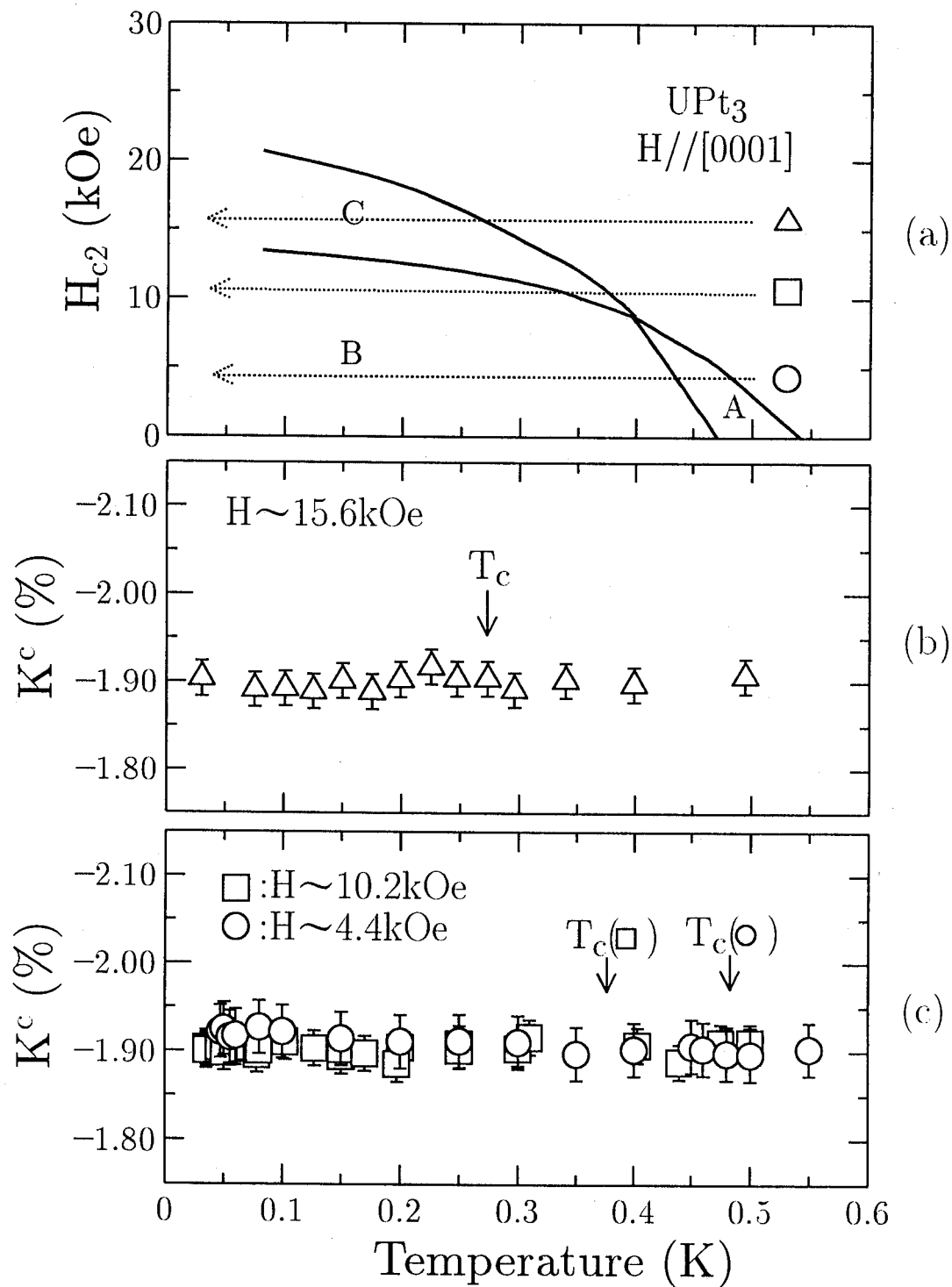
0   0.1   0.2   0.3   0.4   0.5   0.6

Temperature (K)

Figure 5.1.11 (a) Schematic $H - T$ phase diagram for $H \parallel [0001]$ (H_c). Temperature dependence of ^{195}K for H_c at (b) $\sim$ 15.5 kOe (**C**-phase) and (b)$\sim$10.2 kOe (**B**-phase) and $\sim$ 4.7 kOe (**A**- and **B**-phase) below and near T_c.

5.2 Analysis and Discussion

5.2.1 Hyperfine Interaction

The Knight shifts for both directions strongly depend on temperature and well scale to the uniform susceptibility, as mentioned above. The Knight shift couples to the macroscopic susceptibility through the hyperfine coupling, as mentioned in Chapter 2. Namely, the Knight shift components, $K(T)$, can be related to the uniform susceptibility, $\chi(T)$, with temperature as an implicit parameter by a following relation;

$$K^{a,c}(T) = K_s^{a,c}(T) + K_{vv}^{a,c},\tag{5.3}$$

and $K_s^{a,c}(T)$ is related to the temperature dependent susceptibility, $\chi_s^{a,c}$, as

$$K_s^{a,c}(T) = \frac{A_{hf}^{a,c}}{(N_A \mu_B)} \chi_s^{a,c}(T),\tag{5.4}$$

where $A_{hf}^{a,c}$ is the hyperfine coupling constant, N_A the Avogadro number and μ_B the Bohr magneton. $K_s^i(T)$ relates to the "*spin*" part due to U-5f electrons which is generated by the pseudo-spin polarization of quasiparticle bands near the Fermi level, *i.e.* an intraband effect. While K_{vv} is the temperature independent "*Van Vleck*" susceptibility originated from both the orbital parts of Pt 5d-electrons and the intraband mixing effect with other bands distributed over higher energy level than the Fermi level. From a linear relation of the $K(T)$ vs $\chi(T)$ plots (Fig.5.2.1), the hyperfine coupling constants are estimated as $A_{hf}^a \sim A_{hf}^b \sim -84.8$ and $A_{hf}^c \sim -70.9 \mathrm{kOe}/\mu_B$, which are nearly compatible with the previous results [44, 64].

The second term of eq.(5.5), K_{vv}^i, cannot be extracted easily because the temperature dependence of $K(T)$ and $\chi(T)$ is attributed to the "*fictitious spin*" $J = L + S$ in the f-electron system. Although a general procedure to separate the temperature independent part of the Knight shift from the measured one is not yet established as that in the 3d-electron system, we can tentatively estimate the minimum values of K_{vv} by following procedures. In a temperature range compatible to renormalized band width with ~ 10 K near the Fermi level for UPt$_3$ expected from a large γ value of 420 mJ/moleK^2, since the Fermi degeneracy is lifted, $K_s(T)$ relevant to the pseudo-spin polarization is anticipated to exhibit approximately a Curie-Weiss like behavior, whereas the interband mixing effect with other bands distributed in higher energy range than the temperature may gives
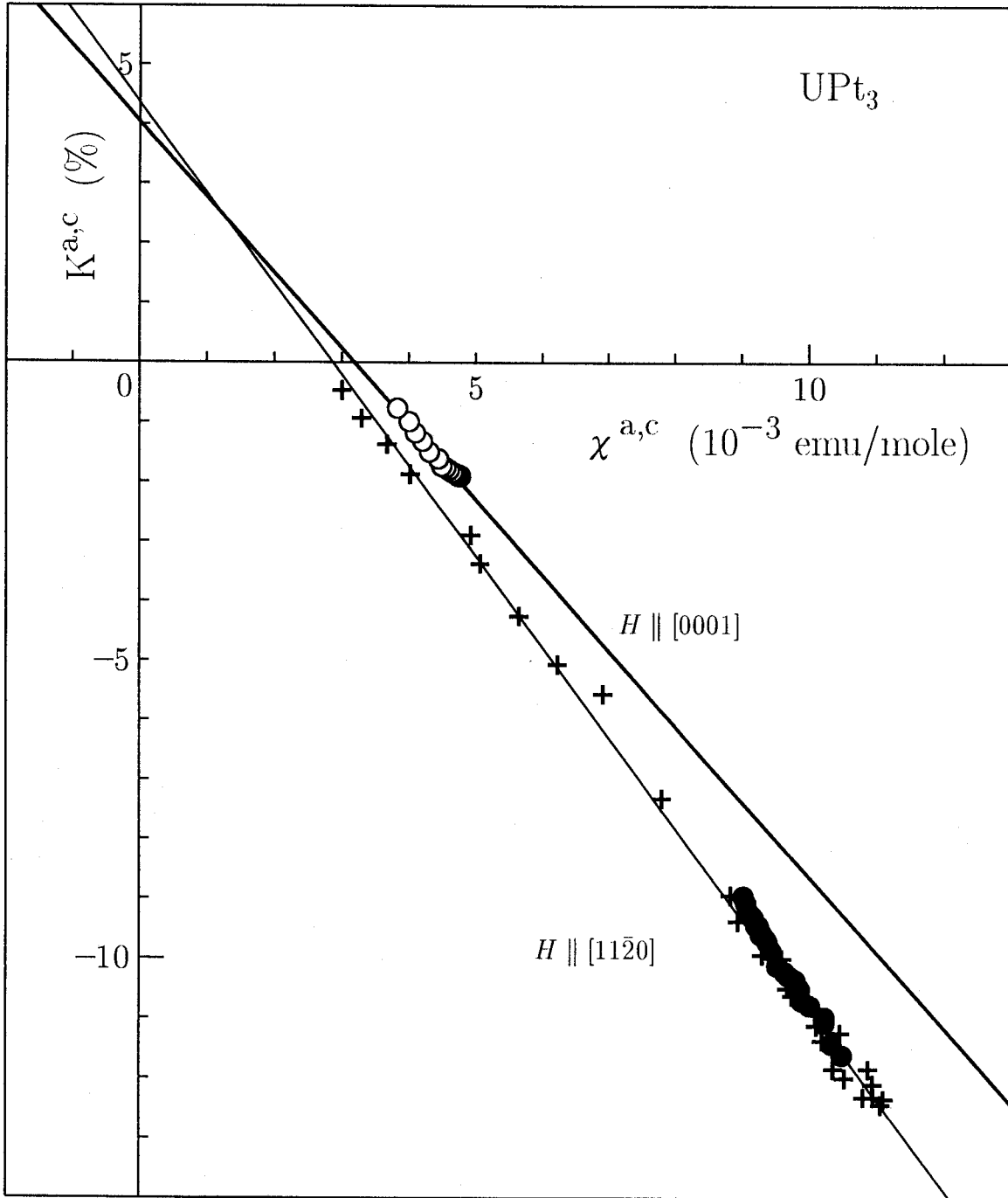
Figure 5.2.1 ^{195}K vs χ plots for H_a and H_c. The data (+) are referred to the previous result [44]. The slope of the solid lines correspond to $A^a_{hf} \sim -84.9$ and $A^a_{hf} \sim -70.8$ kOe/μ_B.

rise to a minimum value of $K_{vv}^{a,c}$, as far as the heavy fermion band picture is maintained. Accordingly, the $K_{obs}^{a,c}$ is described by

$$K_{obs}^{a,c}(T) = \frac{C_{a,c}}{T + \theta_{a,c}} + K_{vv}^{a,c}. \tag{5.5}$$

Actually, as indicated Fig.5.2.2 by solid line, the Knight shift data above 30K are able to be fitted by above formula with $\theta_a = 19.5$, $C_a = -757.4$ and $K_{vv}^a \sim +1.95$ %, and $\theta_c = 14.9$, $C_c = -89.8$ and $K_{vv}^c \sim +0.70$ %. It should be noted that $K_{vv}^{a,c}$ is provided as positive sign on the contrary to negative $K_s^i(T)$, and hence an absolute value for spin part is larger than the measured one. Thus the "*spin*" parts of Knight shift just above T_c are roughly estimated as $K_s^a(T_c) \sim -10.25$ % and $K_s^c(T_c) \sim -2.61$ % by using eq.(5.5) of $K_s^{a,c}(T_c) = K_{obs}^{a,c}(T_c) - K_{vv}^{a,c}$. Furthermore, from the simple estimation for the spin susceptibility in the Fermi liquid state, as discussed in Chapter 4, of

$$\chi_s^i(0) = \frac{\gamma^i g_J \mu_B^2 J(J+1)}{\pi^2 k_B^2} \tag{5.6}$$

by using $\gamma = 420$ mJ/moleK^2, $\chi_s^\perp$ and χ_s^c are obtained as 0.744×10^{-2} and 0.372×10^{-2} (emu/mole), in assumption of $g_J J \sim 1$ and on taking account of the anisotoropy of quasi-particle electron mass expected from the anisotoropy of the initial slope of H_{c2}, *i.e.*, $m_\perp \sim 2m_\parallel$. Then, the "*spin*" part of Knight shift, $K_a^{s,cal}$ and $K_c^{s,cal}$ are evaluated as -11.34% and -4.56%, respectively, from the relation of $K_s = \frac{A_{hf}}{\mu_B N_A} \chi_s$, using the value of $A_{hf}^a \sim -85$kOe/μ_B and $A_{hf}^b \sim -71$kOe/μ_B. These estimations are roughly in agreement with the "*spin*" part of Knight shifts, indicating that $K_s^a(T_c) \sim -10.25$ % and $K_s^c(T_c) \sim -2.61$ % are not ascribed to the "*Van Vleck*" contribution but rather to the "*spin*" parts. Thus from the hyperfine studies, it is expected a drastic change of the Knight shift below T_c for even-parity superconductors in the clean limit.

The precise measurements of the Knight shifts provides the crucial information of **AF** ordering below 5K. In the present study, any anomalies were not observed at around $T_N = 5$K, which is compatible to the resent μSR results [71]. According to the previous report on antiferromagnetic U(Pt$_{0.95}$Pd$_{0.05}$)$_3$ [66] which shows the antiferromagnetic ordering with $\mu_s = 0.6\mu_B$/U below 6K with the same spin arrangement as UPt$_3$, the zero field NMR signals were observed at around 30MHz, which is in consistency with the internal field of 45kOe/μ_B at Pt site. Since the arrangements of the **AF** moments in both are the same, the
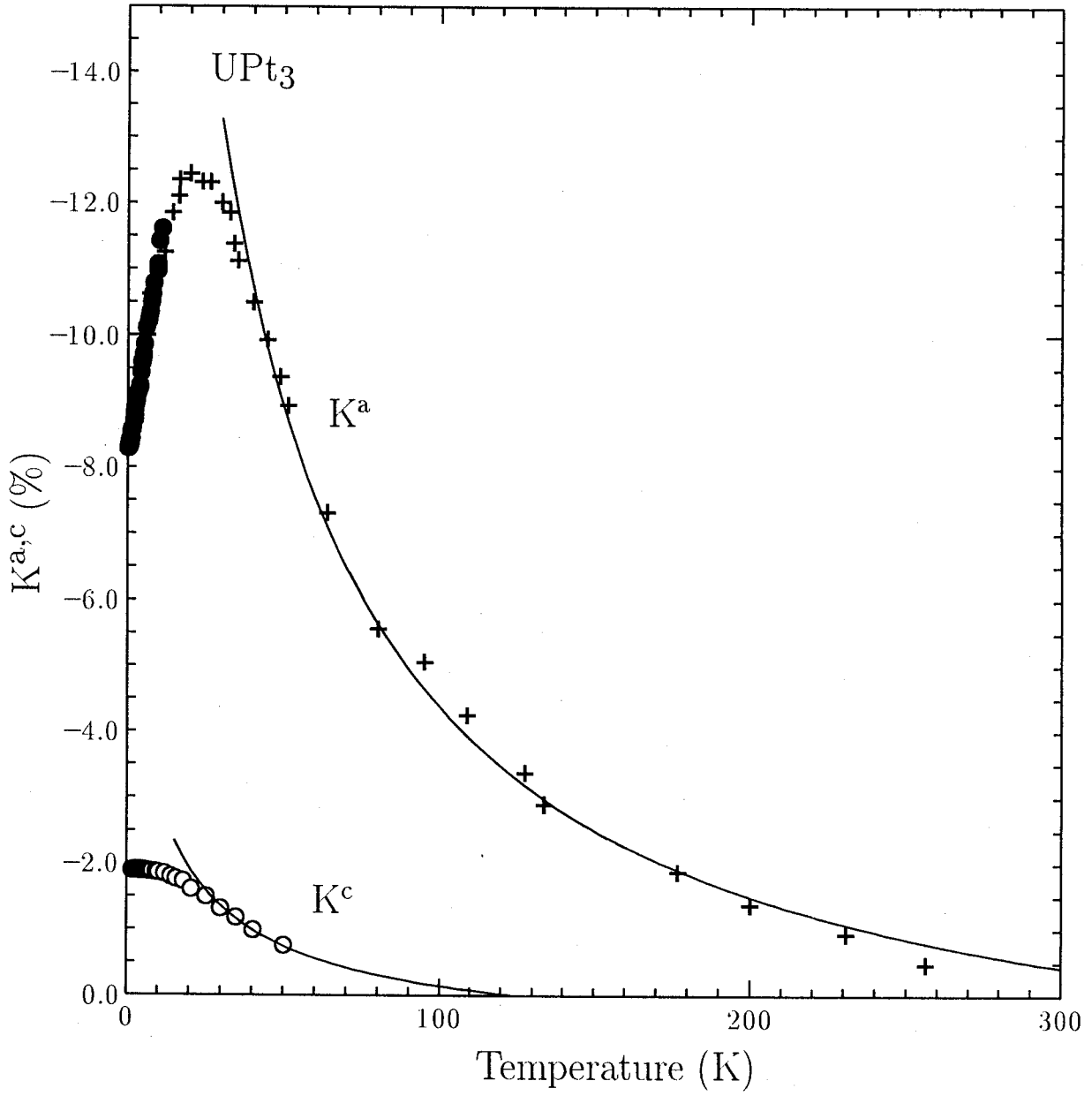
Figure 5.2.2 Temperature dependence of ^{195}Pt Knight shifts, K^a and K^c of single crystal UPt$_3$ for H_a and H_c, respectively. The data (+) are referred to the previous result [44]. The solid lines are the best fits to eq.(5.7) above 30 K, yielding $K^a_{vv} \sim +1.95$ % and $K^c_{vv} \sim +0.70$ % (see text).

68

staggered moment of $0.02\mu_B$ for UPt$_3$ should introduce the internal field of $H_{int} \sim 1.5$kOe at Pt site below T_N =5K. Namely, no anomalies excludes a static long-range AF ordering. A possible explanation for inconsistency between the neutron and NMR results is that the antiferromagnetic moments still fluctuate with the frequency higher than the NMR frequency, that is, the resolution of neutron scattering, ~ 1meV~ 1GHz which is larger than the NMR frequency, $\sim 1\mu$eV~ 1MHz. In order to clarify the magnetic nature, further detailed NMR experiments from dynamical viewpoints (nuclear spin-spin relaxation time, T_2, and spin lattice relaxation time, T_1) are required and, hence,we confine ourselves here to point out that the **AF** ordering is not static long-range type from NMR viewpoints.

5.2.2 Odd-Parity Cooper Pairing in UPt$_3$

In this section, we discuss the Knight shift behavior below T_c.

As clearly seen in the figures, the Knight shift dose not change below T_c independent of the direction of the crystallographic axes and of the superconducting multiphases. Generally for even-parity superconductors in a clean limit, the spin susceptibility, χ_s, below T_c is expressed by [13]

$$\chi_s = -4\mu_B^2 \int_0^\infty N_s(E) \frac{\partial f(E)}{\partial E} dE \qquad (5.7)$$

where $N_s(E)$ and $f(E)$ are the density of state at the Fermi level in the superconducting state and Fermi-Dirac function. In fact, from the Knight shift studies in CeCu$_2$Si$_2$ and UPd$_2$Al$_3$, the significant reduction of the ^{63}Cu- and ^{29}Si-Knight shift in CeCu$_2$Si$_2$ [70] and of ^{27}Al- shift [31, 32] in UPd$_2$Al$_3$ provided an evidence for the even-parity pairing state. In UPd$_2$Al$_3$, it should be note that the reduction of the spin shift was well resolved below T_c independent of crystal directions, in spite of the slight change only by ~ 0.1 %. Thus for the *d-wave* scenario with either A$_{1g}$ or E$_{1g}$, $\chi_s(T)$ should decrease to zero below T_c in a clean limit. As discussed before, since the *spin* parts of $K_s^\perp(T_c) \sim -10.25$ % and $K_s^\parallel(T_c) \sim -2.61$ %, $K_s^{a,c}(T)$ should behave as shown by solid lines in Fig.5.2.3, where the *d-wave* model for E$_{1g}$ representation with $\Delta(T) = 2\Delta \sin\theta\cos\theta$ and $2\Delta_0 = 3.5k_B T_c$ is assumed.

Evidently, the invariance of the spin shift below T_c requires the OP with either an odd-parity pairing with equal spin pairing or an even-parity with the *strong spin-orbit scattering*. If the invariance of spin shift is attributed to the *strong spin-orbit scattering*, the spin-orbit
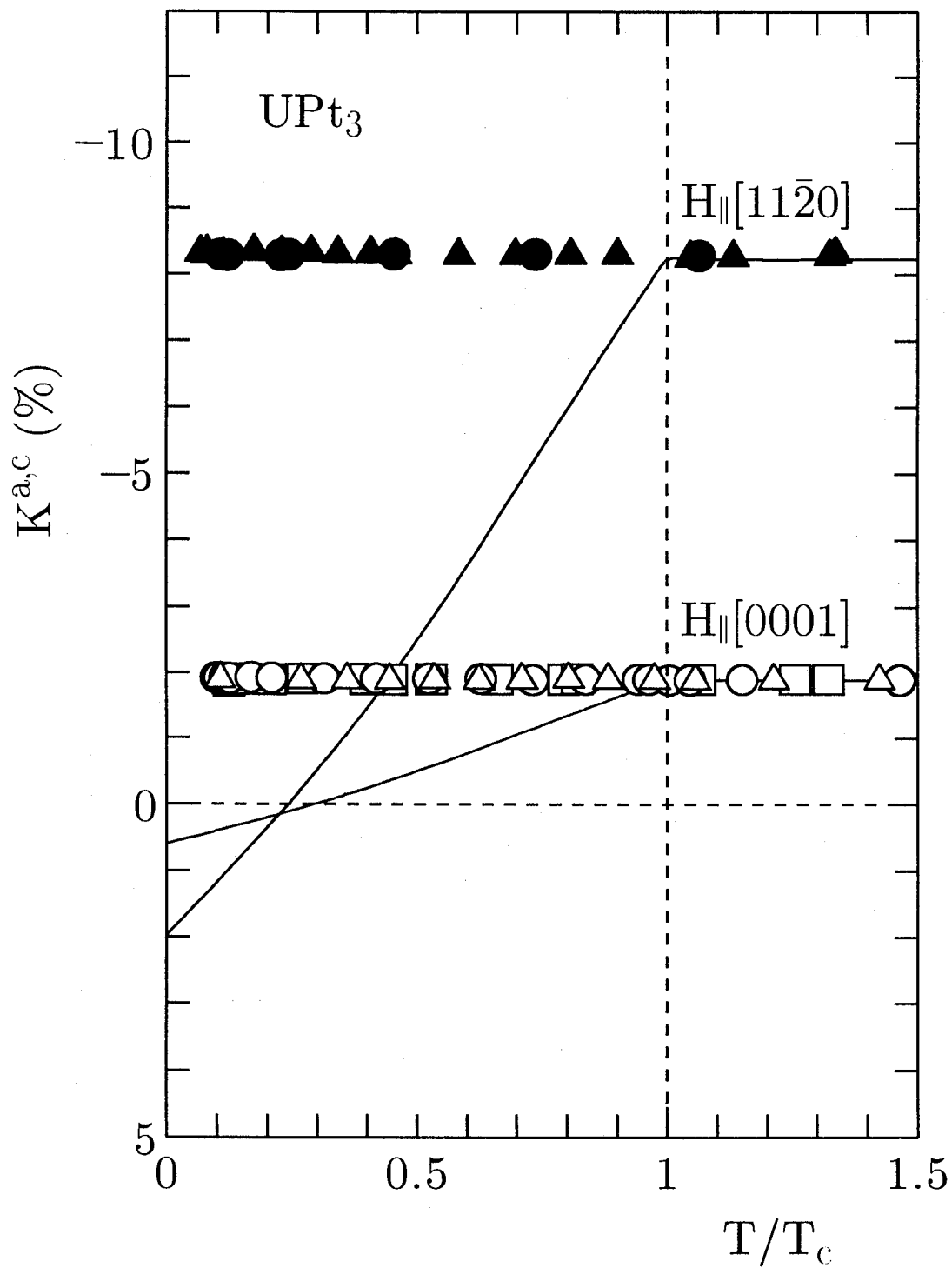
Figure 5.2.3 Temperature dependence of ^{195}K below T_c on a full scale. The solid lines shows the case for even-parity $d - wave$ model with $2\Delta_0 = 3.5k_BT_c$ and $\Delta(\theta) = 2\Delta_0 \sin\theta\cos\theta$.

scattering mean free path, l_{so} in our sample can be estimated easily as 9.4 Å from the formula of [67]

$$\frac{K_s}{K_n} \simeq 1 - 2\frac{l_{so}}{\pi\xi_0}, \quad (l_{so} \ll \xi_0), \tag{5.8}$$

by using the coherence length, $\xi_0 \sim 150$ Å in assumption of $\frac{K_s}{K_n} \sim 0.98$. Here we assume that the reduction of spin shifts occurs within the experimental errors of ~ 0.03 %. This is, however, inconsistent with the criteria of $l_{so} \gg l_{tr}$ for above mechanism because the transport mean free path l_{tr} is larger than 2000 Å from the dHvA experiment [68], meaning that the *strong spin-orbit scattering* mechanism is not the cause of the invariance of the Knight shift and a possibility of d-wave pairing is excluded. Therefore, it is reasonable to consider that an odd-parity in a clean limit is realized in UPt$_3$.

Even in case of an odd-parity superconductivity, the temperature dependence of spin susceptibility below T_c is different from that in the usual triplet state when the **spin-orbit coupling** in the Cooper pairs is strong. Here, we remark on the **SOC** in the Cooper pairs. It is said that, in the heavy fermion systems, the spin-orbit coupling and the crystal field should be taken into account for discussing Cooper pair formation as described in Chapter 2 as follows,

$$\hat{A} \cdot \vec{d}_\alpha(k_i) = A_{\alpha\beta}\vec{d}_\beta(A_{ij}k_j). \tag{5.9}$$

In this case, even for odd-parity pairing, the spin susceptibility, $\chi_s(T)$, should decrease for $H \parallel \vec{d}$ by analogy with even-parity pairing because the spin labels can be no longer treated independently with a symmetry rotation. In fact, the Pauli limiting like saturation of the upper critical field H$_{c2}^c$ reminds us of the odd-parity of the strong **SOC** case when $\vec{d}$-vector is locked to hexagonal c-axis (two dimensional E$_{2u}$ representation based on the **SBF** was proposed to explain such the Pauli limiting like behavior [60]). In E$_{2u}$ representation, the spin susceptibility for [0001] direction, χ_s^c, was predicted to decrease to zero at $T = 0$. By contrast, E$_{1g}$ representation in the **SBF** model, which is also based on the strong **SOC** regime, the spin susceptibility in the basal plane, $\chi_s^a(T)$, in the B-phase is predicted to be reduced to a half of the value at T_c because its "$\vec{d}$-vector" is lying in the basal plane. In any case, the scenarios based on the strong **SOC** case predict an anisotropic decrease of the spin susceptibility even for the odd-parity superconductivity. Our results, however, show the Knight shifts stay constant below T_c independent of crystal directions within a

71

experimental accuracy of $\pm 0.03\%$, unexpectedly, indicating that the strong **SOC** case is unfavorable but rather the weak **SOC** one is realized in UPt$_3$.

Miyake argued that the description based on the weak **SOC** was valid for single heavy-fermion bands which is formed by hybridization between one f-electron per f-site and conduction electrons in Ce based compounds [24]. Although it is not clear whether or not Miyake's arguments can be applied to UPt$_3$ at present, from the experimental view points, it is clear that the superconducting state of UPt$_3$ should be described on the odd-parity in the weak **SOC** regime. In this context, such a one-dimensional model as A$_{1u}$ or A$_{2u}$ [58] seems to be allowed as a possible mechanism of UPt$_3$. Since even the present A$_{1u}$ or A$_{2u}$ scenario based on the **SBF** model, however, requires the "static" magnetic order, which contradicts with both the present and the recent μSR results on the high-quality single crystal UPt$_3$, such a theoretical model that interprets the various experimental results without contradiction have not been provided yet.

In any way, we emphasize that the odd-parity pairing in weak **SOC** case is realized in the superconducting state in UPt$_3$

5.3   Conclusion

In conclusion, we have performed precise NMR measurement for the high quality single crystal UPt$_3$. No anomalies associated with the **AF** ordering could be observed near and below T_N =5 K, suggesting that U-moments still fluctuate at the NMR frequency. The NMR experiment, of course, is the static limit as a microscopic probe. In the superconducting state, [195]Pt-Knight shift does not change within a experimental error of $\pm 0.03\%$ irreducible of both the direction of the crystal axes and of the superconducting multiphases, which is clearly different from the case of UPd$_2$Al$_3$ where the isotropic reduction of the spin susceptibility was observed. From an analysis for the temperature dependence of Knight shift below T_c, the impurities-induced *strong spin-orbit scattering* mechanism is not the cause of the invariance of the spin susceptibility below T_c. These eliminate a possibility of both the even-parity pairing and the odd-parity in the strong **SOC** case, and provide the unique state of an odd-parity paring with the weak **SOC** case in UPt$_3$ system.

6 NMR Studies of CePd$_2$Al$_3$

6.1 Experimental Results

6.1.1 ^{27}Al NMR Spectra

Figure 6.1.1 shows the temperature dependence of ^{27}Al-NMR spectra (I=5/2) at 10.5 MHz for the oriented powder of the annealed sample (PC1) with the c-axis perpendicular to the magnetic field. Above 20 K, the spectrum shows a well separated two dimensional powder pattern, which originates from the combined effect of the electric quadrupole shift and the anisotropic Knight shift within the basal plane.
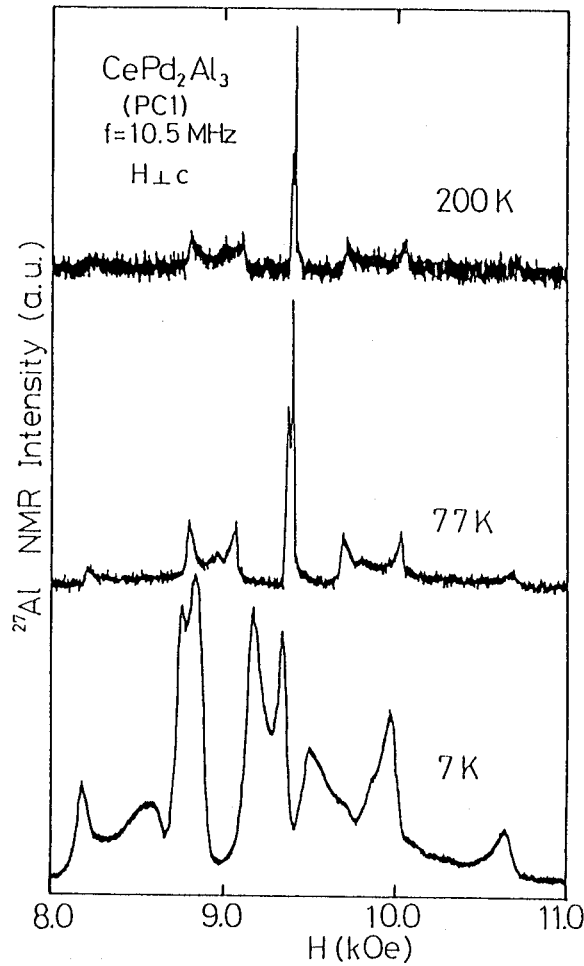

Figure 6.1.1 Temperature dependence of ^{27}Al-NMR spectra at f=10.5MHz for the oriented powder of PC1(annealed sample) with $H \perp$c. Below 20 K, the NMR linewidth increases rapidly with decreasing temperature, dominated by the anisotropic Knight shift within the basal plane.

From the splitting of the satellites at 77 K, the electric quadrupole frequency ν_Q and the asymmetry parameter η are estimated to be $\nu_Q \sim 1.032$ MHz and $\eta \sim 0.328$, respectively,

which are consistent with the previous report [83]. From these values, the NQR frequencies corresponding to $(\pm 1/2 \Leftrightarrow \pm 3/2)$ and $(\pm 3/2 \Leftrightarrow \pm 5/2)$ transitions are estimated as $\nu_{NQR}(LF) = 1.15$ MHz and $\nu_{NQR}(HF) = 2.02$ MHz, respectively, which agree well with the values obtained by ^{27}Al-NQR experiments as described later. Below 20 K, the NMR linewidth, dominated by the anisotropic Knight shift within the basal plane, increases rapidly with decreasing temperature, as clearly seen in Fig.6.1.1.
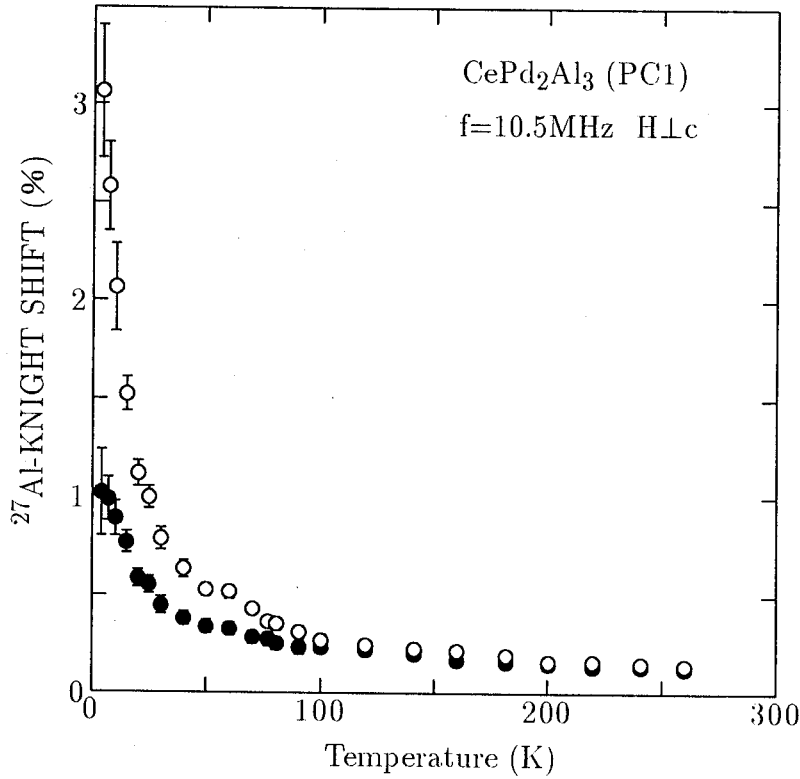

Figure 6.1.2 Temperature dependence of two components of ^{27}Al-Knight shift in the basal plane. Open($\bigcirc$) and closed($\bullet$) circles correspond to the peaks on the lower($\phi = 90°$ or $30°$) and higher($\phi = 0°$) field side of the central line, respectively.

The central spectrum for the $(1/2 \Leftrightarrow -1/2)$ transition is also split by the combined effect of the second-order quadrupole shift and the anisotropic Knight shift. In order to extract the Knight shift, the electric quadrupole shift must be subtracted from the observed shift of each central line, which is expressed in frequency as[31]

$$\Delta\nu = K\gamma_N H_{res} + \frac{\nu_Q^2 - \frac{2}{3}\eta\cos(2\phi)}{2(1+K)\gamma_N H_{res}} \tag{6.1}$$

Here, the second term is the second-order quadrupole shift. ϕ is the azimuthal angle between the certain fixed axis and the magnetic field in the basal plane. The peaks on

74

the higher and the lower field sides of the central line correspond to $\phi = 0°$ and $\phi = 90°$ (equivalent to $\phi = 30°$), respectively. The subtraction of the second-order quadrupole shift was performed by dividing eq.(6.1) by $\gamma_N H_{res}$. Then a linear relation between $\Delta\nu/(\gamma_N H_{res})$ and $1/H_{res}^2$ is expected, giving the value of the Knight shift by extraporlating $1/H_{res}^2$ to zero. For this estimation, the NMR spectrum was taken at 5.5MHz, 10.5MHz and 15.1MHz by sweeping the magnetic field.

The temperature dependence of the two components of the Knight shift in the basal plane, obtained in this way, is shown in Fig.6.1.2. Overall temperature dependence of both shifts is similar to that of the susceptibility[83].

6.1.2 ^{27}Al NQR Spectra

Figure 6.1.3 shows a systematic change of the NQR spectrum of ^{27}Al in the paramagnetic state at 4.2 K for PC1, PC2 and SC1, which corresponds to the ($\pm 3/2 \Leftrightarrow \pm 5/2$) transitions. All the spectra consist of two peaks at around 2.01 and 1.91 MHz for the main and satellite peaks, respectively, indicating that two inequivalent Al-sites exist. The NQR linewidth of main peak, and relative intensities of satellite to main peaks are summarized in Table 3.

Crystal	main peak linewidth (kHz)	relative intensity (%)	
		main	satellite
PC1	40.0	93.5	6.5
PC2	65.7	88.8	11.2
SC1	85.7	76.5	23.5

Table 3 NQR linewidth of the main peaks and the relative intensities of the main and the satellite peaks for PC1, PC2 and SC1 at 4.2 K.

Figure 6.1.4 shows the NQR spectra at 1.3 K. Comparing Fig.6.1.3 with Fig.6.1.4, we see that the linewidth is appreciably broadened for PC1 and PC2, but not for SC1. In the **AF** spin structure determined by the neutron scattering experiment, the hyperfine field induced
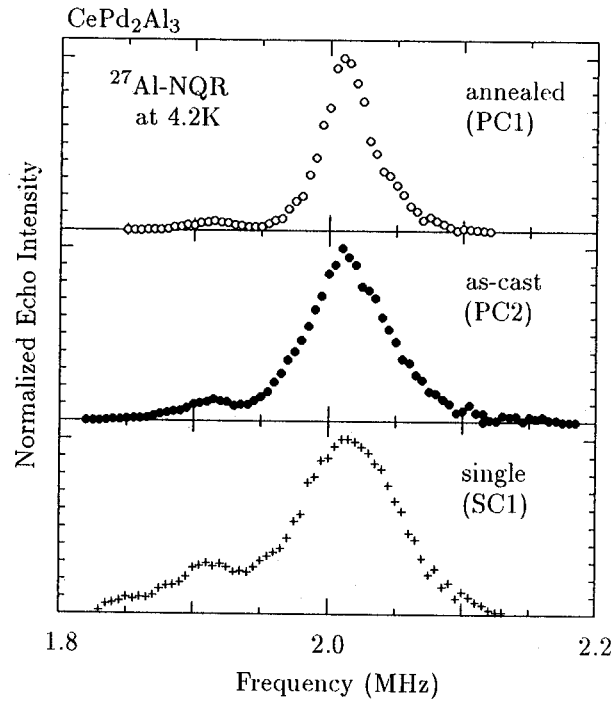
75

Figure 6.1.3 Systematic change of NQR spectrum for ($\pm3/2 \Leftrightarrow \pm5/2$) transition of ^{27}Al ($I = 5/2$) in the paramagnetic state at 4.2K for PC1($\bigcirc$), PC2($\bullet$) and SC1($+$).
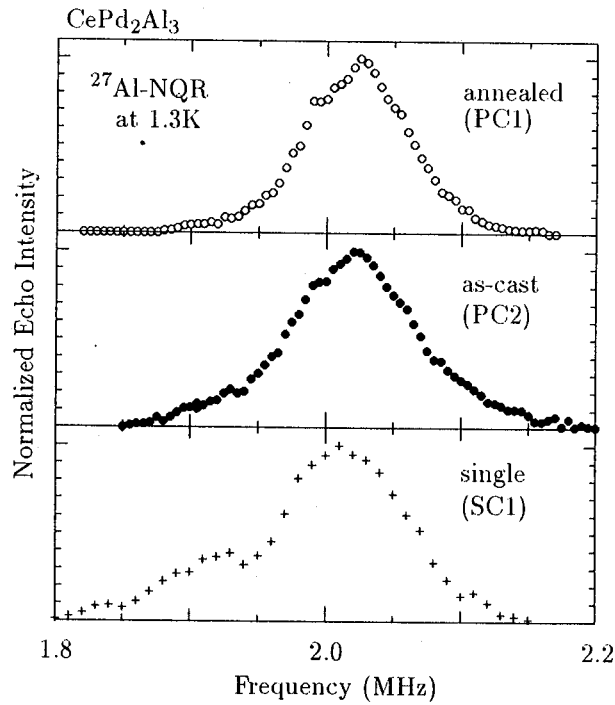

Figure 6.1.4 ^{27}Al-NQR spectra for ($\pm3/2 \Leftrightarrow \pm5/2$) transition at 1.3 K for PC1($\bigcirc$), PC2($\bullet$) and SC1($+$). We note that the linewidth is considerably broadened for PC1 and PC2, but not for SC1, indicating that no long-range order occurs for SC1.

by the onset of the **AF** order should be canceled out at the Al-site, since the ideal Al-site in the PrNi$_2$Al$_3$ structure occupies the magnetically symmetric site. This is, however, not the case because of the distribution of the occupation over two possible Al-sites, as described later. The broadening of the NQR spectrum can be an evidence for the appearance of the magnetic ordering. Therefore, from the temperature dependence of the NQR spectrum, it is concluded that, to some extent, a static magnetic correlation develops at low temperatures even for the as-cast polycrystal (PC2), similar to the annealed polycrystal (PC1), which exhibits the **AF** ordering. There is no sign of some static correlations in the single crystal (SC1).

6.1.3 ^{27}Al Nuclear Spin-lattice Relaxation Rate $1/T_1$

In Figs. 6.1.5 and 6.1.6, we show the NMR and NQR relaxation behaviors of ^{27}Al nuclei, respectively. For PC1 and PC2, T_1 of ^{27}Al above 20 K was measured by the NMR at 10.5 MHz, while below 20 K T_1 was measured by the NQR method for the $(\pm 3/2 \leftrightarrow \pm 5/2)$ transition in zero field. The magnetization recovery for the NMR transition of $(-1/2 \leftrightarrow 1/2)$ is given by

$$\frac{M(\infty) - M(t)}{M(\infty)} = 0.02857 \exp(-t/T_1) + 0.18 \exp(-6t/T_1) + 0.7936 \exp(-15t/T_1), \quad (6.2)$$

while the recovery for NQR transition of $(\pm 3/2 \leftrightarrow \pm 5/2)$ is as follows,

$$\frac{M(\infty) - M(t)}{M(\infty)} = \frac{3}{7} \exp(-3t/T_1) + \frac{4}{7} \exp(-10t/T_1) \quad (6.3)$$

Figure 6.1.7 shows the temperature dependence of $1/T_1$ of ^{27}Al for PC1, PC2 and SC1. In the paramagnetic state, $1/T_1$'s for both polycrystals show almost the same temperature dependence, in agreement with the result reported by Fujiwara *et al.*[83] In the temperature range of 20−100 K, $1/T_1$ is temperature independent, which is commonly observed for the heavy fermion systems such as described in Chapter 4. This feature provides an evidence that the system can be described as an assembly of the local moments[84, 85, 86]. Below 20 K, which is comparable to the Kondo temperature, $T_K \sim 19$ K, deduced from the neutron scattering experiment, $1/T_1$ begins to decrease gradually with decreasing temperature,
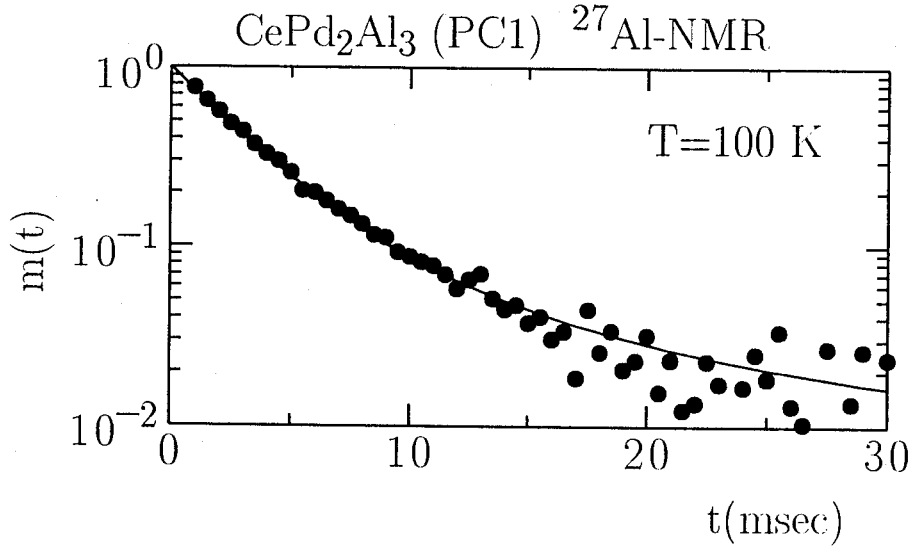
Figure 6.1.5 Typical behavior of nuclear magnetization recovery for $(-1/2 \Leftrightarrow +1/2)$ transition of annealed $CePd_2Al_3$. The solid line is the least square fitting to eq.(6.2).
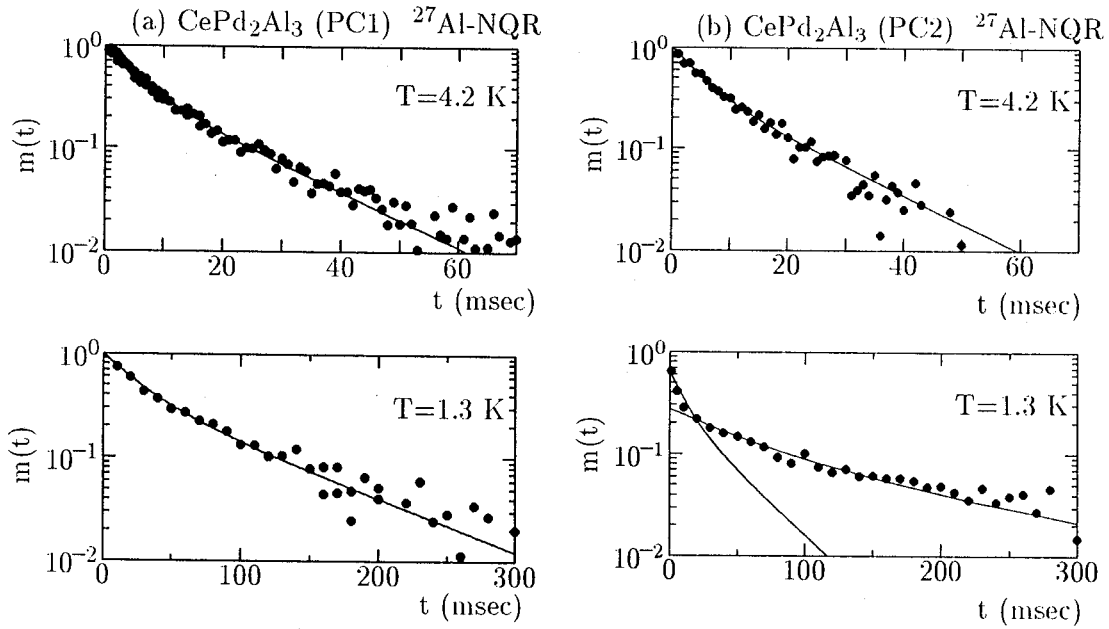

Figure 6.1.6 Typical behaviors of nuclear relaxation for $(\pm 3/2 \Leftrightarrow \pm 5/2)$ transition of (a) annealed and (b) as-cast $CePd_2Al_3$. The solid lines are the least square fitting to eq.(6.3).

implying that the system enters a crossover regime towards the coherent Kondo state, *i.e.* the heavy Fermi liquid state below T_K. Before the heavy Fermi liquid state is fully established, the system, however, undergoes an antiferromagnetic transition at T_N=2.7 K for PC1.
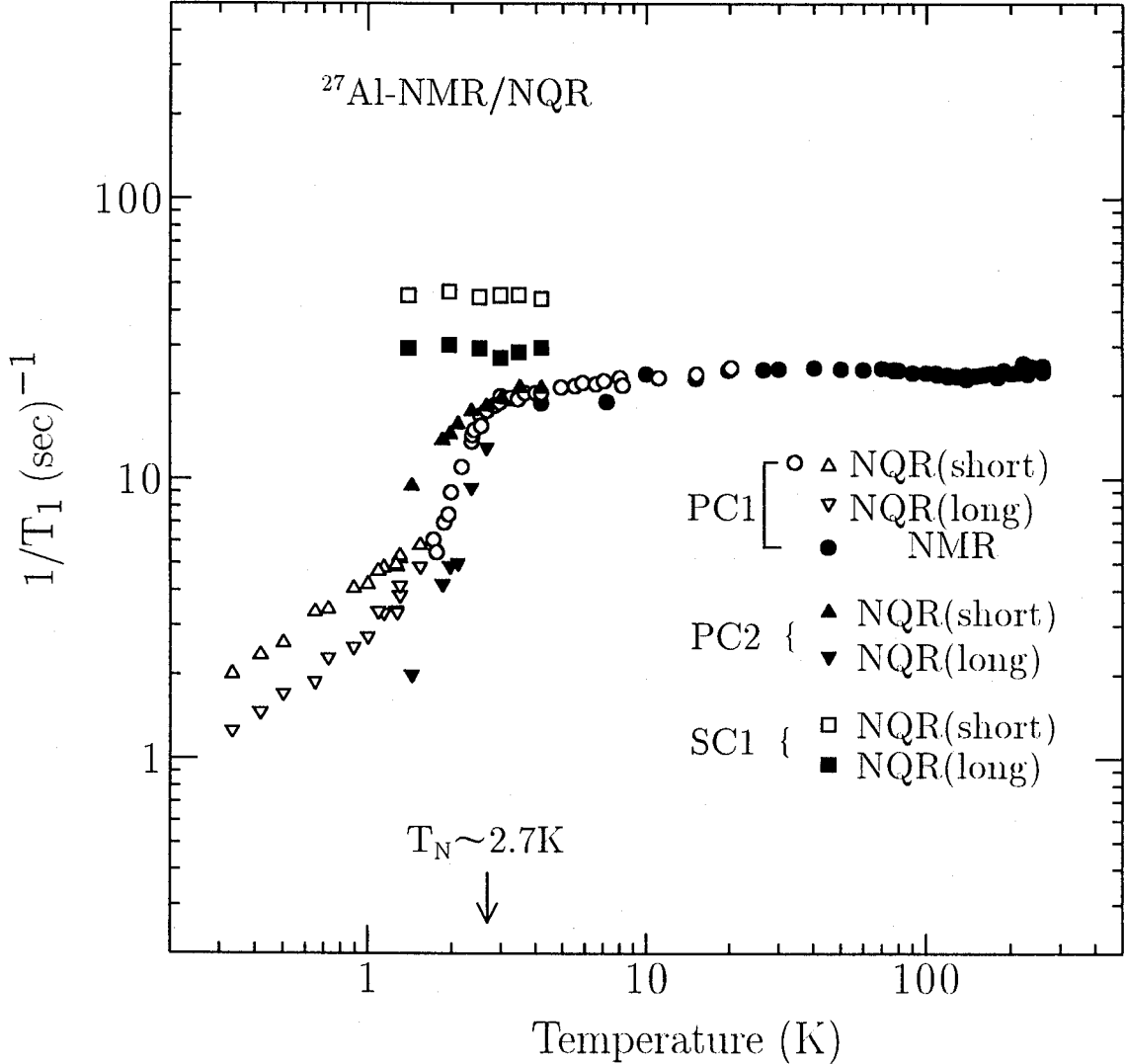

Figure 6.1.7 Temperature dependence of $1/T_1$ of ^{27}Al for PC1, PC2 and SC1. $1/T_1$ above 20 K was measured by NMR at f=10.5MHz($\bullet$), and below 20 K was measured by NQR for ($\pm 3/2 \Leftrightarrow \pm 5/2$) transition at zero magnetic field. $1/T_1$ for PC1 was uniquely determined above 1.5 K ($\bigcirc$), while far below T_N short($\triangle$) and long($\triangledown$) components of T_1 were tentatively extracted because of the distribution of T_1. The distribution of T_1 for PC2 and SC1 appears in the high temperature region. The short and the long components for PC2 are denoted by symbols $\blacktriangle$ and $\blacktriangledown$, respectively, and those for SC1 are indicated by $\square$ and $\blacksquare$.

Below T_N=2.7 K, $1/T_1$ for PC1 drops rapidly without the effect of the critical fluctuation near the ordering temperature. Below 1.5 K, $1/T_1$ cannot uniquely be determined due to

the distribution of T_1. It has been found that $1/T_1$ for PC2, where the clear onset of the AF ordering cannot be evidenced from bulk measurements, exhibits a much larger distribution of $1/T_1$ below 2.7 K than that for PC1. In a clear contrast to the case for polycrystals, $1/T_1$ for the single crystal is largely distributed above and below 2.7 K and does not experience any anomalies around 2.7 K. Both the short and long components of $1/T_1$ stay constant in the measured temperature range. No sign of magnetic ordering could be observed.

6.2 Analysis and Discussion

6.2.1 Hyperfine Interaction

First we begin to discuss the hyperfine interaction. Differently from U-based compounds where the configuration of $5f$ electrons in U-ion is undecided, the Hund ground state due to configuration of $4f^1 5s^2 p^6$ of Ce^{+3} can be determined uniquely and the state is defined by the total angular momentum, J, because the ion Ce^{+3} has a single f electron. In Ce-123 system, the lowest J manifold ($J = 5/2$) is split into three doublets by the crystal electric field (CEF). Then the temperature dependence of the susceptibility is expressed as

$$\chi_{total}^i(T) = \frac{Ng_J^2\mu_B^2}{\sum_{n=0,1,2}\exp(-\frac{E_n}{k_BT})}\left\{\sum_{n=0,1,2}\frac{|<n|J_i|n>|^2}{k_BT}exp(-\frac{E_n}{k_BT})\right.$$
$$\left.-2\sum_{n=0,1,2}\sum_{m\neq n}\frac{|<n|J_i|m>|^2}{E_m-E_n}exp(-\frac{E_n}{k_BT})\right\}, \qquad (6.4)$$

where the suffix "i" specifies the direction of the crystal axis. g_J is the Lande factor, μ_B the Bohr magneton, N the Abogadro's number and k_B the Boltzmann factor. Here, the simple form of the susceptibility for Ce^{3+} ions does not incorporate the RKKY type exchange interaction into itself. The sum "n" goes over the three doublets denoted as $|n>$ ($n = 0, 1, 2$).The first term arises from the respective doublets (hereafter called as "spin" part). The second term originates from the excited state doublets. The CEF splitting scheme in $CePd_2Al_3$ is assigned as the ground state, $|0>= \Gamma_7 = |\pm 1/2 >$ with $E_0 = 0$ K, the first excited, $|1>= \Gamma_9 = |\pm 3/2 >$ with $E_1 =33$K, and the second excited, $|2>= \Gamma_8 = |\pm 5/2 >$ with $E_2 = 800$ K [78]. Since the experiment was made up to higher temperature region than $\Delta_1 = E_1 - E_0 = 33$ K, the contribution to the total susceptibility from the first excited state should vary with temperature, including the "spin" part as well,

whereas, that from the second excitation is temperature independent and gives rise to Van Vleck part, because $\Delta_2 = E_2 - E_1 = 767$ K is significantly larger than $\Delta_1 = 33$ K and the temperature region where the experiment was made. Equation (6.4) is thus decomposed into two contributions as,

$$\chi_{total}^i(T) = \chi_s^i(T) + \chi_{vv}^i \tag{6.5}$$

$\chi_s(T)$ and χ_{vv} are the "spin" and the Van Vleck part for f-electrons, respectively. The contribution from the conduction electrons of s-, p-, and d-states to χ_{total} is evaluated as $2.3^{-9} \text{m}^3/\text{mole}$ from the non-magnetic $LaPd_2Al_3$, which is negligibly smaller by two orders of magnitude than the total susceptibility. χ_{vv} is roughly estimated as the order of 10^{-9} cm^3/mole from the eq.(6.4), which is also negligible. The Knight shift of ^{27}Al is expressed as

$$K_{Al}^i(T) = K_s^i(T) + K_{vv}^i + K_c. \tag{6.6}$$

Here, K_s means the "spin" part of the Knight shift originated from the transferred hyperfine interactions, which is composed of the isotropic and the anisotropic part via $s - f$ and $p - f$ hybridizations, respectively, and from the temperature dependence of the second term of eq.(6.4) associated with Δ_1. K_{vv} is the Van Vleck shift related to χ_{vv}. K_c is the Knight shift from the conduction electrons at Al sites. Since K_{vv} and K_c are temperature independent, the temperature dependence of K_s arises only from χ_s. From eqs.(6.5) and (6.6). the Knight shift components, $K_{Al}(T)$ in the basal plane is related to $\chi_{total}^{\perp}(T)$ with temperature as an implicit parameter by

$$K_s^{\perp}(T) = \frac{A_{hf}^{\perp}}{N\mu_B}\chi_s^{\perp}(T). \tag{6.7}$$

Since $\chi^{\parallel}$ is almost temperature independent with a magnitude by one order of smaller than $\chi^{\perp}(T)$ as estimated from the anisotropic susceptibility data on single crystal[78], it is possible that $K_s^{\perp}(T)$ for oriented powder (PC1) is tentatively plotted against $\chi^{\perp}(T) = \frac{3}{2}\chi_{poly}(T) - \frac{1}{2}\chi^{\parallel} \sim \frac{2}{2}\chi^{poly}(T)$.

In fact, the $K^{\perp}$ vs $\chi_{poly}(T)$ plot provides a linear relation above 20K as shown in Fig.6.2.1. From the result that an extrapolation to $\chi = 0$ intersects at almost zero Knight shift$\sim 0.08\%$, the temperature independent Van Vleck part is actually negligible within the experimental accuracy. Then the hyperfine coupling constants in the basal plane are

81

estimated as $A_{hf} = 2.059$ kOe/μ_B and 0.850 kOe/μ_B. The isotropic and the anisotropic hyperfine fields within the basal plane are evaluated as $A_{iso} = 1.455$ kOe/μ_B and $A_{ani} = 0.605$ kOe/μ_B, respectively.
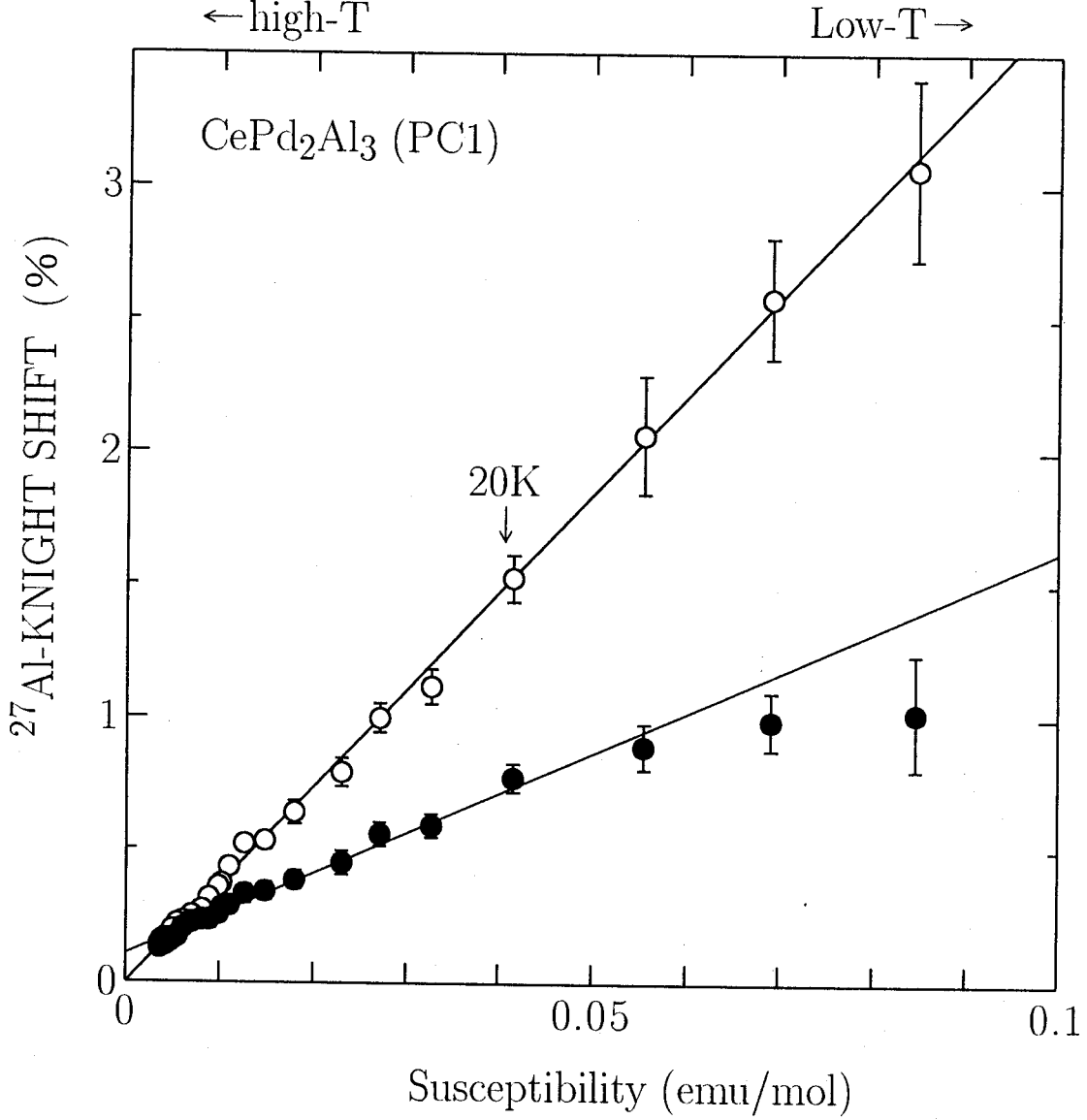

Figure 6.2.1 Two components of ^{27}Al Knight shift vs the susceptibility plots, with temperature as an implicit parameter, by using $2/3\chi_{\perp}(T) \sim \chi_{poly}(T)$.

6.2.2 Magnetic and Structural Instability in Ce-123 System

We discuss a possible origin for two kinds of the NQR peaks. The frequency at the main peak is in good agreement with the value extracted from the NMR spectrum. Hence it is

concluded that the main peak corresponds to the signal from the regular Al-site. There are two possibilities for the origins of the satellite peak, namely, the replacement of Al atoms into "regular" Pd-site [74] or the displacement of Al atoms along c-axis [79]. In the former case, the dipole field at the Pd-site is estimated as $\sim$0.5 kOe in the **AF** ordered state with the saturation moment of about $\sim 0.5\mu_B$. In addition, by taking into consideration the transferred hyperfine interaction due to the hybridization between Ce-f and Al-s,p electrons, the Al nuclei occupying the "regular" Pd-site should feel a large internal field by the onset of **AF** ordering, resulting in an appreciable decrease of the NQR intensity below T_N. However, this is not the case because the integrated intensity of the NQR spectrum multiplied by temperature, $I.I. \times T$, at 1.3 K is almost equal to that at 4.2 K within an error of $\sim$ 2 % for both PC1 and PC2. Therefore, the satellite is not attributed to Al atoms replaced into the Pd-site, although a possibility of the Pd-Al atomic disorder cannot be ruled out completely. From view points of the Al-NQR experiments together with the result of the structural analysis by the neutron scattering experiment[78], it is reasonable that Al atoms are displaced along the c-axis, yielding possible two Al-sites.

Next we argue the relationship between the **AF** ordering and the structural disorder. It is noteworthy that both the linewidth of the main peak and the relative intensity of the satellite to the main at 4.2 K increase significantly for nonordering PC2 and SC1, as summarized in Table 3. From the results of the NQR experiments, it is proposed that Al atoms can occupy two possible sites in the Al layer, induced by either disorder(PC2) or vacancies(SC1) even though the lattice symmetry remains unchanged. It is known that, in general, large anisotropy between the inplane exchange interaction parameter, $J_\perp$, and the interplane one, J_c, make the magnetic ordering temperature, T_N or T_C, decrease in the usual three dimensional Heisenberg model. The small value of $T_N \sim 2.7$ K in the Ce-123 system implies the large anisotropy of the exchange interactions. J_c is expected to be small in contrast to $J_\perp$, because the inplane Ce atoms are closely packed with Pd atoms, whereas those along the c-axis is well separated by the single Al layers. Since J_c involves the RKKY-type interaction through the conduction electron polarization in the Al-layer between two magnetic layers, any disorder in the Al-layer could prevent the development of the interplane magnetic coupling, J_c, via the Al layer which stabilizes the antiferromagnetic

long range order.

In any case, we emphasize a close relationship between the disappearance of the long range **AF** ordering and the structural disorder in the Al layer from the NQR view point. In order to further characterize the magnetic properties, we discuss the results of the nuclear-spin-lattice relaxation rate, $1/T_1$.

From the fact that the satellite line of the NQR spectrum still remains even for PC1, the site-occupation at two Al-sites is considered to cause a distribution of the low-energy excitation inherent to this unique heavy-fermion antiferromagnet. Even in such a situation, short and long components of T_1 were tentatively extracted from the relaxation function of the nuclear magnetization to see the T dependence of $1/T_1$ far below T_N. It has been found that $1/T_1$ for PC2, where the clear onset of the AF ordering cannot be evidenced from bulk measurements, exhibits a much larger distribution below 2.7 K than that for PC1. This is because the Al atoms occupy two sites much more randomly for PC2 than for PC1 as expected from the NQR spectrum, hence the paramagnetic region remains partially in the lower temperature region than 2.7 K. It is likely that the short component of T_1 originates from such paramagnetic regions induced by the Al-site disorder, while the magnetically ordered region gives rise to the long component of T_1 and causes the broadening of the NQR spectrum as indicated in Fig.6.1.7. Thus the short-range "static" magnetic correlation develops below T_N for PC2 and the **AF** ordering is not fully of a long-range type. In a clear contrast to the case for the polycrystals, $1/T_1$ for the single crystal is largely distributed above and below 2.7 K and does not experience any anomalies around 2.7 K. Both the short and long components of $1/T_1$ keep constant values in the temperature range of measurement. No sign of magnetic ordering could be observed. From the measurements of the NQR spectrum and T_1, it is thus confirmed that the single crystal $CePd_2Al_3$ experiences neither the long-range **AF** ordering nor the development of the short-range static magnetic correlation because of the Al-deficiency in addition to the site-randomness over two Al-sites. Apparently, ^{27}Al-NQR and NMR studies are decisive in proving that the occupation and distribution of Al atoms over two sites control dramatically the magnetic nature and mask more or less the intrinsic magnetic feature inherent to the ideal $CePd_2Al_3$. If the sample where only one Al-NQR signal is observed is prepared,

more detailed information could be obtained on the magnetic excitations in this unique heavy-fermion antiferromagnetic state.

6.3 Conclusion

We have investigated the microscopic magnetic properties in a series of $CePd_2Al_3$ systems by means of ^{27}Al-NMR/NQR measurements. As suggested from susceptibility, specific heat, ^{27}Al-NQR, neutron scattering and μSR experiments [80], the difference in the magnetic behavior among various samples of $CePd_2Al_3$ are interpreted from the present study as follows:

(1) In the annealed polycrystal (PC1), considerable amount of Al atoms occupy an ideal Al-site in the $PrNi_2Al_3$-type structure to such an extent that the long-range antiferromagnetic ordering can fully develop below $T_N=2.7$ K. However, a presence of the small site-distribution over two Al-sites is responsible for the distribution of the magnetic excitation spectrum in the low temperature region well below T_N and for masking the intrinsic feature inherent to the ideal $CePd_2Al_3$. In this sense, the magnetic coherence length along the c-axis, ξ_c is not expected to be infinite, though it might be significantly large.

(2) In the as-cast polycrystal(PC2), it is evident that two Al-sites are occupied more randomly than in PC1. This large distribution of Al atoms over two sites causes the inhomogeneous antiferromagnetic ordering. The short-range "static" magnetic correlation develops below nearly the same temperature as $T_N=2.7$ K, although ξ_c will remain finite, and as a result, induces a hyperfine broadening of the Al NQR spectrum.

(3) In the single crystal(SC1), both inhomogeneous effects of the site-randomness over two sites and the Al-deficiency destroy both the long-range AF ordering and the short-range static AF correlation, diminishing the exchange coupling strength, $J_\parallel$, below a critical value, and ξ_c will almost be zero.

Thus from a clear description of the magnetism in the various $CePd_2Al_3$ samples. we have highlighted an intimate relationship between structural effects and the magnetic character in this compound.

Acknowledgements

References

Heavy Fermion System

[1] G.R. Stewart, Rev. Mod. Phys. **56**, 755 (1984).

[2] F. Steglich, J. Aarts, C.D. Bredl, W. Lieke, D. Meschede, W. Franz, and H. Schafer, Phys. Rev. Lett. **43**, 1892 (1979).

[3] H.R. Ott, H. Rudiger, Z. Fisk, and J.L. Smith, Phys. Rev. Lett. **52**, 679 (1984).

[4] M.B. Maple, J.W. Chen, Y, Dalichaouch, T. Kohara, C. Rossel, M.S. Torikachvili, M.W. McElfresh, and J.D. Thompson, Phys. Rev. Lett. **56**, 185 (1986)

[5] C. Geibel, S. Thies, D. Kaczorowski, A. Mehner, A. Grauel, B. Seidel, R. Hefrich, K. Petersen, C.D. Bedl, and F. Steglich, Z Phys. **B83**, 305 (1991)

[6] C. Geibel, C. Schank, S. Thies, H. Kitazawa, C.D. Bredl, A. Bohm, M. Rau. A. Grauel, R. Caspary, R. Helfrich, U. Ahlheim, G. Weber, and F. Steglich, Z.Phys **B84**, 1 (1991).

Nuclear Magnetic Resonance

[7] see *e.g.*, A. Abragam, *Principles of Nucclear Magnetism*, (Clarendon Press, Oxford, 1961); C.P. Slichter, *Principle s of Magnetic Resonance (Splinger Series in Solid State Science)*, (Springer Verlag, Berlin, 1990), vol.1.

[8] G.C. Carter, L.H. Bennet, and D.J., Kahan, *Metallic Shifts in NMR*, eds. by B. Chalmers, J.W. Christian, and T.B. Massalski, (PERGAMON PRESS, Oxford, New York, Toront, Sydney, Paris, Frankfurt), vol.20.

[9] T. Moriya, Prog. Theor. Phys. **16**, 23 (1956).

[10] T. Moriya, J. Phys. Soc. Jpn. **18**, 516 (1963).

[11] J. Korringa, Physica **16**, 601 (1950).

[12] see *e.g.*, D.E. MacLaughlin, in *solid state Phys.*, eds. by H. Ehrenreich, F. Seitz, and D. Turnbull, (Academic Press, New York, 1976), vol. 31, p.1.

[13] K. Yosida, Phys. Rev. **110**, 769 (1958).

[14] L.C. Hebel, and Slichter, Phys. Rev. **113**, 1504 (1959).

[15] H.L. Fine, M. Lipsicas and M.Strogin, Phys. Lett. **29A**, 336 (1969)

[16] Y. Masuda and A.G. Redfield, Phys. Rev. **125**, 159 (1962).

[17] K. Asayama, in *Selected Topics in Superconductivity*, eds. L.C. Gupta, and M.S. Multani, (World Scientific), vol.1.; ibid. in *Magnetism and Superconductivity in Itinerant Electron System*, eds. A. Kawabata, and H. Yasuoka, (SHOKABO TOKYO), p.60, in Japanease.

Superconductivity

[18] J. Bardeen, L.N. Cooper, and J.R. Schrieffer, Phys. Rev. **108**, 1175 (1957).

[19] P.W. Anderson and P. Morel, Phys. Rev. **123**, 1911 (1961).

[20] R. Balian, and N.R. Werthamer, Phys. Rev. **131**, 1553 (1963).

[21] G.E. Volovik, and L.P. Gor'kov, Sov. Phys. JETP **61**, 843 (1985)

[22] M. Sigrist, and K. Ueda, Rev. Mod. Phys. **63**, 239 (1991)

[23] P.W. Anderson, Phys. Rev. **B30**, 4000 (1984).

[24] K. Miyake, in *Theory of Heavy Fermions and Valence Fluctuations*, eds. T. Kasuya and T. Saso., P256 (Springer, Berlin, 1986)

UPd_2Al_3

[25] N. Sato, T. Sakon, N. Tkeda, T. Komatsubara, C. Geibel, and F. Steglich, J. Phys. Soc. Jpn. **61**, 32 (1992).

[26] A. de Visser, H. Nakotte, L.T. Tai, A.A. Menovsky, S.A.M. Mentink, G.J. Nieuwen-huys, and J.A. Mydosh, Physica **C179**, 84 (1992).

[27] R. Caspary, P. Hellmann, M. Keller, G. Sparn, C. Wassilew, R. Köhler, C. Geibel, C. Schank, F. Steglich, and N.E. Phillips, Phys. Rev. Lett. **71**, 2146 (1993).

[28] T. Sakon, K. Imamura, N. Koga, N. Sato, and T. Komatsubara; Physica **B199&200**, 154 (1994).

[29] A.Krimmel, P.Fischer, B.Roessli, H.Maletta, C.Geibel, C.Schank, A.Grauel, A.Loidol, and F.Steglich, Z. Phys. B-Cond. Matter **86**, 161 (1992).

[30] K. Gloos, R. Modler, H. Schimanski, C.D. Bredl, C. Geibel, F. Steglich, A.I. Buzdin, N. Sato, and T. Komatsubara, Phys. Rev. Lett. **70**, 501 (1993).

[31] M. Kyogaku, Y. Kitaoka, K. Asayama, C. Geibel, C. Shank, and F. Steglich, J. Phys. Soc. Jpn. **62**, 4016 (1993); ibid. **61**, 2660 (1992).

[32] M. Kyogaku, Y. Kitaoka, K. Asayama, N. Sato, T. Sakon, T. Komatsubara, C. Geibel, C. Shank, and F. Steglich, Physica **B186&188**, 285 (1993).

[33] R. Feyerherm, A. Amato, F.N. Gygax, A. Schenk, C. Geibel, F. Steglich, N. Sato, and Y. Komatsubara, Phys. Rev. Lett. **73**, 1849 (1994).

[34] Y. Kohori, K. Matsuda, and T. Kohara, Physica **B206&207**, 622 (1995); ibid. Solid state commun.(1995)

[35] S. Schmitt-Rink, K. Miyake, and C.M. Varma, Phys. Rev. Rett. **57**, 2575 (1986); K. Miyake, private communication ; Y. Kitaoka, K. Ishida, and K. Asayama, J. Phys. Soc. Jpn. **63**, 2052(1994).

[36] K.Ishida, Y. Kitaika, T. Yoshitomi, N. Ogata, T. Kamino, and K. Asayama, Physica **C179**, 29 (1991).

[37] K. Oda, T. Kumada, K. Sugiyama, N. Sato, T. Komatsubara and M. Date, J.Phys. Soc. Jpn. **63** 3115(1994).

[38] A. Amato, R. Feyerherm, F. N.Gygax, A. Schenck, M. Weber, R. Caspary, P. Hellmann, C. Shank, C. Geibel, F. Steglich, D.E. MacLaughlin, E.A. Knetsch, and R.H. Heffner, Eurphys. Lett. **19**, 127 (1992).

[39] L. Paolasini, J.A. Paixão, G.H. Landel, A. Delapalme, N. Sato, and T. Komatsubara, J. Phys. Cond. Matter **5**, 8905 (1993).

UPt$_3$

[40] See *e.g.*, A. de Visser, A. Menovsky, and J.J.M. Franse, Physica **B147**, 81 (1987); L. Taillefer, J. Frouquet, and G.G. Lonzarich, Physica **B169**, 257 (1990).

[41] A.I. Goldman, G. Shirane, G. Aeppli, E. Bucher, and J. Hufnagl, Phys. Rev. **B36**, 8523, (1987).

[42] G. Aeppli, E. Bucher, C. Broholm, J.K. Kjems, J. Baumann, and J. Hufnagl, Phys. Rev. Lett. **60** ,615 (1988); G. Aeppli, D. Bishop, C. Broholm, E. Bucher, K. Simensmeyer, M. Steiner, and N. Stüsser, Phys. Rev. Lett. **63**, 676 (1989).

[43] A. Schestrom, M-F. Xu, Y. Hong, D. Bein, M. Levy, B.K. Sarma, S. Adenwalla, Z. Zhao, T. Tokuyasu, D.W. Hess, J.B. Ketterson, J.A. Sauls, and D.G. Hinks, Phys. Rev. Lett. **62**, 332 (1989).

[44] Y. Kohori, T. Kohara, H. Shibai, Y. Oda, T. Kaneko, Y. Kitaoka, and K. Asayama, J. Phys. Soc. Jpn. **56**, 2263 (1987); ibid. Jpn. J. Appl. Phys. Suppl. **26**, 1239 (1987);

[45] R.A. Fisher, S. Kim, B.F. Woodfield, N.E. Phillips, L. Taillefer, K. Hasselbach, J. Frouquet, A.L. Giorgi, and J.L. Smith, Phys. Rev. Lett. **62**, 1411 (1989).

[46] K. Hasselbach, L. Taillefer, and J. Fluquet, Phys. Rev. Lett. **63**, 93 (1989).

[47] B.S. Shivaram, Y.H. Jeong, T.F. Rosenbaum, and D.G. Hinks, Phys. Rev. Lett. **56**, 1087 (1986).

[48] C. Broholm, G. Aeppli, D.J. Kleiman, D.R. Harshmann, D.J. Bishop, E. Bucher, D.Ll. Williams, E.J. Ansaldo, and R.H. Heffner, Phys. Rev. Lett. **65**, 2062 (1990).

[49] Y. Kohori, T. Kohara, H. Shibai, Y. Oda, Y. Kitaoka, and K. Asayama, J. Phys. Soc. Jpn. **57**, 395 (1988); Y. Kohori, H. Shibai, T. Kohara, Y. Oda. Y. Kitaoka, and K. Asayama, J. Mag. Mag. Mater. **76&77**, 478 (1988).

[50] G.M. Luke *et al.* Phys. Rev. Lett. **71**, 1446 (1993); ibid. Phsica **B186**, 264 (1993).

[51] C. Stassis, J. Arthur, C.F. Majkrzak, J.D. Axe, B. Batlagg, J. Remaeika, Z. Fisk, J.L. Smith, and A.S. Edelstein, Phys. Rev.**B34**, 4382 (1986).

[52] V. Müller, Ch. Roth, D. Maurer, E.W. Scheidt, K. Lüders. E. Bucher, and H.E. Bömmel, Phys. Rev. Lett. **58**, 1224 (1987).

[53] Y. Qian, M-F. Xu, A. Schenstrom, H-P. Baum, J.B. Ketterson, D. Hinks. M. Levy, and B.K. Sarma Solid state commun. **63**, 599 (1987).

[54] S. Addenwella, S.W. Lin, Q.Z. Ran, Z.Zhao, J.B. Ketterson, J.A. Sauls, L.tailleher, D.G.Hinks, M.Levy, and B.K.Sarma, Phys. Rev. Lett. **65**, 2298 (1990)

[55] B. Bogenverger, H.v. Löhneysen, T. Trappmann, and L. Taillefer. Physica **B185&186**, 248 (1993).

[56] G. Goll, H.v. Löhneysen, and I.K. Yanson. Phys. Rev. Lett. **70**, 2008 (1993)

[57] H.v. Löhneysen, Physica **197**, 551 (1994).

[58] K. Machida and M. Ozaki, Phys. Rev. Lett. 71, 2146 (1993); K. Machida, T. Ohmi and M. Ozaki, J. Phys. Soc. Jpn. **62**, 3216 (1993).

[59] K.Machida, M.Ozaki, and Ohmi, J. Phys. Soc. Jpn. **64**, 1064 (1995)

[60] C.H.Choi and J.A.Sauls, Phys. Rev. Lett. **66**, 484 (1991).

[61] S.M. Hayden, L. Taillefer, C. Vettier, and J. Flouquet, Phys. Rev. **B46**, 8675 (1992)

[62] R. Joynt, V.P. Mineev, G.E. Volovik, and M.E. Zitomirsky, Phys. Rev. **B42**, 2014 (1990).

[63] M.E. Zitomirsky, and I.A. Luk'yananchuk, Sov. Phys. JETP Lett. **58**, 131 (1993); M.E. Zitomirsky, and K. Ueda, unpublished.

[64] M. Lee, G.F. Moores, Y.-Q. Song, W.P. Halperin, W.W. Kim, and G.R. Stewart, Phys. Rev. **B48**, 7392 (1993).

[65] A.I. Goldman, G. Shirane, G. Aeppli, B. Batlogg and E. Bucher, Phys. Rev. **B34**, 6564 (1986).

[66] Y. Kohori, M. Kyogaku, T. Kohara, K. Asayama, H. Amitsuka, and Y. Miyako, J. Mag. Mag. Mater. **90&91**, 510 (1990).

[67] P.W. Anderson, Phys. Rev. Lett. **3**, 325 (1959)

[68] N. Kimura, R. Settai, Y. Ōnuki, H. Toshima, E. Yamamoto, K. Maezawa, H. Aoki, and H. Harima, J. Phys. Soc. Jpn. **64**, 3881 (1995); private communication, N. Kimura, and Y. Ōnuki.

[69] T. Sakakibara *et al.*, unpublished.

[70] Y. Kitaoka, H. Yamda, K. Ueda, Y. Kohori, T. Kohara, and K. Asayama, Jpn. J. Appl. Phys. Suppl. **26**, 1221 (1987).

[71] P.D. de Rétier, A. Huxley, A. Yaouanc, J. Flouquet, P. Bonville, P. Imbert, P.Pari, P.C.M. Gubbens, and A.M. Mulders, Physics letters **A205**, 239 (1995).

CePd$_2$Al$_3$

[72] H. Kitazawa, C. Schank, S. Thies, B. Seidel, C, Geibel, and F. Steglich, J. Phys. Soc. Jpn **61**, 1461 (1992).

[73] E. Bauer, R. Hauser, E. Gratz, C. Schaudy, M. Rotter, A. Lindbaum, D. Gignoux, and D.Schmitt, Z. Phys **B92**, 411 (1993).

[74] S.A.M. Mentink, N.M. Bos, G.J. Nieuwenhuys, A.A. Menovsky, and J.A. Mydosh, Physica **B186&188**, 497 (1993).

[75] S. Mitsuda, T. Wada, K. Hosoya, and H. Kitazawa, J. Phys. Soc. Jpn. **61**, 4667 (1992).

[76] A. Amato, C. Geibel, E.N. Gygax, R.H. Heffner, E. Knetsch, D.E. MacLaughlin, C. Schank, F. Steglich, and M. Weber, Z. Phys **B96**, 159 (1992).

[77] A. Donni, P. Fischer, B. Roessli, and H. Kitazawa, Z. Phys **B** (1993) in press.

[78] S.A.M. Mentink, G.J. Nieuwenhuys, A.A. Menovsky, J.A. Mydosh, A. Drost, E. Frikkee, Y. Bando, T. Takabatake, P. Boni, P. Fischer, A. Furrer, A. Amato, and A. Schenck, Physica **B199&200**, 143 (1994).

[79] S.A. M.Mentink, N.M. Bos, G.J. Nieuwenhuys, A. Drost, E. Frikkee, L.T. Tai, A.A. Menovsky, and J.A. Mydosh, Physica **B186&188**, 460 (1993).

[80] S.A.M. Mentink, G.J. Nieuwenhuys, A.A. Menovsky, J.A. Mydosh, H. Tou, and Y. Kitaoka, Phys. Rev. **B49**, 15759 (1994).

[81] T. Sakon, K. Imamura, N. Takeda, N. Sato, and T. Komatsubara, Physica **B186&188**, 297 (1993).

[82] Y. Dalichaouch, M.C.de Andrade, and M.B. Maple, Phys. Rev. **B46**, 8671 (1992).

[83] K. Fujiwara, Y. Yamanashi, and K.Kumagai, Pysica **B199&200**, 107 (1994).

[84] H. Nakamura, Y. Kitaoka, K. Asayama, and J. Flouquet, J. Phys. Soc. Jpn. **57**, 2644 (1988).

[85] Y. Kitaoka, K. Ueda, T. Kohara, Y. Kohori, and K. Asayama, *Theoretical and experimental aspect of valence fluctuations and Heavy Fermion* eds. L.C. Gupta and S.K. Malik (Plenum Publishing Corporation 1987) p.297.

[86] T. Kohara, Y. Kohori, K. Asayama, Y. Kitaoka. M.B. Maple, and M.S. Torikachvili, Solid State Commun. **59**, 603 (1986).